Title
Myopia control in guinea pigs

Author
Garcia, Mariana

Publication Date
2014

Peer reviewed|Thesis/dissertation

Myopia control in guinea pigs

By

Mariana Borges Garcia

A dissertation submitted in partial satisfaction of the

requirement for the degree of

Doctor of Philosophy

in

Vision Science

in the

Graduate Division

of the

University of California, Berkeley

Committee in charge:

Professor Christine F. Wildsoet, Chair
Professor Kevin E. Healy
Professor Nancy McNamara

Fall 2014

Myopia control in guinea pigs

By

Mariana Borges Garcia

University of California, Berkeley

Abstract

Myopia control in guinea pigs

By

Mariana Borges Garcia

Doctor of Philosophy in Vision Science

University of California, Berkeley

Professor Christine Wildsoet, Chair

Myopia, or nearsightedness, is a common refractive error characterized by an abnormally large increase in eye elongation that leads to a mismatch between the eye's refracting power and the location of the retina. Besides causing blurry vision when left uncorrected, myopia carries a significant risk of vision-threatening complications such as glaucoma, retinal detachment, myopic maculopathy, and choroidal neovascularization. Billions of dollars are spent worldwide on the correction of myopia and treatment of its associated complications. In addition to the threat it poses to the ocular health of working-age populations, the steady climb in myopia prevalence reported in most countries adds urgency to the need for innovative and reliable myopia-control therapies. Taking inspiration from the concept behind scleral buckling surgery – in which a strip of cadaver sclera is used to brace the weakened posterior pole of the eye – we sought to develop a hydrogel-based therapy with the intended action of slowing or preventing subsequent excessive elongation, by way of rehabilitating the myopic sclera in the early stages of the disease.

Chapter 2 describes the development of a guinea pig myopia model, for use in testing our experimental myopia-control therapy. Guinea pigs have emerged as a popular mammalian myopia model because of their ease of housing and husbandry, relatively large eyes, and better visual acuity than other laboratory rodents (mice and rats). After establishing a breeding colony using breeders donated from a myopia lab at the University of Auckland, we successfully induced myopia in guinea pigs using a form deprivation model. In the course of our studies, we also tried to induce myopia using defocusing lens and form deprivation in guinea pigs from a commercial research supplier. To our surprise, those animals proved resistant to any kind of myopia-inducing stimuli. The research implications of such potential strain-related variability in responses are discussed, including the need to exercise due caution in comparing results from different myopia research laboratories.

In Chapter 3, we detail the optimization and *in vitro* characterization of a hyaluronic acid (HyA) hydrogel investigated as a myopia-control therapy. Using parallel plate rheology we determined the modulus of hydrogels of two different monomer contents, 2.0 and 3.3 weight percent by volume. Both were much softer than the native sclera, i.e. 200 and 800 Pa compared to ~2 MPa. Through cytotoxicity and proliferation assays we found that both softer and stiffer hydrogels were biocompatible with guinea pig scleral fibroblasts, although proliferation rates were higher for cells cultured on the tissue culture polystyrene control surface. Interestingly, cell proliferation proved to be independent of the concentration of the bsp-RGD(15) cell-binding peptide included in the hydrogel. This suggests that scleral fibroblasts were able to engage with other binding sites on the scaffold, perhaps hyaluronan receptor CD44. Likewise, cells were observed to migrate through

hydrogels with no bsp-RGD(15) peptide in a novel migration assay in which cells were allowed to first form a stable monolayer before being exposed to the hydrogels.

Chapter 4 presents the results of *in vivo* testing of 200 Pa HyA hydrogel containing 380 μM of cell-binding peptide in our established guinea pig myopia model. After a 7-day period of myopia induction through form deprivation, guinea pigs received a posterior sub-Tenon's capsule injection of either HyA hydrogels or the triethanolamine buffer used to prepare the hydrogel (sham treatment). After an additional three weeks of form deprivation, both groups of treated guinea pigs (hydrogel and sham) exhibited a significant amount of myopia control, as indicated by normalization of the axial lengths of treated eyes relative to their contralateral (fellow) eyes. In fact, the treatment effects were not significantly different from each other. The myopia control effect is tentatively attributed to thickening of Tenon's capsule at the surgical site, with the secondary effect of enhancing the mechanical stability of the posterior sclera. The changes in Tenon's capsule could be the product of a wound healing response triggered by the surgical manipulation. Functional measurements (flash electroretinograms and visual acuity) revealed no evidence of adverse effects of the treatments. Intraocular pressure was also unaffected by them. In discussing the findings of this study, two possible novel myopia-control therapies are proposed for further investigation: an HyA hydrogel-based implant customized to also deliver an anti-myopia drug for additional control, and a sub-Tenon's capsule surgical manipulation, of the type used for sham injections of buffer.

Dedicated to the memory of Liete Rocha Borges

Table of Contents

Abstract 1
List of figures v
List of tables viii
List of abbreviations ix

Acknowledgments xi

Chapter 1. Background

1.1 Introduction: Myopia and its public health impact 1
1.2 The myopic sclera 2
1.2.1 A brief overview of scleral structure 2
1.2.2 Scleral biochemistry and its changes with myopia 3
1.2.3 Biomechanical changes in the myopic sclera 4
1.3 Current strategies for myopia control 5
1.3.1 Pharmacological intervention 5
1.3.2 Surgical interventions and use of biomaterials 6

Dissertation approach and outline 7

Chapter 2. A tale of two guinea pigs – characterization of a guinea pig myopia model

2.1 Introduction 9
2.2 Animal models in myopia research – a brief review 9
2.2.1 Common animal models of myopia 11
2.2.1.1 Monkeys 11
2.2.1.2 Chicks 11
2.2.1.3 Tree shrews 12
2.2.1.4 Mice 13
2.2.1.5 Guinea pigs 14
2.3 Materials and Methods 15
2.3.1 Animals 15
2.3.2 Lenses and diffusers 15
2.3.3 Measurements 16
2.3.4 Experimental Treatments 16
2.3.5 Statistical analyses and data representation 17
2.4 Results 17
2.4.1 Elm Hill guinea pigs treated with negative lenses and diffusers 17

2.4.1.1 Refraction and axial length changes 17
2.4.1.2 Visual acuity changes 22
2.4.2 New Zealand guinea pigs treated with diffusers 23
2.4.2.1 Refraction and axial length changes 23
2.4.2.2 Visual acuity changes 26
2.4.3 Comparing the form deprivation responses in New Zealand and Elm Hill guinea pigs 27
2.5 Discussion 29
2.6 Conclusion 33

Chapter 3. *In vitro* characterization of mammalian scleral fibroblast behavior on synthetic hyaluronic acid-based hydrogels

3.1 Introduction 34
3.2 Materials and methods 36
3.2.1 Establishment and maintenance of primary cultures of guinea pig scleral fibroblasts 36
3.2.2 Characterization of cell growth on hyaluronic acid-based hydrogels 37
3.2.2.1 Synthesis of hyaluronic acid-based hydrogels 37
3.2.2.2 Cell viability and proliferation on hyaluronic acid-based hydrogels 40
3.2.2.3 Migration through hyaluronic acid-based hydrogels 40
3.3 Results 43
3.3.1 Rheological characterization of hyaluronic acid-based hydrogels 43
3.3.2 Cell viability and proliferation on hyaluronic acid-based hydrogels 44
3.3.3 Migration through hyaluronic acid-based hydrogels 47
3.4 Discussion 48
3.5 Conclusion 50

Chapter 4. Myopia control in guinea pigs through hydrogel-mediated scleral support and regeneration

4.1 Introduction 51
4.2 Materials and methods 52
4.2.1 Animals 52
4.2.2 Experimental design 52
4.2.3 Diffusers 53
4.2.4 Sub-Tenon's capsule surgery 54
4.2.5 Magnetic Resonance Imaging (MRI) 55

4.2.6 Measurements 55
4.2.6.1 Refractive errors and ocular biometry 55
4.2.6.2 Functional testing and IOP measurement 56
4.2.6.3 Statistical analyses and data representation 57
4.2.7 Histological studies 58
4.3 Results 58
4.3.1 Effect of hydrogel/sham surgeries on axial components and refractive error 58
4.3.2 Retinal function and visual acuity in guinea pigs after hydrogel/sham surgery 66
4.3.3 Intraocular pressure in guinea pigs after hydrogel/sham surgery 68
4.3.4 MRI localization of implant and histology analyses after 28 days of treatment 69
4.4 Discussion 71
4.5 Conclusion 77

Chapter 5. Summary and future directions

5.1 Dissertation summary 78
5.2 Future directions 79

References 81

Appendix 1. Calculation of a correction factor for the refractive error data presented in Chapter 4 98

Appendix 2. *In vitro* compatibility studies of N-isopropylacrylamide-based semi- interpenetrating polymer networks with guinea pig scleral fibroblasts 101

Appendix 3. Preliminary *in vivo* hydrogel injection studies 106

List of figures

Figure 1.1. Schematic illustration of emmetropic, myopic, and corrected myopic eyes 1

Figure 2.1. Guinea pig fitted with a diffuser on its left eye, the right eye serves as an untreated contralateral control 15

Figure 2.2. Axial length and refraction data for Elm Hill guinea pigs after 28 days of negative lens or diffuser treatment 18

Figure 2.3. Longitudinal changes (mean ± SEM) over the experimental period in interocular axial length and refraction for Elm Hill guinea pigs treated with -10 D, -5 D, 0 D lenses and diffusers ..19

Figure 2.4. Interocular axial length plotted against interocular refractive differences at baseline (day 0) and at day 28 20

Figure 2.5. Change in interocular differences in anterior chamber depth (ACD), lens thickness, and vitreous chamber depth (VCD) for Elm Hill guinea pigs after 28 days of negative lens or diffuser treatment 21

Figure 2.6. Change in interocular axial length (y-axis) plotted against change in interocular vitreous chamber depth (x-axis) after 28 days of treatment in Elm Hill guinea pigs treated with negative lenses or diffusers 21

Figure 2.7. Change in interocular difference in retinal thickness, choroidal thickness, and scleral thickness after 28 days of negative lens/diffuser treatment in Elm Hill guinea pigs 22

Figure 2.8. Visual acuity (VA) measurements of Elm Hill guinea pigs after 28 days of negative lens or diffuser treatment, measured with an OptoMotry instrument 23

Figure 2.9. Total change in treated and control values of axial length and refraction for New Zealand (NZ) guinea pigs after 28 days of diffuser treatment 24

Figure 2.10. Change in interocular differences (mean ± SEM) in axial length and refractive error, plotted against treatment day, for New Zealand guinea pigs treated with diffusers for 28 days 24

Figure 2.11. Change in anterior chamber depth (ACD), lens thickness, and vitreous chamber depth (VCD) for New Zealand guinea pigs after 28 days of diffuser treatment 25

Figure 2.12. Interocular differences in axial length (y-axis) plotted against interocular differences in refractive error or vitreous chamber depth at baseline and after 28 days of treatment 26

Figure 2.13. Change in retinal thickness, choroidal thickness, and scleral thickness for treated and control eyes after 28 days of diffuser treatment in New Zealand guinea pigs 26

Figure 2.14. Visual acuity (VA) measurements of treated and control eyes of New Zealand guinea pigs after 28 days of diffuser treatment, acquired with an OptoMotry virtual cylinder 27

Figure 2.15. Changes in interocular differences (treated minus control), in axial length and refractive error for the Elm Hill and New Zealand (NZ) guinea pigs after 28 days of diffuser treatment 27

Figure 2.16. Interocular differences (treated minus control), in visual acuity measured in Elm Hill and New Zealand guinea (NZ) pigs after 28 days of diffuser treatment 28

Figure 3.1. Schematic for hydrogel synthesis 39

Figure 3.2. Setup for migration assay through hyaluronic acid hydrogels 41

Figure 3.3. Steps in the image processing algorithm used to analyze images acquired in the migration assay 42

Figure 3.4. Graph of pixel brightness versus slice number, with fitted Gaussian function, used to identify the reference position for the Z-stack 43

Figure 3.5. Rheological characterization of polymerized 2 and 3.3 wt% hyaluronic acid hydrogels with 380 μM RGD, plotted as complex shear modulus as a function of frequency, measured by oscillatory parallel plate rheology 44

Figure 3.6. Z-stack projections of guinea pig scleral fibroblasts stained with calcein AM (indicator of live cells, green) and ethidium homodimer (indicator of dead cells, red), acquired after 2 days of 2D culture on 200 and 800 Pa hydrogels with varying RGD (cell-binding peptide) concentration 44

Figure 3.7. Guinea pig scleral fibroblast counts derived from cultures over 14 days on 200 Pa (A) and 800 Pa (B) hyaluronic acid hydrogels, with RGD concentrations varying from 0-380 μM, and tissue culture polystyrene (C, control) 45

Figure 3.8. Guinea pig scleral fibroblast numbers after 14 days of culture on 200 Pa (A) and 800 Pa (B) hyaluronic acid hydrogels, with RGD concentrations varying from 0-380 μM, or on tissue culture polystyrene (TCPS, control) 46

Figure 3.9. Results of rheological measurements on 2.0 (A) and 3.3 (B) wt% hydrogels of varying RGD concentrations after 14 days of cell culture 46

Figure 3.10. Graph of scleral fibroblast migration through 0 μM RGD (left panel) and 380μM RGD (right panel) hydrogels, both 200 Pa, after 2 days of culture 48

Figure 4.1. Schematic representation of experimental design and measurements 53

Figure 4.2. Representative guinea pigs used as animal models in this study, showing the position of the hook Velcro segments and a fitted diffuser 54

Figure 4.3. Guinea pig eye enucleated 2 weeks after a ~100 μL sub-Tenon's capsule injection of 800 Pa, 380 μM RGD HyA hydrogel and embedded in Optimal Cutting Temperature (OCT) compound 55

Figure 4.4. Representative guinea pig ERG response 57

Figure 4.5. Axial length data for NZ guinea pigs after 28 days of Diffuser, Diffuser + HyA, or Diffuser + Sham treatment 59

Figure 4.6. Change in interocular axial length difference over time for all treated groups 60

Figure 4.7. Change in axial length in treated eyes plotted against change in axial length in fellow (control) eyes 61

Figure 4.8. Change in interocular differences of anterior chamber depth and lens thickness for guinea pigs treated with Diffusers, Diffusers+HyA, and Diffusers+Sham 62

Figure 4.9. Panel A: CID in axial length plotted against CID in vitreous chamber depth after 28 days of treatment with Diffusers, Diffusers + HyA, or Diffusers + Sham. Panel B: Change in interocular differences of Vitreous Chamber Depth for guinea pigs treated with Diffusers, Diffusers+HyA, and Diffusers+Sham. 63

Figure 4.10. Change in interocular differences of retinal thickness, choroidal thickness, and scleral thickness for guinea pigs treated with Diffusers, Diffusers+HyA, and Diffusers+Sham 63

Figure 4.11. CIDs for refractive errors (Panel A) and changes in refractive error over the total treatment period for treated and control eyes (Panel B) of guinea pigs treated with Diffusers, Diffusers+HyA, and Diffusers+Sham..... 65

Figure 4.12. CID in axial length plotted against CID in refractive error for the Diffuser group alone (A) and all three treatment groups (B) 66

Figure 4.13. Changes in interocular differences for refractive errors over time for all treated groups, all measured under cycloplegia 66

Figure 4.14. Interocular differences in wave amplitudes and time-to-peak (implicit times) obtained from ERG recordings from treated and control eyes from guinea pigs in the Diffusers + HyA and Diffusers + Sham groups..... 68

Figure 4.15. Interocular difference in visual acuity measured at the end of the 28-day study in guinea pigs treated with Diffusers, Diffuser + HyA, and Diffuser + Sham 69

Figure 4.16. Intraocular pressure (reported as interocular difference, treated-control) measured at the end of the 28-day study in guinea pigs from the groups Diffuser + HyA, and Diffuser + Sham 70

Figure 4.17. Image of an eye and surrounding orbital structural, recorded with a 7 T MRI after injection of HyA hydrogel under Tenon's capsule..... 70

Figure 4.18. Guinea pig eyes stained with Hematoxylin & Alcian Blue (top row) and Hematoxylin & Eosin 71

Figure 4.19. Bisected enucleated eye embedded in OCT (A) and Alcian Blue-stained frozen section from the same eye (B), 5 weeks after HyA hydrogel implantation 73

Figure 4.20. Hematoxylin & Eosin-stained sections of Diffuser + Sham eyes 74

List of tables

Table 2.1. Summary of the current, most widely used animal myopia models discussed in this chapter, with the advantages and disadvantages of each. * number of related publications as of May 2014. 10

Table 2.2. Examples of studies that employ the guinea pig as an animal model of myopia 14

Table 2.3. Comparison of axial lengths, refractive errors, and visual acuities of fellow (control) eyes of guinea pigs from the Elm Hill and New Zealand populations 28

Table 2.4. A sample of guinea pig myopia studies published between 2003 and 2013 30

Table 3.1. Average moduli of hydrogels after 14 days of cell culture 47

Table 4.1. Change in dimensions of ocular components over the 28-day treatment 64

Table 4.2. Mean and standard deviation values for amplitude and implicit time (time-to-peak) of three ERG waves, measured in the treated and control eyes of Diffuser+HyA and Diffuser+Sham guinea pigs 68

List of abbreviations

7-MX	7-methylxanthine
ACD	Anterior chamber depth
AL	Axial length
ANOVA	Analysis of Variance
cd	Candela
D	Diopter
DMEM	Dulbecco's Modified Eagle's Media
DMSO	Dimethyl sulfoxide
ECM	Extracellular matrix
EDC	Ethyl-(3-dimethylaminopropyl)carbodiimide hydrochloride
ERG	Electoretinogram
FBS	Fetal Bovine Serum
GAG	Glycosaminoglycan
HCl	Hydrochloric acid
HOBt	1-Hydroxybenzotriazole hydrate
HyA	Hyaluronic acid
IOP	Intraocular pressure
LT	Lens thickness
m	meter
MAI	Poly(methylacrylate-co-2-hydroxyethyl acrylate)
mmHg	Millimeters of mercury
MMP	Matrix metalloprotease
MRI	Magnetic Resonance Imaging
ms	millisecond
NaCl	Sodium chloride
NaOH	Sodium hydroxide
New Zealand	NZ
NIPAAm	N-isopropylacrylamide
ortho-k	Orthokeratology
pen/strep	Penicillin/streptomycin
PGMA	Poly(glyceryl methacrylate)
PHEA	Poly(2-hydroxyethyl acrylate)
pHEMA	Poly(2-hydroxyethyl methacrylate)
PhNR	Photopic negative response
PLGA	Poly(lactic-co-glycolic)
PVP	Poly(vinyl-pyrrolidone)
RPE	Retinal pigment epithelium
s	second
SD	Standard deviation
ST	Scleral thickness
T	Tesla
TCEP	Tris(2-carboxyethyl) phosphine hydrochloride
TCPS	Tissue culture polystyrene
TEA	Triethanolamine buffer
TGF-β	Transforming growth factor - β

TIMP	Tissue inhibitor of metalloprotease
UV	Ultraviolet
VCD	Vitreous chamber depth
Visual acuity	VA

Acknowledgments

I have been incredibly fortunate in all the professional and personal support I received during my PhD. Thank you to my advisor Christine Wildsoet, for the gift of such an incredible project, concern for my professional and personal well-being, and for giving me so much scientific freedom to pursue my curiosity. I am also thankful to my co-advisor and committee member Kevin Healy, for encouraging me to become an integral part of his lab and for all the years of advice. Thanks are also due to Nancy McNamara, for being so generous with her time over the past few years and for providing such insightful comments on my dissertation.

The members of the Wildsoet and Healy labs have been instrumental in helping me complete this project. Amit Jha's scientific generosity and expertise with hydrogels made all the difference in my work, and I will always be thankful for the role he played in my research. I am grateful for the fruitful scientific discussions and encouragement provided by David Hammond, Prema O'Brien, Ravi Metlapally, Yan Zhang, Lisa Ostrin, and Diane Nava. James Su was a patient and supportive mentor during my first two years at Berkeley. Peter Chen and Feng Zhao provided valuable insight during the optimization of the guinea pig surgeries. Brittany Ng helped monitor the guinea pigs during my last semester, allowing me to finish experiments and expedite my writing. Naomi Kohen, Felicia Svedlund, Eda Altiok, Natalie Marks, and Anusuya Ramasubramanian were a wonderful support group for many years and made lab a truly joyful environment.

Professor John Phillips and his team at the University of Auckland provided the guinea pigs for our animal colony – without them the vast majority of this work would never have come to fruition. I am also thankful to the veterinary and animal care staff at UC Berkeley, in particular Kelly Jensen, Kristina Jones, Lindsey Jennings, Anthony McGinnis, and Sparkle Phillips.

None of this work would have been possible without the financial support from the National Institutes of Health, National Science Foundation Graduate Research Fellowship, Ezell Fellowship, and the Minnie Turner Award.

I am extremely grateful to my parents, Alvaro and Iara, and to my sister Raquel, for a lifetime of love and encouragement, and for teaching me to find enthusiasm and strength even in the most exhausting circumstances. My housemates Chat Hull, James Gao, and Helene Moorman transformed our house into a home, and made my years at Berkeley incredibly special. Biggest thanks of all goes to my husband and best friend Adam Morgan – sharing my life with you makes everything better.

Chapter 1. Background

1.1 Introduction: Myopia and its public health impact

Most animals are born hyperopic (farsighted). During development, they undergo a highly regulated process termed emmetropization, through which the length of the eye grows to approximately match its refracting power (with contributions from the cornea and the lens). Failures in emmetropization are the underlying cause of refractive errors [1]. Myopia – commonly called nearsightedness – is a refractive error in which parallel light rays entering the eye are focused in front of the retina (Figure 1.1) [2].

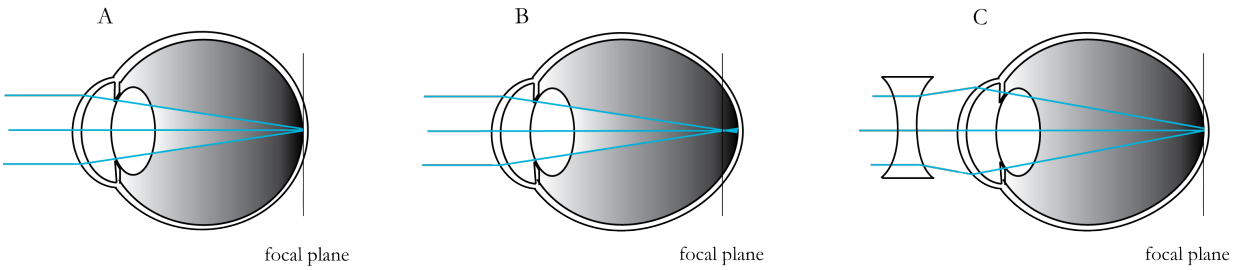

Figure 1.1. Schematic illustration of emmetropic (A), myopic (B), and corrected myopic (C) eyes. In an emmetropic eye (A), light rays are brought to focus on the retina, while in myopic eyes the focal plane is shifted to the vitreous chamber (B). Upon correction with a negative lens of the appropriate power, the focal plane is shifted back to the retina (C).

Myopia is the result of an altered retinal signaling cascade that culminates in altered biochemistry of the sclera (outermost eye wall), leading to an increased creep response and subsequent axial expansion of the eye. Even though myopia was recognized as an ocular condition by the ancient Greeks (Aristotle noted that nearsighted people had a tendency to squint and write in small script), it was only in 1611 that the optical abnormality of the myopic eye was described by Kepler. It was not until one century later that this optical focusing defect was related to an increase in ocular axial length [2]. Even now, much of the general public still regards myopia as simply a minor inconvenience; however, a growing body of evidence points towards the fact that this seemingly inoffensive condition poses significant risks to the ocular health of working-age people around the world.

Myopia is estimated to affect 22% of the world's population, i.e., 1.5 billion people [3]. It is the second leading cause of preventable blindness in developing countries[4], and incurs a financial burden of over 5 billion dollars in the United States alone [5]. Myopia has reached epidemic levels in industrialized East Asian countries such as Singapore, China, Japan, and South Korea, affecting 80-90% of teenagers graduating high school [6]. Recent years have also seen an increase in the prevalence of the once uncommon high myopia (sometimes referred to as pathological or degenerative myopia, defined as refractive error greater than -6 D). For example, a 2005 Singaporean study found that over 18% of 7-year old children are high myopes[7]. High myopia carries an increased risk of

staphylomas – areas of localized mechanical failure and outward distention of the posterior sclera – and a greatly increased risk of sight-threatening diseases such as choroidal neovascularization (newly formed vessels originating in the choroid invade the retina), lacquer cracks (breaks in Bruch's membrane that underlies the retinal pigment epithelium), chorioretinal atrophy (atrophy of the neural retinal and choroid), retinoschisis (splitting of the neural retina), and macular holes (retinal defects in the macula, the region of the retina responsible for high-resolution vision) [6,8,9]. It is estimated that up to 70% of high myopes suffer from sight-threatening pathologies [10], and myopic macular degeneration is already the predominant cause of monocular blindness and third leading cause of bilateral blindness in Japan [11]. It is important to note, however, that all levels of myopia carry an increased risk of most of the above ocular pathologies [12]

The total economic burden of myopia is not only the result of the costs incurred by medical care and optical correction; with myopia affecting younger and younger children (allowing more time for the disease to progress to higher levels), it is inevitable that productive years over which individuals can contribute to society will progressively decrease. With an increasing number of people suffering from myopia globally and the age of onset becoming progressively lower, it is imperative that new methods of myopia control be developed and implemented.

The cause(s) of myopia remain unresolved. It was originally believed to have mostly genetic causes, with little influence from the environment [13]. However, early animal studies demonstrating that eye length could be altered through visual manipulation gave more weight to the role of the visual environment in myopia development [14]. Furthermore, recent epidemiological studies point to a protective effect of outdoor activities, and some (but not all) studies have reported a link between myopia and intense near work. Together, these results have shifted opinion towards myopia being a complex multifactorial disease, in which both predisposing genes and environmental influences play roles.

1.2 The myopic sclera

1.2.1 A brief overview of scleral structure

The sclera is the white outer shell of the eye. As alluded to above, it provides mechanical support to the delicate internal ocular neural and vascular tissues (retina and choroid respectively), and, when in a healthy state, it can resist significant mechanical forces from internal (intraocular pressure) and external (extraocular muscles) sources. Most vertebrates have a bilayered sclera, consisting of an inner cartilaginous layer and an outer fibrous collagenous layer. Interestingly, eutherian mammals (including primates) lack the cartilage component and have a fibrous-only sclera [15]. In most animals the thickness of the sclera is not uniform throughout the eye; in humans, it ranges from 1.00-1.36 mm at the posterior pole to 0.40-0.60 mm at the equator. It is covered on its external surface by two vascularized, fascial layers: the episclera and Tenon's capsule. The episclera is a transitional layer connecting the sclera with Tenon's capsule, which consists of a hypocellular layer of randomly arrayed collagen bundles that run parallel to the scleral surface. Tenon's capsule is firmly attached at the limbus, but becomes more loosely attached and thus slightly mobile about 3 mm posteriorly, probably merging with the connective dural sheath of the optic nerve and with the fibrous bands that connect the eyeball to the orbit. Furthermore, Tenon's capsule has been identified as an important site of attachment of pulleys for the extraocular muscles [16].

Due to its low turnover of both cells and matrix, the sclera has a low metabolic requirement and is largely avascular, deriving its nutrition from the episcleral and choroidal vessels. Any inflammatory

cells infiltrating the sclera are derived from these two sources and it is rare for new blood vessels to form within the sclera [16]. Most importantly in the context of this dissertation, the sclera's biochemical and biomechanical properties are responsible for maintaining the shape of the eye, and consequently are directly implicated in myopia development[17]. Myopic scleras are thinner and more extensible than healthy scleras, with a reduced extracellular matrix (ECM) content that reflects the decreased synthesis and increased degradation by resident scleral fibroblasts. Section 1.2.2 will discuss the biochemical changes described for myopic scleras, while section 1.2.3 will elaborate on how these biochemical changes affect the mechanical behavior of the tissue.

1.2.2 Scleral biochemistry and its changes with myopia

The sclera is a fibrous viscoelastic connective tissue in which a relatively sparse fibroblast population is enmeshed in an extracellular matrix comprised of collagen (50% dry weight, 80-90% of which is collagen I), proteoglycans, free glycosaminoglycans (GAGs), and a small amount of elastic fibers (elastin) [18,19]. The most abundant proteoglycans in human sclera are decorin, biglycan, and aggrecan[20], while the most predominant GAGs are dermatan sulphate, chondroitin sulphate, hyaluronic acid, and heparan sulphate, [21]. Proteoglycans consist of a core protein with attached GAG side chains, forming a bottle brush-like structure; they constitute approximately 0.7-0.9% of scleral dry weight and occupy the interfibrillar spaces of the scleral matrix. The GAG side chains impart a negative charge to the proteoglycans and are essential for tissue hydration and elasticity, for they sequester water within the scleral ECM [15,16]. They also play a key role in modulating the arrangement and assembly of collagen fibers [15]. For example, the proteoglycan decorin has been shown to increase the diameter of collagen fibrils *in vitro* [22].

The opaque nature of the sclera is a product both of the varying diameters of the collagen fibrils and of the anisometropic nature of the lamellae into which they are organized, causing light to scatter instead of entering the eye in an organized way (as is the case with the transparent cornea) [21]. Scleral collagen fibers and lamellae vary greatly in thickness and orientation, adjacent lamellae being rotated with respect to each other, with scleral fibroblasts sandwiched in between. Scleral collagen fibrils have also been shown to vary in diameter, from 25-300 nm [23].

Scleral fibroblasts maintain and remodel their native matrix through the secretion of a variety of enzymes, including matrix metalloproteases (MMPs) and their inhibitors – tissue inhibitors of metalloproteases (TIMPs). Mammalian scleral fibroblasts have been found to express mRNA for MMP-1, MMP-2, MMP-3, MMP-9, TIMP-1, and TIMP-2 [24,25] and genes for MMP 1-3, 7-17, 20, and 24 [26]. In healthy scleral tissue, matrix degradation is balanced by new matrix production. This balance is impaired in "diseases" such as myopia.

It is common to read in the literature that the sclera has a low cellularity compared to other tissues in the body, but few studies have endeavored to determine scleral fibroblast density. General estimates can be gleaned from molecular biology studies of scleral matrix composition, which often normalize data to DNA content. For example, a study measuring increased aggrecan content in chick scleras after a 5-day form deprivation treatment reported 42.5 and 23 μg of DNA in the anterior and posterior sections of the sclera, respectively [27]. Note, however, that these data relate to the bilayered avian sclera, and thus includes a population of scleral chondrocytes. Approximations can also be made by drawing parallels with the cellularity of the corneal stroma, which has been estimated at $818x10^3 \pm 186x10^3$ keratocytes per cornea [28]. Despite their presumably low number, scleral fibroblasts can exert influence over large areas of tissue due to their extended cytoplasmic extensions, through which they interact with adjacent cells and with the matrix [16].

Interactions between cells and matrix are largely mediated by integrins, a large family of transmembrane proteins composed of two main classes of subunits, termed α and β. The subunits α1-6, α9-11, αv, β1, β4, β5, and β8 have been identified in mammalian sclera [29]. Besides mediating cell-matrix attachments, integrins also act as powerful intermediaries in the cellular mechanotransduction pathway, through which they sense mechanical cues from the environment. Integrin expression is reduced during myopia development, thereby diminishing the extent of cell-matrix interaction and interfering with the cell's ability to respond to mechanical cues from the ECM. The myopic sclera also exhibits decreased levels of cytokines such as transforming growth factor - β (TGF-β) – which can upregulate collagen and proteoglycan synthesis by scleral fibroblasts [30] – and of adhesion-modulating glycoproteins such as fibronectin and laminin [31].

Fundamental to the eye size changes in myopia is the altered remodeling of the scleral ECM. Increased production of MMPs by scleral fibroblasts [32], coupled to decreased production of TIMPs, decreased proliferation of fibroblasts, and decreased ECM synthesis, results in a marked decrease in the total scleral ECM content, leading to thinning and mechanical weakening of the tissue [15,33–36]. Underlying the overall thinning of the myopic sclera are reductions in the sizes of the collagen fiber bundles and of the fibrils themselves. Being now mechanically weaker than normal, the myopic sclera is less able to withstand the normal stresses imparted by intraocular pressure and may stretch as a consequence [37].

1.2.3 Biomechanical changes in the myopic sclera

The mechanical properties of the sclera are highly dependent on the nature and arrangement of its collagen fibers. The architecture of healthy sclera – collagen crosslinked into fibrils, which in turn are arranged into lamellae that are anisotropically oriented throughout the sclera – is disturbed during myopia development, giving rise to abnormal mechanical properties [38].

Studies in animal models have provided the most insight into the scleral changes underling myopia. The scleras of myopic eyes exhibit a more pronounced creep response (higher elongation under constant load) compared to that of normal scleras, with this difference being especially pronounced at the posterior pole[39–41]. As noted above, this altered mechanical behavior has been linked to scleral thinning, which goes hand-in-hand with reductions in collagen I and GAG content, an increase in the percentage of small collagen fibrils in the scleral matrix, and disruption to the interwoven arrangement of collagen lamellae[15,41]. Based on studies in animal models, these changes appear to occur early in myopia development [42] and are reversible, if myopia-inducing treatments are terminated and eyes are allowed to undergo myopia recovery. During the recovery process, MMP activity decreases while TIMP activity, as well as proteoglycan and GAG synthesis increase [36,37]. Creep experiments in tree shrews have correlated myopia recovery with a reduction in scleral creep response [39]. However, in chicks these reversals in scleral biochemistry do not immediately translate into changes in scleral creep, as revealed by a study examining the creep response of myopic and recovering chick eyes[43]. These observations highlight not only the important role of the sclera in myopia development, but also the dynamic remodeling process exhibited by a tissue that was once believed to be simply an inert casing.

Taken together, all these factors paint a picture that can help us understand the chain of events behind the mechanical behavior of myopic sclera. Synthesis of matrix components such as proteoglycans and GAGs is influenced in part by the tension within the matrix, which is transmitted to the scleral fibroblasts through mechanosensors such as integrins. As a result of a yet to be fully understood myopia-generating signaling cascade, the expression of integrin subunits decreases[44],

diminishing the ability of scleral fibroblasts to respond to changes in eye wall stress. Resulting reductions in matrix production in conjunction with increases in matrix degradation due to higher MMP secretion ultimately lead to significant changes in tissue hydration and thickness.

1.3 Current strategies for myopia control

For the most part, management of myopia is limited to correcting the mismatch between the eye's optical power and its length through spectacles, contact lenses, or refractive surgery. These treatments can overcome the blur experienced by myopes, but they do not control myopia progression [45].

Currently there are few therapies for limiting myopia progression. Several optical therapies involving multifocal spectacle and contact lenses and orthokeratology (ortho-k) are currently under investigation [46–49]. Recent small scale contact lens trials have reported promising results and are now leading into larger clinical studies, with several myopia-control contact lenses already being marketed in Asia (Myovision™,Misight™). However, since myopia onset occurs in early childhood and control is most efficacious when started as early as possible, optical therapies such as contact lenses are not always practical. The remainder of this section will focus on pharmaceutical and surgical strategies for myopia control.

1.3.1 Pharmacological interventions

The only myopia control pharmaceutical agent in wide use is topical ophthalmic atropine, a non-selective cholinergic muscarinic antagonist. The majority of early studies of this drug employed a 1% solution that, while efficacious, had many ocular side-effects including photophobia, accommodation paralysis, pupil dilation, and corneal allergies. These side-effects still limit atropine's long-term use and have largely restricted its adoption to East Asian countries with high myopia prevalence [50]. More recently, lower doses have been tested to find an atropine concentration that can control myopia progression with fewer side-effects. A recent study in which Singaporean children were treated with 0.01% atropine demonstrated positive results [51], although questions still remain as to the long-term efficacy of this treatment and what would happen to myopia progression upon its termination.

A more selective muscarinic antagonist, pirenzepine, has also been tested for its myopia-control properties. Unlike atropine, which binds to all muscarinic cholinergic receptors (M1-M5), pirenzepine binds only to the M1 receptor subtype [52]. It was hoped that pirenzepine's narrower selectivity would decrease the ocular side-effects compared to those associated with atropine use. Although clinical trials in the US and Asia found a 50% decrease in myopia progression over 12 months, additional follow-up studies have not been conducted. Despite the lower side-effects associated with pirenzepine, one reason for the relatively low enthusiasm towards this drug is the required twice-daily administration, with inevitable implications in terms of treatment compliance [53].

A more novel pharmacological approach to myopia control has been the oral administration of 7-methylxanthine (7-MX), an adenosine receptor antagonist derived from caffeine. 7-MX was tested for safety in a 36-month study in Danish children in which a small myopia control effect was observed[54]; it is now approved for use at a higher dose in Denmark. 7-MX also continues to be tested in animal models in order to understand its mode of action. Experiments in form-deprived guinea pigs and rabbits found a significant reduction in myopia progression and concurrent

thickening of the posterior sclera, with an increase in median collagen fibril diameter [55,56]. Questions remain, however, as to the potential adverse effect of systemic 7-MX on other connective tissues.

1.3.2 Surgical interventions and use of biomaterials

There is only one surgical scleral-based myopia control procedure currently in clinical use: scleral buckling surgery, in which a scleral strip from a cadaver donor eye is used to encircle the ocular globe and brace the posterior pole [57,58]. This procedure has been largely restricted to cases of high myopia (typically after the development of staphylomas and/or central retinal complications), due to its invasive nature and requirement of general anesthesia. There are also no standardized surgical procedures for scleral buckling; different surgeons are known to vary their techniques with respect to graft placement, graft shape and size, and extent of tension exerted by the graft [59]. This lack of standardization might be responsible for the variable success rate reported for this therapy [58]. The long-term fates of such grafts also remain unknown [57].

Synthetic materials, as an alternative to cadaver sclera, have seen limited testing, although there is a strong need for research in this area since the increase in myopic population means that the supply of suitable donor tissue is threatened[60]. Strips of poly(2-hydroxyethyl methacrylate) (pHEMA) and injections of in situ polymerizing poly (vinyl-pyrrolidone) (PVP) have both been tested as scleral therapies in a chick myopia model [61]. After three weeks of treatment, the pHEMA implant was encased in a fibrous capsule and led to significant scleral thickening. Despite the potential mechanical support offered by the pHEMA strips, these implants did not impact ocular elongation. The injections of PVP formed a thin film over the scleral surface and caused a thickening of the cartilage layer. Once again, however, tissue thickening did not impact the rate of eye growth. In a follow-up study, myopic chicks received sub-Tenon's capsule injections of a more bioactive hydrogel that allowed for cell infiltration and matrix degradation[62]. The N-isopropylacrylamide (NIPAAm)-based semi-interpenetrating hydrogels were crosslinked with MMP-degradable crosslinkers and possessed binding sites for scleral fibroblasts. Extensive cell infiltration into the implanted hydrogels as well as scleral thickening was observed in the treated chicks, but there was no subsequent control of myopia progression. Though both these studies did not lead to hydrogel-mediated myopia control, they demonstrated that synthetic hydrogels could be implanted against the sclera for prolonged periods of time, and in fact were a starting point for the experiments described in this dissertation.

We can look to the treatment of retinal detachment for the most extensive exploration of biomaterial-based scleral buckles. In this context, buckles are used to indent the sclera to bring the choroid in closer contact with the retina [63]. Their use is not without complications; issues associated with buckle use include implant extrusion, chronic inflammation and irritation, changes to intraocular pressure, decreased eye motility, and susceptibility to infection [64]. Research in this area has been ongoing since the 1930s, and although its goal is not to strengthen the sclera, it can shed light on promising alternatives to cadaver sclera. Both degradable and non-degradable materials have been tested as buckles for retinal detachment. Early buckles were quite crude and made from polyethylene tubing. Sutures were placed into the tube's lumen and used to tension it against the sclera; the lumen was also used as a reservoir for antibiotics, in an attempt to ward off infections. However, polyethylene tube implants still caused infections and over time would erode the sclera and choroid. Non-degradable silicone buckles were more flexible than polyethylene and therefore less likely to chafe against the host tissue. In addition, they often became encased in a fibrous capsule, possibly adding to the buckle's ability to brace the eye wall. The stable capsule also made it easier for surgeons to remove the implant in cases where new surgeries were required. Unlike hydrogel-based buckles, which will be discussed shortly, those made out of silicone were less subject

to fragmentation. Unfortunately, patients that received silicone buckles were still likely to develop infections[63,65]. The last widespread innovation in this front was the introduction of hydrogel buckles in the 1980s. Hydrogels present several advantages such as low modulus, defined and controllable swelling, and potential to act as drug depots for antibiotics and anti-inflammatory drugs. Poly(glyceryl methacrylate) (PGMA), poly(2-hydroxyethyl acrylate) (PHEA), and poly(methylacrylate-co-2-hydroxyethyl acrylate) (MAI) have been tested as potential buckle materials[63,66]. Of these three materials, MAI, was the most successful due to its better post-swelling properties; unlike PGMA it retains good tensile strength, and unlike PHEA it has a lower tendency to fragment. MAI is still commercially available under the name MIRAgel[67]. Regretably, MIRAgel-treated patients must still contend with complications such as occasional fragmentation and foreign body giant cell granulomatous reactions[65].

Degradable materials tested as buckles include stabilized fibrin, absorbable gut, and collagen. Despite presenting a few advantages (ability to be impregnated with antibiotics and to be formed in a precise shape, resorption decreases chances of implant extrusion), these materials have not been widely pursued because of their tendency to trigger a constant low-grade inflammation, which can lead to vision complications such as vitreous haze and macular edema [63].

Dissertation approach and outline

The work described in this dissertation aims to control myopia progression through hydrogel-mediated scleral regeneration, thereby compensating for the loss of scleral ECM and preventing extreme eye elongation.

An injectable hyaluronic acid-based hydrogel has been investigated as an early-stage myopia intervention therapy, using a mammalian model for myopia. It is intended to serve as a scaffold for cell infiltration and matrix deposition, and thus as a mechanism for increasing the thickness of the sclera (particularly at the vulnerable posterior pole) and controlling eye elongation. This work could represent a significant step forward toward an early intervention, long-term myopia control therapy that could be safely administered to young patients. The injectable nature of the hydrogel confers an additional advantage to this therapy over scleral buckling, for it can be administered by intraorbital sub-Tenon's capsule injection, a significantly less invasive surgery.

This dissertation is organized into the three sections describing three distinct aims (Chapters 2, 3, and 4). A concluding chapter (Chapter 5) summarizes the dissertation's main findings and discusses potential future directions for the project.

- **Chapter 2: Establishment and characterization of a mammalian (guinea pig) myopia model,** in which animals from different suppliers were subjected to different myopia-inducing paradigms (form-deprivation and negative lenses of different powers). Through these experiments, we found a guinea pig population that does not become myopic, regardless of the "strength" of the stimulus. This phenomenon has never before been reported in the literature and points to genetic determination of susceptibility to myopia.

- **Chapter 3: *In vitro* development studies involving a range of hyaluronic acid-based hydrogels and biocompatibility studies using guinea pig scleral fibroblasts**. The proliferation and migration responses of isolated guinea pig scleral fibroblasts were examined in hyaluronic acid-based hydrogels of different moduli and concentrations of a cell-binding peptide, compatible with delivery by injection *in vivo*. A novel migration assay – consisting of

establishing a cell monolayer prior to submitting the cells to migration challenge – and an automated analysis script were developed as part of this aim.

- **Chapter 4: *In vivo* myopia control studies involving juvenile guinea pigs and injectable hyaluronic acid-based hydrogels.** Guinea pigs with low levels of myopia were treated with sub-Tenon's capsule injections of hydrogel or buffer (sham) as an early myopia control intervention. Myopia progression was monitored through A-scan ultrasonography and refraction measurements; ocular health was also assessed at the end of the 4-week experiment through tests of intraocular pressure, visual acuity, and retinal function. The implants and adjacent ocular tissues were examined histologically postmortem for evidence of resident cells in the implants and changes to native scleral structure.

Chapter 2: A tale of two guinea pigs - characterization of a guinea pig myopia model

2.1 Introduction

Experiments with animal models are one of the pillars of myopia research, and over the last 30-40 years they have helped shed light onto the mechanisms controlling emmetropization and refractive error development. Induction, control, and prevention of the disease in animals can answer key questions and provide important insight into the pathology of myopia. It was through animal studies that active emmetropization – the process by which the eye matches its length to the optical power of its refractive surfaces through adjustments to its growth – was first confirmed. The development of animal models of myopia started in the 1970s, when a serendipitous observation was made during a study of the monkey visual cortex: monkeys with monocularly sutured eyelids were found to have more elongated eyes [68]. These results, along with a parallel observation in chicks [69], opened up a new era of investigation involving myopia induction in chicks, primates, guinea pigs, and, more recently, mice. It is now well known that form-deprivation and negative lenses can lead to an acceleration of eye growth coupled to myopia, while positive lenses cause a decrease in growth rate and hyperopia. Additionally, visual manipulation in animals with severed optic nerves revealed the control of emmetropization to be chiefly retinal in origin, not central – that is, eyes can emmetropize without receiving input from the brain [70]. The fact that similar manipulation of visual experience in so many animals disrupts emmetropization suggests that it developed early in vertebrate evolution, to minimize refractive errors and increase the chances of survival [71]. The story of myopia animal models reflects advances in measurement technology (for example, the ability to measure minute changes in eye length has paved the way for the development of a mouse model) and illustrates the creativity of vision scientists.

Over the last few years, guinea pigs have emerged as an important myopia animal model, combining the advantages of mammalian eyes (e.g. fibrous-only sclera) with the ease of housing and husbandry not possible for other mammalian models such as primates and tree shrews. Despite the increasing number of labs adopting the guinea pig as their model, few groups have reported the wide variation in critical ocular characteristics that can occur between animals sourced from different populations. This chapter will describe experiments behind the establishment of a guinea pig myopia model at our lab, through which we discovered that guinea pig populations respond idiosyncratically to myopia-inducing stimuli.

2.2 Animal models in myopia research – a brief review

An ideal animal model of disease should exhibit similarity to the human disease phenotype, close resemblance to human anatomy and physiology, as well as genetic similarity between individuals of the same species. From a practical perspective, easy husbandry and the ability to gather data from large sample sizes with a reasonable expense of time and money are relevant. Naturally, no single animal embodies all these characteristics, but instead each species embodies different aspects of the "ideal model".

Unexpected and unorthodox animals have been explored as myopia models. Examples include the pigeon [72], kestrel [73], squirrel [74], some kinds of fish [75,76], and the squid [77]. Some animals have been mostly abandoned as myopia models, such as the cat [78–80] – once a common model for visual development and one of the earliest animals tested as a myopia model – and the rabbit[81,82]. The more long-lived myopia models still in use today are the tree shrew, chicken, and monkey (rhesus and marmoset). The remainder of this section will briefly summarize the animal models most heavily used by current research groups, highlight their advantages and disadvantages, and finish with the rationale for our choice of the guinea pig for the myopia-control studies detailed in Chapter 4. Key advantages and disadvantages of the models discussed are also summarized in Table 2.1.

Table 2.1. Summary of the current, most widely used animal myopia models discussed in this chapter, with the advantages and disadvantages of each. * number of related publications as of May 2014.

Animal model (*Number of papers/abstracts published**)	**Advantages**	**Disadvantages**
Rhesus macaques *(85)*	As primates, most closely emulate human eye anatomy, physiology, and features of myopic eyes	- Slow maturation - Difficult and expensive to acquire & maintain - Require relatively long treatment periods to elicit significant eye length changes - Variability in response to myopia-inducing stimuli compared to other models
Marmosets *(28)*	All the advantage of primate model, but with faster development and more frequent breeding in captivity	Difficult and expensive to acquire & maintain
Chickens *(1,079)*	- Rapid response to form deprivation and compensation a wide range of defocusing lens powers - Rapid development - Readily available; ability to obtain large sample sizes in relatively short time	- Large choroidal contribution to defocus responses makes it difficult to draw clear parallels to mammalian models - Bilayered sclera, with an inner cartilage layer that contributes significantly to tissue rigidity and influences its overall mechanical response - Accommodation involves corneal as well as lenticular component, ruling it out use for testing contact lenses as an anti-myopia treatment
Tree shrews *(100)*	- Consistent response to negative defocus and form deprivation - Many features of its ocular development are similar to humans	- Difficult to handle due to territoriality, aggressive behavior, and high susceptibility to social stress - Difficult and expensive to acquire & maintain - Variable response to positive defocusing lenses
Mice *(65)*	- Genetic manipulation feasible - Readily available - Ability to generate large sample sizes quickly	- Nocturnal and not highly dependent on vision, leading to questions about precision of emmetropization - Small eyes demand highly precise axial length measurements using specialized advanced technology
Guinea pigs *(178)*	- Precocial species; born with open eyes and well developed vision - Mammalian ocular structure and physiology - Gentle temperament	- Lower visual acuity than humans, monkeys, and chicks - Response to myopia-inducing stimuli can be colony-dependent

2.2.1 Common animal models of myopia

2.2.1.1 Monkeys

The earliest studies of eye growth manipulation were performed on rhesus macaques, which were found to become myopic when raised with nearwork-restricted visual stimuli [83]. More systematic studies in which the lids of young monkeys were purposefully sutured shut to study refractive error regulation revealed that depriving eyes of form vision is a reliable method for inducing myopia in young animals. This method is commonly referred to as form deprivation myopia [14]. This somewhat primitive system of form deprivation was later replaced by translucent diffusers, which, along with defocusing lenses, remain the most common tool for manipulating eye growth. Form deprivation myopia has also been associated with human ocular disorders that prevent clear vision, such as congenital cataracts, eyelid ptosis, or keratitis [84]. For lens-induced myopia, which makes use of negative lenses, a parallel has been drawn with lags of accommodation as experienced during reading; in both cases, the ocular plane of focus lies behind the retina (hyperopic defocus). More recently, attention has also been drawn to influences of ocular shape in retinal defocus, specifically to the possibility that hyperopic defocus experienced by the retinal periphery of prolate eyes may represent a stimulus for myopia.

Studies in rhesus macaques have contributed to our understanding of key issues in the myopia field, including the respective roles of the fovea and peripheral retina in emmetropization [85–87], potential protective role of bright light in combating myopia development [88,89], and time-course of myopia recovery upon termination of myopia-inducing stimuli [90,91].

Marmosets are New World primates that have been used as an alternative primate model to macaques due to their significantly smaller size, rapid development, and ready ability to breed in captivity [92]. They respond consistently to both myopia-inducing paradigms [93,94], and have been a used to study issues such as the relationship between animal age and ability to respond to myopia-inducing stimuli [95,96] and the relationship between accommodation and myopia development [94,97]. Experiments examining the sclera of myopic marmosets have also confirmed the reduction in extracellular matrix synthesis previously reported in chicks [36,93].

The greatest advantage of monkeys as a model for myopia is their close resemblance to humans in terms of their ocular optics, accommodation mechanism, binocular vision, color vision, acuity, and visual development [71]. The evolutionary distance between humans and other myopia models still represents the greatest disadvantage of models such as chicks and guinea pigs. Unfortunately, it is not straightforward to obtain young monkeys in sufficient numbers to ensure statistical significance, and the costs of keeping animals for prolonged periods of time can be prohibitive for smaller research groups. Marmosets also present these difficulties; even though they can be bred more easily in captivity, they tend to have small litters (rarely more than 1 infant). An additional concern is the fact that there is a large variation in the responses of individual animals to both form deprivation[98] and defocusing lenses [99].

2.2.1.2 Chicks

The 1978 finding that the vision of young chicks could be manipulated to produce myopia [69] could be considered one of the most significant advances in the field of myopia research. Chicks remain the most common myopia research model and are typically the first animal in which new discoveries are made. Among their greatest advantages are the facts that they are highly visual (highest acuity of

non-primate models for myopia), easy to obtain and house, mature quickly, and can be raised in large numbers, thus ensuring faster research progress. Chicks respond to form-deprivation by rapidly becoming myopic [100]. They were the first model tested with optical defocusing lenses, with the surprising discovery that their eyes can compensate bidirectionally to a wide range of optical defocus imposed with positive and negative lenses ^{101–103}. Chick responses to myopia-inducing stimuli are remarkably reliable if the experimental conditions are properly controlled, with anatomical changes easily detected within minutes of visual manipulation [104].

Unfortunately, chick models also present a number of disadvantages as models for human myopia: they accommodate through both corneal and lenticular mechanisms [105,106] and possess a bilayered sclera (with an inner cartilage layer imparting significant rigidity to the tissue). The two scleral layers respond differently during myopia development, with the fibrous layer thinning (as in humans) and the cartilaginous layer thickening [27]. Also unlike humans, chick eyes are laterally placed (as opposed to front-facing). On the other hand, this has the merit of being coupled to independent ocular control, allowing monocular manipulation with effects largely confined to the treated eye and causing minimal behavioral disruption. Perhaps the most significant difference between the chick and other animal models is the dramatic modulation in choroidal thickness seen during active emmetropization. In chicks, a well-developed network of choroidal lymphatic vessels allows for large and rapid changes in choroidal thickness. Such variations typically precede those in the sclera; upon imposed optical defocus, they serve to move the retina forward (with positive lenses) or backward (with negative lenses) towards the altered focal plane [107]. This discovery of defocus-driven changes in choroidal thickness in chicks lead to related investigations in other animal models. Similar responses, albeit on much smaller scales, have now been confirmed in mammalian and primate animal models [108,109]. A recent study found this phenomenon to also occur in humans [110].

Despite the differences discussed above, many of the results from chick studies have been successfully translated to mammalian models [71]. In fact, some anatomical differences have been the source of important discoveries. For example, atropine – a non-selective cholinergic muscarinic receptor antagonist that remains the only drug in clinical use for myopia control – was initially thought to act via receptors on the ciliary muscle, at a time when overuse of accommodation tied to excessive nearwork was still believed to be the main culprit in myopia development. Myopia control experiments in chicks found that atropine was effective in controlling eye elongation, despite the fact that chick ciliary muscle does not possess muscarinic receptors for atropine, having nicotinic receptors instead[111,112]. Atropine's ability to control myopia progression in chicks – despite its inability to block accommodation – eliminated the accommodation pathway as the mode-of-action for this drug, and opened the door to wider exploration of anti-myopia drug targets.

2.2.1.3 Tree shrews

Tree shrews are small, non-rodent, primate-like animals native to the tropical forests of southeast Asia[113]. They exhibit diurnal behavior and have a cone-dominated retina, fibrous-only scleras, mature significantly more quickly than monkeys, and have a relatively short gestation period (43 days)[71,114]. Their ocular development and structures are quite similar to humans, despite their somewhat fatter lens and thus larger lens thickness-to-axial length ratio[115]. Tree shrew eyes respond to both form deprivation and defocusing lenses, though their response to positive lenses is limited [116]. Ocular changes can be detected less than two days after initiation of myopia-inducing stimuli[39] and proceed reliably in a manner similar to human myopia, with vitreous chamber elongation and scleral thinning[115,117–119].

Tree shrews have been used as a model for a large number of studies, especially those investigating molecular signaling pathways[33,120–124] and optical therapies for myopia control in mammals[116,125,126]. Our understanding of myopia-induced changes in the mammalian sclera owes much to the contributions from tree shrew studies, which have explored the effect of myopia on scleral biochemistry and biomechanics[24,30,35,40,42,127–132].

The main disadvantages of the tree shrew as an animal model are its high maintenance requirements and low availability, for Thailand ceased all tree shrew exports in 1980 and establishment of new colonies depends on donations from existing research groups[133].

2.2.1.4 Mice

The greatest limitation of the animal models described so far is the difficulty they pose to researchers aiming to probe the genes associated with myopia development. For decades, myopia research lagged behind other scientific fields due to its inability to generate reliable genetic disease models. The interactions of genes and environment appear so thoroughly intertwined in myopia development, at least from a human epidemiological standpoint, that it has been difficult to separate the relative contributions of each factor. The generation of the mouse myopia model allows for a closer examination of the role of 'susceptibility' genes identified in large human population studies and could make it easier to tease apart the contribution of genes and environment to myopia development.

The mouse is the most recently developed myopia model and offers several advantages, including a completely sequenced genome that can be probed to understand complex signaling pathways, the ability to manipulate genes and environment in the same animal, as well as a short gestation and large litter size that together allow the testing of large sample sizes in a short time period [134]. On the negative side, mice have extremely small eyes, are nocturnal with a rod-dominated retina, and have very poor visual acuity – 0.4 cycles/degree [135]. The small size of mice eyes makes measurements of refractive error and axial length quite difficult, as the axial elongation-to-diopter of myopia ratio is below the tolerance of most A-scan ultrasonography setups: 5.4-6.5 μm per 1 D myopic shift [136]. For this reason, researchers have had to resort to more advanced technologies for measuring ocular dimensions, e.g., low or partial coherence interferometry [137,138], laser micrometry [139], or Magnetic Resonance Imaging [140]. Refractive error measurements have also proved challenging; while most published studies have used an automated infrared photorefractor, there is significant variation in refraction reported by various research groups around the world, despite similarities in the ages and strains of animals used [134].

These shortcomings notwithstanding, mice have been avidly adopted into the myopia community and have been shown to respond appropriately to both form-deprivation [141] and negative lenses (imposed hyperopic defocus) [142]. Debate remains over whether lens-induced changes represent responses to defocus as opposed to form-deprivation, due to the large depth-of-focus of the mouse eye relative to the imposed defocus. A close look at the results of mice myopia studies reveals another intriguing fact: a wide inter-animal variation in eye elongation and refractive development, as characterizes most other animal models, despite the fact that mice are the only model in which controlled genetic lines can be produced.

2.2.1.5 Guinea pigs

Myopia experiments with guinea pigs first date to 1995, to a study in which guinea pigs were found to compensate more to imposed hyperopic than to myopic defocus[143]. They have since become an increasingly popular myopia model, combining the advantages of mammalian models (fibrous-only sclera, phylogenically closer to humans than chicks), with the small size and ease of handling/housing of chickens. Their eyes are significantly larger than those of mice, making it possible to detect changes in optical dimensions using the high frequency ultrasonography systems available to most myopia research groups. Unlike monkeys and tree shrews, guinea pigs are precocial animals (born with open eyes and well developed vision) [144], and as such can be enrolled into myopia studies just a few days after birth. Guinea pigs are easier to handle than tree shrews, which are notoriously aggressive, territorial, and susceptible to handling stress. They are also (theoretically) easier to obtain than rhesus monkeys, marmosets, and tree shrews, although, as reported in this chapter, the animal source needs to be considered carefully since not all guinea pig populations are susceptible to myopia-inducing stimuli. Guinea pig visual acuity is approximately 1.0 cycles/degree, making it significantly higher than that of mice, although substantially lower than that of chicks (6.0-8.6 cycles/degree) [145,146].

Since their introduction as an animal model, the process of emmetropization of guinea pigs has been well characterized[147,148]. Their ability to respond to form deprivation[108] has also been studied, as has their response to both positive and negative lenses, which occurs in a dose-response manner[149]. Guinea pigs have now been used as an animal model in a wide range of studies; some examples are summarized in Table 2.2.

Table 2.2. Examples of studies that employ the guinea pig as an animal model of myopia

Reference number	Study topic
150	Eye shape development
151	Effect of albinism on myopia development
152,153	*In vitro* and *ex vivo* assessment of fibroblast mechanical properties after myopia development
154	Myopia control through multifocal dual-powered lenses
55,155,156	Myopia control through pharmacological agents
157	Role of temporal and spatial stimuli in emmetropization
158–161	Role of chromatic aberration on myopia development
162	Role of flicker on myopia development
163	Effects of visual integration of hyperopic stimuli
155,156,164–174	Myopia-related signaling in the retina
165,169,173,174,177,178	Myopia-related signaling in the choroid
161,165,169,173,179,180	Myopia-related signaling in the sclera

In the course of our initial work to establish a guinea pig myopia model in our laboratory, we found that animals from different approved sources responded differently to myopia-inducing stimuli, one population proving to be completely nonresponsive to them. As alluded to above, large inter-animal variability in responses have been reported previously in rhesus macaques, although colony-specific differences have not. In the study described in this chapter, we systematically compared the responses of two pigmented guinea pig populations to negative lenses and form deprivation myopia-inducing paradigms.

2.3 Materials and methods

2.3.1 Animals

Two different lines of pigmented guinea pigs were used in this study, obtained from Elm Hill Labs (Chelmsford, MA) and University of Auckland, New Zealand.

Elm Hill line: Pregnant pigmented English Short Hair guinea pigs were purchased at the 2nd week of pregnancy and housed alone until they gave birth.

New Zealand line: Male and female pigmented guinea pigs were generously provided by Prof. John Phillips (University of Auckland, NZ) and housed in pairs, in oval-shaped breeding tubs; their offspring were used in this study.

For both populations, pups were weaned at 5 days of age and housed as single sex pairs in transparent plastic wire-top cages, in a room with 12h/12h light/dark cycle. Cages measured 16 inches wide by 20 inches long and had a layer of low-dust aspen shavings as bedding. The animals had free access to water and vitamin C-supplemented food, and received fresh fruit and vegetables three times a week as diet enrichment. All animal care and treatments in this study conformed to the ARVO Statement for the Use of Animals in Ophthalmic and Vision Research. Experimental protocols were approved by the Animal Care and Use Committee of the University of California, Berkeley.

2.3.2 Lenses and diffusers

The lens/diffuser manufacture and attachment protocols were adapted from those implemented in chicks [103]. All treatments were monocular, the untreated contralateral eye serving as a control (Figure 2.1).

Figure 2.1. Guinea pig fitted with a diffuser on its left eye, the right eye serves as an untreated contralateral control.

Lenses and diffusers were mounted on Velcro ring supports, made by punching a 1.8 cm central hole through a 3.5 cm circular hook Velcro® disc (part # 192346, Velcro Industries). The lenses were custom-made from polymethylmethacrylate (Valley Contax), with a back optic radius of 8 mm and overall diameter of 17 mm. They were glued onto the hook Velcro® supports along with a 2 cm-diameter plastic washer (to impart rigidity) (Seastrom Manufacturing) using UV-curing glue (Norland Optical Adhesion 68, Part # 6801, Norland Products). A similar method was used to manufacture the diffusers, which were made from sheets of white styrene (Midwest Products Co, Part # 701-01), hot-molded into semi-circular domes and attached to Velcro® supports as described

for the lenses. Before fitting the diffusers, their transmittance was measured using a light meter (ILT1700, International Light Technologies). Only diffusers with transmittance of 15±1% were used for the study. To attach the lenses/diffusers to the guinea pigs, rings of loop Velcro were first prepared from discs using a 1.8 cm punch; four 1/8 sections of the circles were symmetrically affixed to the fur surrounding one of the guinea pig's eyes using a small amount of gel cyanoacrylate glue (SureHold® Plastic Surgery) [108]. Lenses/diffusers were fitted when the guinea pigs were 7 (New Zealand population) or 10 (Elm Hill population) days old and worn for 28 days. Animals were monitored hourly during the 12-hour light cycle to ensure that the lenses/diffusers remained in place. Lenses were cleaned 1-2 times daily; diffusers were cleaned as necessary.

2.3.3 Measurements

Both refractive error and axial ocular dimensional data were collected over the experimental period. Refractive errors were measured immediately before the initiation of treatments (baseline), as well as at the end of weeks 2 and 4 of the experiment. Cycloplegic refractions were measured using streak retinoscopy on awake animals, 30 minutes after instillation of 1% cyclopentolate hydrochloride (Bausch & Lomb). Refractive errors are reported as Spherical Equivalent Refractions (average of the results for the two principal meridians).

Axial length measurements were made more regularly, twice a week, over the 28-day duration of the experiment. Axial ocular dimension data were obtained with a high frequency A-scan ultrasonography custom-built system comprising a Panametrics ultrasound probe (P725-025-SU-R100) driven by a Panametrics amplifier (5072PR). For this procedure, animals were first placed under gaseous anesthesia (2.5-3% isoflurane in oxygen), with eyelid retractors inserted to hold eyes open during measurement [183]. Each measurement comprised an average of at least 7 recordings. Measurements on individual animals were conducted at the same time of day to prevent any possible confounding effects of circadian rhythms of eye growth [184]. The ultrasonography measurement system has a resolution of 10 μm and outputs peaks for the cornea, front of the lens, back of the lens, vitreous/retina interface, retina/choroid interface, choroid/sclera interface, and back of the sclera. Axial length was calculated by adding the axial dimensions of the anterior chamber, lens, and vitreous chamber.

Because early results with the Elm Hill animals indicated an apparent lack of sensitivity to myopia-inducing stimuli, the decision was made to measure their visual acuity to rule out a related abnormality. Visual acuity was therefore measured on all animals on experimental day 28 (end of the treatment), using an OptoMotry device (Cerebral Mechanics). The instrument takes advantage of optokinetic responses; specifically, moving/revolving stimuli elicit involuntary ocular and/or head and body movements. The device allows presentation of drifting sine wave grating stimuli of varying frequency and contrast in a virtual cylinder, with the direction of motion reversed at regular intervals. Guinea pigs were tested using 100% contrast stimuli and a drift speed of 12 degrees/second. Testing made use of a staircase method, with each spatial frequency being tested five times. In the case of the guinea pig, which has minimal capacity for eye and head movements, body movement was tracked as evidence of resolution.

2.3.4 Experimental treatments

Elm Hill guinea pigs were subjected to both form deprivation and optical defocus treatments. At 10 days of age, the guinea pigs were fitted either with -10 D (n=6), -5 D (n=5), 0 D (n=4) lenses, or with diffusers (n=9). All animals underwent all measurements as described above.

The New Zealand guinea pigs were subjects to diffuser treatments only. At 7 days of age, the guinea pigs were fitted with diffusers (n=9). All animals underwent all measurements described above.

2.3.5 Statistical analyses and data representation

Statistical analyses were performed with Graphpad Prism 6. Much of the data are reported as interocular differences (treated eye minus control eye) or changes in the interocular differences over the 28-day treatment. For both groups of animals, the differences between diffuser-treated and contralateral control (fellow) eyes were determined for all measured parameters and subsequently analyzed using a Wilcoxon Matched Pairs Test. To assess the responses of the Elm Hill animals to the different treatments (3 different lenses and diffusers), interocular differences (treated eye minus control eye) were compared using a Kruskal-Wallis test, with Dunn's multiple comparisons post-hoc test. To compare the responses to form deprivation (diffusers) of the Elm Hill and New Zealand lines, interocular differences (treated eye minus control eye) were compared using a Mann-Whitney test. Data are also graphically represented as box-and-whisker plots, with the middle line indicating the median value of the data set, the box encompassing the 25^{th}-75^{th} percentiles, and the whiskers reaching the minimum and maximum data values. Whenever data are explicitly written in the text, they are written as mean ± standard deviation (SD).

2.4 Results

2.4.1 Elm Hill guinea pigs treated with negative lenses and diffusers

2.4.1.1 Refraction and axial length changes

The Elm Hill guinea pig population did not become myopic, either when exposed to negative lenses or form deprivation treatments. Figure 2.2 shows axial length (2.2A and 2.2B) and refractive error (2.2C and 2.2D) data from this experiment.

For animals fitted with lenses, including the highest power (-10 D) lens, interocular differences in axial length were minimal, as were interocular differences in refractive error. Likewise, form deprivation failed to significantly enhance ocular elongation or induce a myopic shift in the refractive error of treated eyes. Interestingly, the form deprivation group exhibited slightly greater elongation of both their treated and fellow control eyes compared to the changes in the lens-treated groups. A seasonal variation of eye growth and slightly larger animal size seems the most parsimonious explanation for this intergroup difference, given that the untreated as well as treated eyes showed similar trends. While the form deprivation experiments were carried out at different times, animals were tested during the summer months only, three animals being treated in June/July 2010, and the remaining six being treated in June 2013. In contrast, the lens treatment experiments were performed between February 2010 and December 2011. Animals in the form deprivation group recorded a higher weight increase than those in the lens treatment groups, with this difference being of borderline statistical significance (Form deprivation group: 284.00 ± 36.90g, All lens groups: 246.70 ± 50.00 g. $p = 0.051$, Mann-Whitney test).

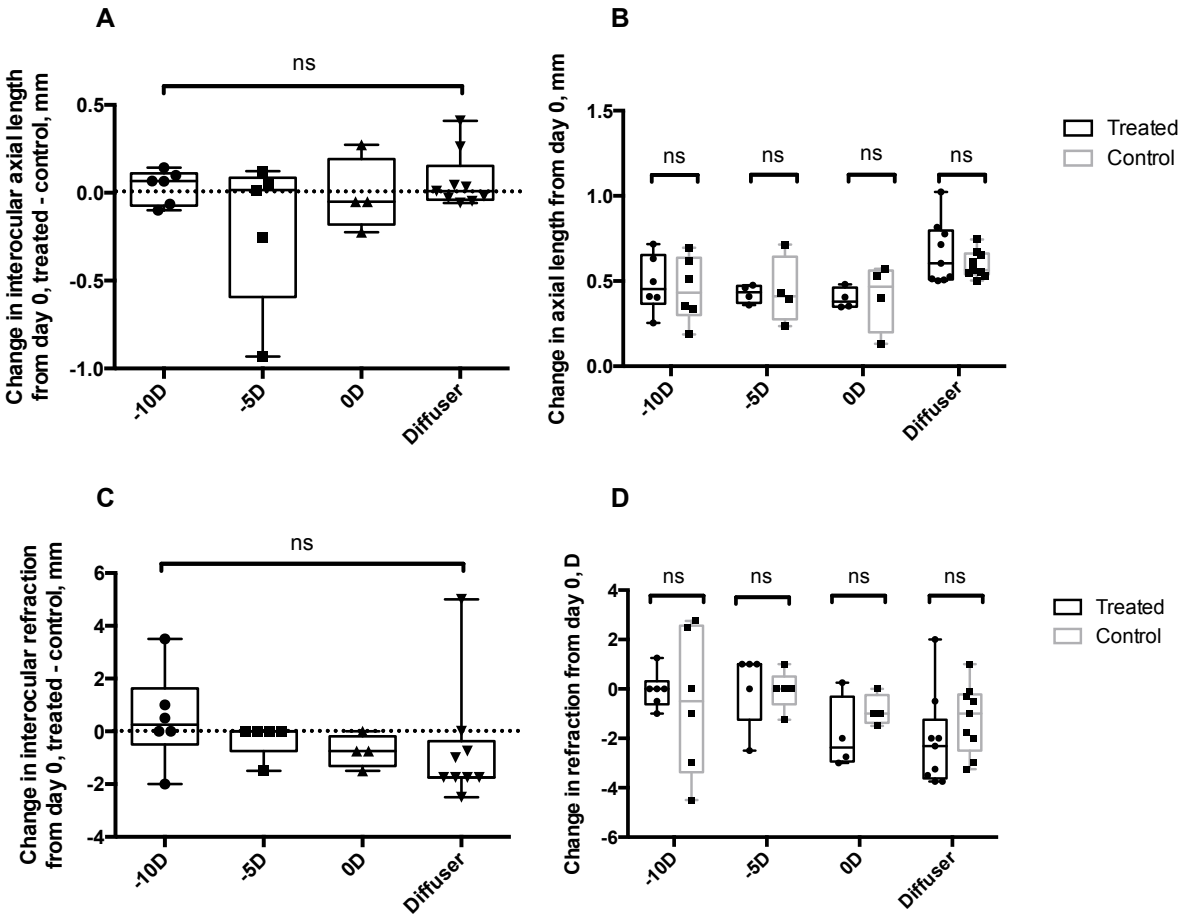

Figure 2.2. Axial length (A and B) and refraction (C and D) data for Elm Hill guinea pigs after 28 days of negative lens or diffuser treatment. A and C depict total change in interocular differences (treated minus control) of guinea pigs treated with -10, -5, and 0 D lenses and diffusers; data for individual animals also shown, with a dotted line at zero, the value at which the change in the treated eye is equal to the change in the control eye. Values above this line indicate that the treated eyes were more elongated (A) and more hyperopic (C) than contralateral controls (none of the inter-group differences significant, Kruskal-Wallis test). B and D depict changes in treated (black bars) and control (gray bars) eyes (differences between matching treated and fellow eye pairs not significant, Wilcoxon test).

In relation to refractive errors, for both the -10 D and the -5 D lens groups the changes in treated eyes were similar to those of control eyes and not significantly different (-0.04±0.75 D in treated eye, vs. -0.54±2.91 D in fellow eye for -10 D lens, and 0.10±1.52 D in treated eye, vs. -0.05±0.80 D in fellow eye for -5 D lens; Wilcoxon test). The mean refractive errors for the treated eyes of both the 0 D lens and diffuser groups were slightly myopic relative to those of their controls (-1.87±1.48 D in treated eye, vs. -0.87±0.63 D in fellow eye for 0 D lens; -2.12±1.88 D in treated eye, vs. -1.22±1.40 D in fellow eye for diffuser), although here again, the differences were not statistically significant (Wilcoxon test). Nonetheless, for the Diffuser and 0 D groups, most guinea pigs had negative refractions in their treated eyes (seven out of nine and three out of four, respectively). In comparison, for the -10 D and -5 D groups, only one out of six and one out of five animals respectively had negative refractions in their treated eyes at day 28.

The results for axial length changes were in agreement with the refractive error data, with none of the groups showing significantly increased elongation of their treated eyes relative to their contralateral controls. For the -10 D lens and Diffuser groups the mean value was consistent with treated eyes being marginally longer than contralateral controls (by 0.03±0.1 mm in the -10 D lens group and 0.07±0.16 mm in the diffuser group), albeit not significantly so. On the other hand, the treated eyes in the -5 D group were, on average, *shorter* than their controls, despite exposure to myopigenic stimuli (interocular difference of -0.20±0.43 mm). The mean for the 0 D group was approximately zero (-0.01±0.21 mm). Five out of the nine animals in the Diffuser group had a longer treated eye compared to the control eye. For the lens-treated guinea pigs, both the -10 D and -5 D groups had a relatively high proportion of longer treated eyes, four out of six and three out of five, respectively. In the 0 D group, only one out of the four animals had a longer treated eye.

Temporal changes in interocular axial length and interocular refraction over the experimental period are reported in Figure 2.3. Notice that there was a temporary shortening of the treated eye in both the -5 D and -10 D lens groups (at days 3 and 7, respectively), but this trend is followed by a swift "recovery" that brings the treated eye back to a length similar to that of controls. For the -5 D and -10 D lens groups, treated eyes showed a relative myopic shift at day 14, but by day 28 these interocular differences had disappeared. The other two groups (0 D lens and Diffuser) did not undergo such oscillations in refractive error, instead changing slowly over the course of the experiment to reach the low levels of relative myopia described above.

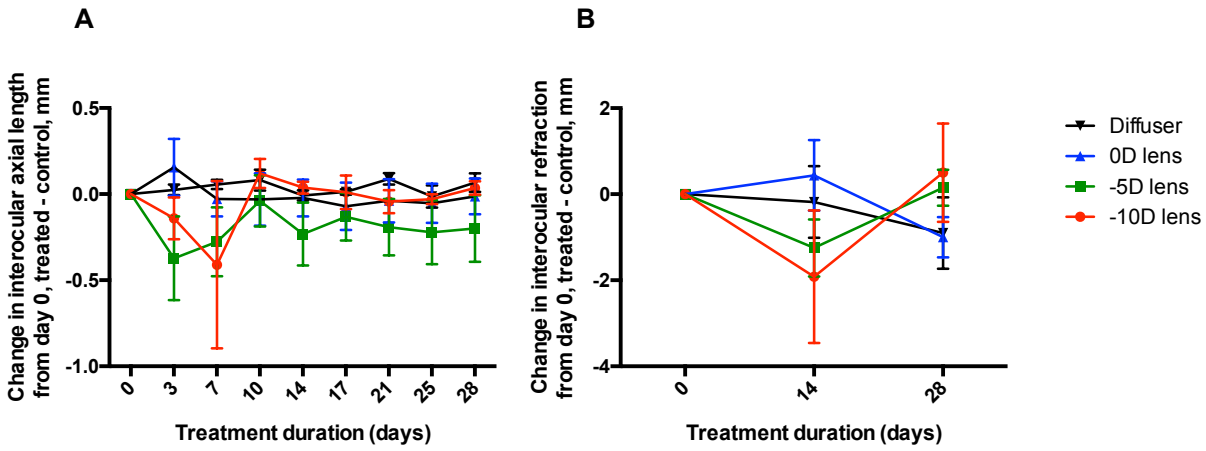

Figure 2.3. Longitudinal changes (mean ± SEM) over the experimental period in interocular axial length (A) and refraction (B) for Elm Hill guinea pigs treated with -10 D, -5 D, 0 D lenses and diffusers.

To further examine the treatment effects, interocular differences in axial length and refractive error at the beginning and end of the 28-day experiment are plotted against each other in Figure 2.4. No strong trends were evident, reflecting the lack of any definitive treatment effect and the inter-animal variability. Prior to treatment (at baseline; Fig. 2.4A), the treated eyes of guinea pigs in the Diffuser and 0 D lens group trended slightly towards hyperopia, while those in the -5 D lens group trended towards myopia. For the -10 D lens group, axial lengths of treated eyes were initially slightly shorter than their fellows, although no differences in refractive error were documented (Fig. 2.4A). After 28 days of treatment with negative lenses or diffusers, the interocular differences in axial length of all groups were centered near zero, while the matching interocular differences in refractive errors were

more widely distributed, being centered around low myopia for the 0 D lens, -5 D lens, and Diffuser groups. Thus these analyses further confirm the lack of axial myopia in treated eyes, despite the presence of myopia-inducing stimuli.

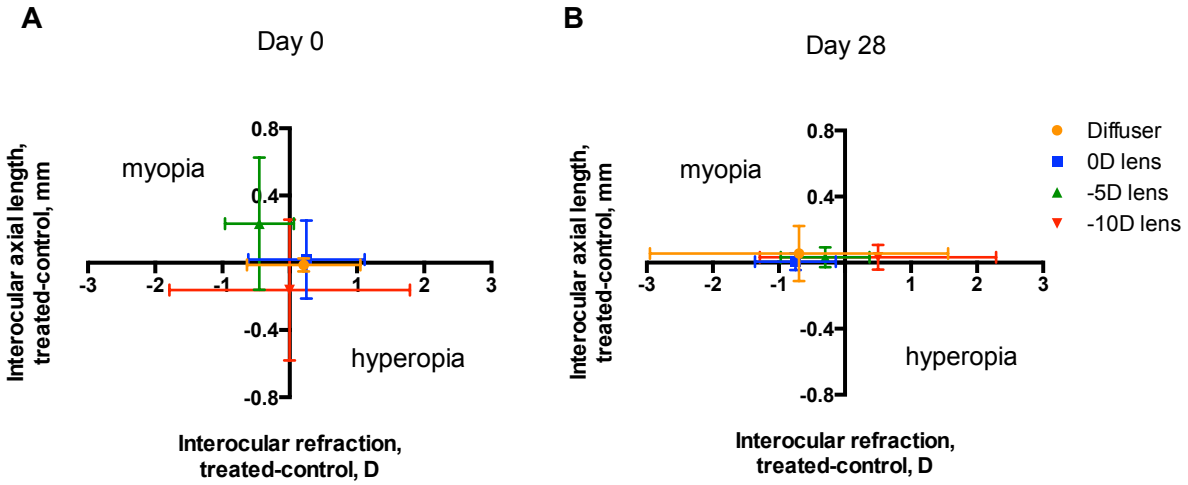

Figure 2.4. Interocular axial length plotted against interocular refractive differences at baseline (day 0, A) and at day 28 (B). Points in the upper left quadrant would indicate axial myopia (treated eyes are longer and have more negative refractions than control eyes), while points in the lower right quadrant would indicate axial hyperopia (treated eyes are shorter and have more positive refractions than control eyes).

As mentioned earlier, axial length is calculated by combining the axial dimensions of the anterior chamber, lens, and vitreous chamber. Figure 2.5 presents the change in interocular differences over the treatment period for each of these components. Once again, no significant differences were found between the groups for any of the three measured components. For all treatment groups, treated eyes had relatively longer anterior chamber depths compared to their contralateral control eyes, although for the lens-treated groups the changes were not lens power-dependent. The crystalline lenses of treated eyes in the Diffuser group were slightly thicker than controls (mean interocular difference 0.05±0.06 mm), and this was also the only group to record a significant difference between treated and control eyes. Intriguingly, all lens-treated guinea pigs showed the opposite trends, i.e., treated eyes had thinner lenses, although as mentioned previously the changes never reached statistical significance.

Enhanced eye elongation in response to myopia-inducing stimuli typically reflects changes in vitreous chamber dimensions. That is, axial length and vitreous chamber depth (VCD) changes are generally tightly correlated. As shown in Figure 2.5C, the change in interocular VCD for the Diffuser group had a very narrow distribution centering slightly below zero (mean: -0.02±0.05 mm). The mean value for the -5 D lens group was also negative, but with a wider distribution (-0.20±0.37 mm). In contrast, the mean for the -10 D lens group was positive (0.04±0.10 mm), while the value for the 0 D lens group was approximately zero (0.01±0.26 mm), with relatively large distributions in both cases. None of these treatment effects proved to be statistically significant, nor were any of the intergroup differences. There were only limited parallels between the VCD and axial length data, reflecting the minimal treatment effects; mean changes in interocular differences were negative for both parameters for the -5 D lens group and positive for the -10 D lens group.

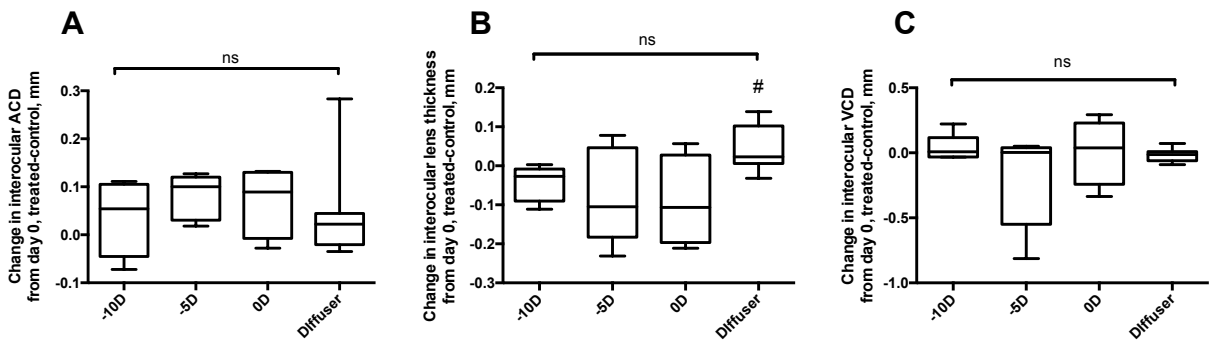

Figure 2.5. Change in interocular differences in anterior chamber depth (ACD) (A), lens thickness (B), and vitreous chamber depth (VCD) (C) for Elm Hill guinea pigs after 28 days of negative lens or diffuser treatment. None of the inter-group differences are significant (Kruskal-Wallis test). Differences between the treated and control eyes (Wilcoxon test) were also not significant for any parameter-group combination, except for lens thickness in the Diffuser-treated group. # indicates $p<0.05$.

The relationship (or lack thereof) between changes in axial length and vitreous chamber depth are shown graphically in Figure 2.6. Points in the upper right quadrant of the graph correspond to treatment-induced increases in axial length resulting from increases in vitreous chamber depth. However, only the -10 D lens group shows such a relationship between these two parameters. For the Diffuser group, the slight elongation in axial length cannot be attributed to vitreous chamber depth elongation. Rather, it is likely due to thickening of the lens, as shown in Figure 2.5B. On the other hand, the mean for the -5 D lens group is located in the lower left quadrant, implying that the relative shortening of the vitreous chambers of treated eyes underlies the previously described relative axial length shortening for this group. Nonetheless, the large standard deviation associated with latter data cannot be ignored, weakening the strength of any arguments made in relation to these data. For the 0 D lens group there was minimal change in either metric, as expected.

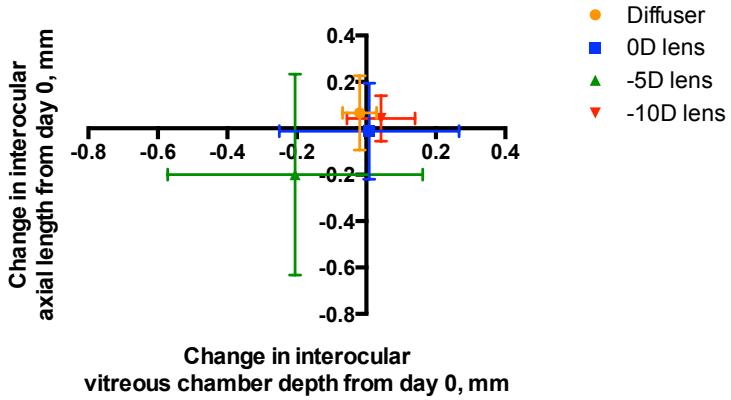

Figure 2.6. Change in interocular axial length (y-axis) plotted against change in interocular vitreous chamber depth (x-axis) after 28 days of treatment in Elm Hill guinea pigs treated with negative lenses or diffusers.

Lastly, we looked for possible treatment-induced changes in the interocular thicknesses of the retina, choroid, and sclera (Figure 2.7). No significant differences were found in the total change in choroidal and scleral thicknesses for any treatment group. Mean choroidal thicknesses were

successively reduced for -10 D, -5 D, and 0 D lenses, while the opposite phenomenon was observed for scleral thickness. In both choroid and sclera measurements, form-deprived eyes had similar thickness changes to their contralateral controls (0.02±0.01 vs 0.03±0.03 mm respectively for choroid thickness, 0.01±0.01 vs. 0.03±0.02mm respectively for scleral thickness). The only metric in which there was a difference in the groups' responses was retinal thickness, where the change in interocular difference in the form deprived eyes was significantly different from that of 0 D lens-treated eyes. Once again, for the lens-treated eyes the retinal thickness was successively thinner for the -10 D, -5 D and 0 D lens groups.

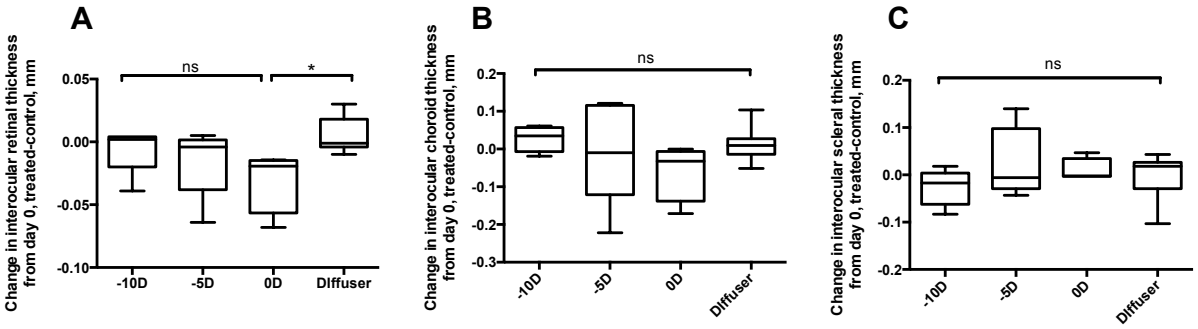

Figure 2.7. Change in interocular difference in retinal thickness (A), choroidal thickness (B), and scleral thickness (C) after 28 days of negative lens/diffuser treatment in Elm Hill guinea pigs. Inter-group differences assessed via Kruskal-Walis test, * indicates $p<0.05$. There were no significant differences between treatment and control eyes in any of the measured parameters (as assessed by Wilcoxon test).

2.4.1.2 Visual acuity changes

Measurements of visual acuity, although not typically performed in myopia development studies, can potentially provide insight into an animal's visual development. Assessments of visual acuity were performed on all treated animals at the end of the 28-day negative lens/diffuser treatment. Figure 2.8 shows interocular differences in visual acuities at day 28 (Figure 2.8A), as well as visual acuities for treated and control eyes (Fig. 2.8B). Once again, we found no significant interocular differences in visual acuities for any of the treatment groups. Nonetheless, it is interesting that the visual acuities of treated eyes in the -10 D and -5 D lens groups tended to be lower than those of control eyes (though not statistically significant). This is perhaps a product of chronic defocus, as these groups recorded the least treatment effects, measured in terms of changes in interocular differences in axial length and refractive error.

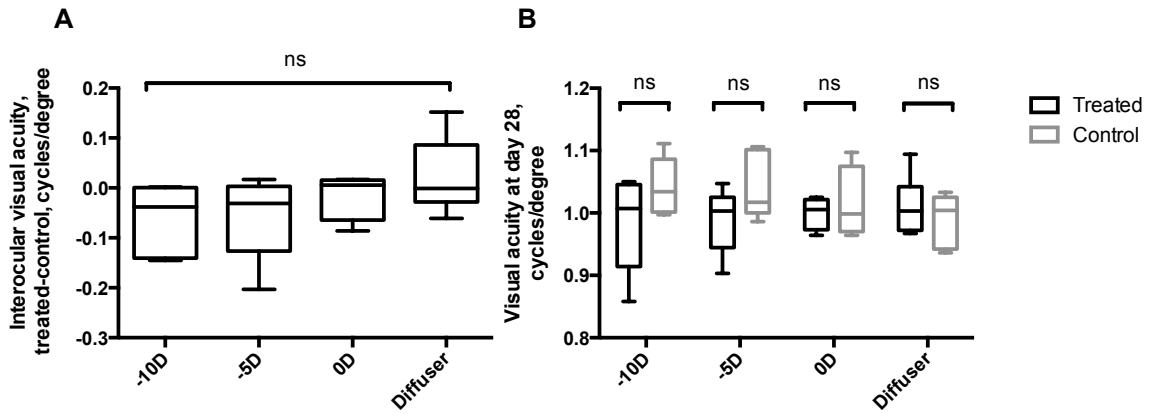

Fig 2.8. Visual acuity (VA) measurements of Elm Hill guinea pigs after 28 days of negative lens or diffuser treatment, measured with an OptoMotry instrument. Panel A shows interocular differences (treated minus control) for guinea pigs treated with -10 D, -5 D, 0 D lenses and diffusers (inter-group differences assessed with Kruskal-Wallis test); Panel B shows data for treated (black bars) and control (gray bars) eye plotted separately (difference between pairs assessed with Wilcoxon test).

2.4.2 New Zealand guinea pigs treated with diffusers

Upon establishing that the guinea pigs purchased from the Elm Hill colony did not respond to any myopia-inducing stimuli, we set out to obtain breeders from a guinea pig colony proven to be sensitive to myopic-inducing stimuli. To that end, we established a breeding colony using guinea pigs generously donated by Prof. John Phillips, whose lab had reported successfully inducing form deprivation myopia in their animals [152]. After establishment of the colony, these "New Zealand" animals were treated with diffusers (to elicit form deprivation myopia), being the paradigm previously used successfully with this population. The decision to confine our studies using the New Zealand animals to form deprivation was also consistent with our over-riding objective, which was to produce myopic animals for the testing of a myopia-control therapy targeting the sclera, and not to study the molecular mechanisms underlying the development of experimental myopia.

2.4.2.1 Refraction and axial length changes

The changes in axial length and refractive error for treated and control eyes of the New Zealand guinea pig population can be seen in Figure 2.9.

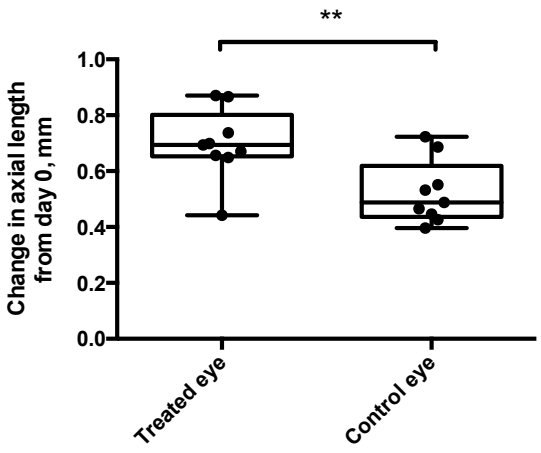

Figure 2.9. Total change in treated and control values of axial length (A) and refraction (B) for New Zealand (NZ) guinea pigs after 28 days of diffuser treatment. Differences assessed with Wilcoxon test. * $p<0.05$, ** $p<0.01$.

The axial length and refractive error data collected from New Zealand guinea pigs confirmed their sensitivity to form deprivation. The diffuser-treated eyes elongated significantly more than the control eyes (Figure 2.9A), with a mean change in interocular difference of 0.17±0.12 mm (treated minus control). Concomitantly with this increase in axial length of treated eyes, there was a myopic shift in the refractions of diffuser-treated eyes (Figure 2.9B), which on average became -4.58 ± 2.92 D more myopic than controls (change in interocular difference).

The changes in interocular differences in both axial length and refraction over the course of the experiment are shown in Figure 2.10. Approximately half of the changes in refraction occurred by day 14, midway through the treatment period. The plot of interocular differences in axial lengths, which were monitored more frequently, revealed that approximately half of the diffuser-induced axial elongation had occurred in the first week of form deprivation (increase in interocular difference at day 7 was 0.103 ± 0.102 mm).

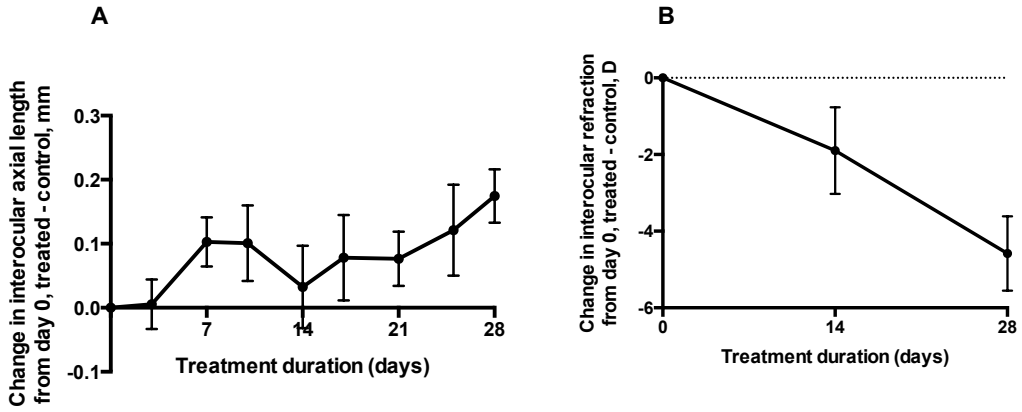

Figure 2.10. Change in interocular differences (mean ± SEM) in axial length (A) and refractive error (B), plotted against treatment day, for New Zealand guinea pigs treated with diffusers for 28 days. All measurements are normalized to day 0 values.

We once again examined the primary source of the ocular elongation described above. Figure 2.11 shows the changes in anterior chamber depth, lens thickness, and vitreous chamber dimensions for both treated and control eyes over the form deprivation treatment period. The dimensions of the anterior chamber and lens of the treated eyes were essentially identical to those of the control eyes. The change in interocular difference for these two parameters was -0.004±0.08mm and 0.02±0.09mm, respectively. In contrast, the vitreous chamber depths of diffuser-treated eyes were significantly longer than those of control eyes, with a change in interocular difference of 0.15±0.12 mm. Thus the increased axial elongation in treated eyes can be attributed largely to an increase in vitreous chamber depth.

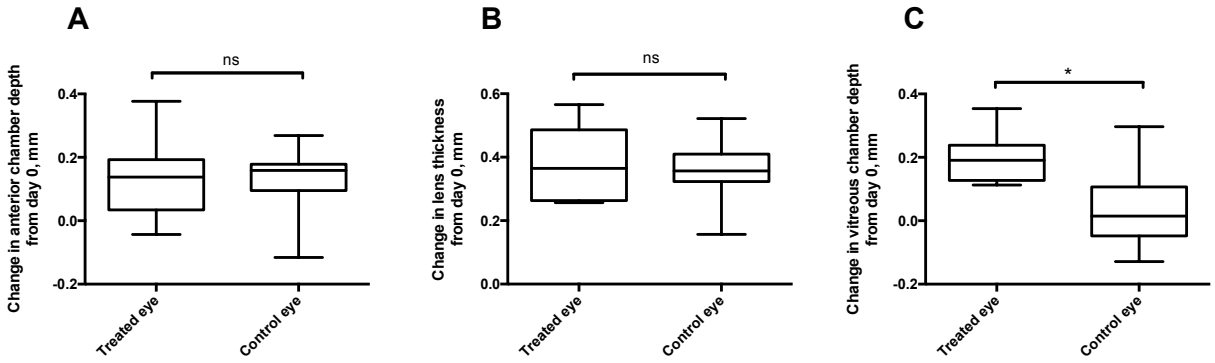

Figure 2.11. Change in anterior chamber depth (ACD) (A), lens thickness (B), and vitreous chamber depth (VCD) (C) for New Zealand guinea pigs after 28 days of diffuser treatment. Differences between treated and control eyes assessed with Wilcoxon test. * $p<0.05$.

Figure 2.12 elaborates further on the relationships between axial length, vitreous chamber depth, and refractive error, both at baseline (black data point) and at the end of treatment (orange data point). Figure 2.12A illustrates the relationship between interocular differences (treated minus control) in axial length and refraction. At baseline (black data point), there was very little difference between treated and control eyes in terms of either axial length or refractive error. Compared to the Elm Hill guinea pigs, the inter-animal variability in New Zealand animals was smaller (compare with Figure 2.4A). After 28 days of form deprivation treatment (orange data point), all animals showed myopic shifts in refractive errors, as reflected in the negative interocular differences. Furthermore, interocular differences in axial length were now positive, reflecting the increased elongation of treated eyes. This pattern is consistent with axial myopia, as is typical of form deprivation myopia in animal models. Figure 2.12B figure shows the interdependence between changes in vitreous chamber depth and axial length; the Day 28 data point lies in close proximity to the dotted line, which represents equality between increases in axial length and increases in vitreous chamber depth).

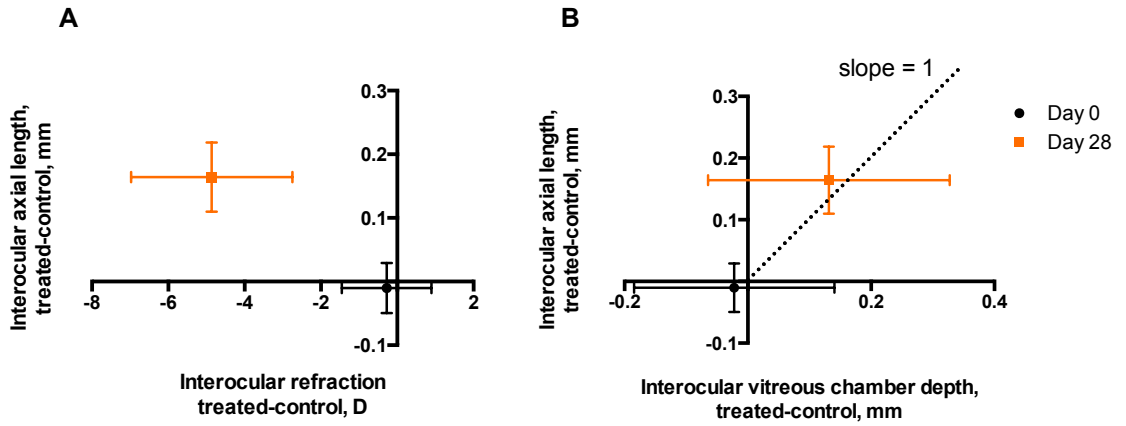

Figure 2.12. Interocular differences in axial length (y-axis) plotted against interocular differences in refractive error (A) or vitreous chamber depth (B) at baseline and after 28 days of treatment. For panel A, points in the upper left quadrant correspond to axial myopia, i.e. treated eyes are longer and have more negative refractive errors than control eyes). In panel B, the dotted line, with a slope of 1, represents equal differences in axial length and vitreous chamber depth.

The effects of the diffuser treatment on the thicknesses of the retinas, choroids, and scleras of New Zealand guinea pigs are shown in Figure 2.13, which plots changes for treated and control eyes for each of these parameters. There were almost no differences in the mean values between treated and control eyes for any of these parameters; the mean change in interocular differences for retina, choroid, and sclera are approximately zero (0.006±0.03, -0.003±0.04, and -0.005±0.02 mm, respectively). As can be inferred from these values and from Figure 2.13, there were no statistically significant differences between treated and control eyes for any of these parameters (Wilcoxon test).

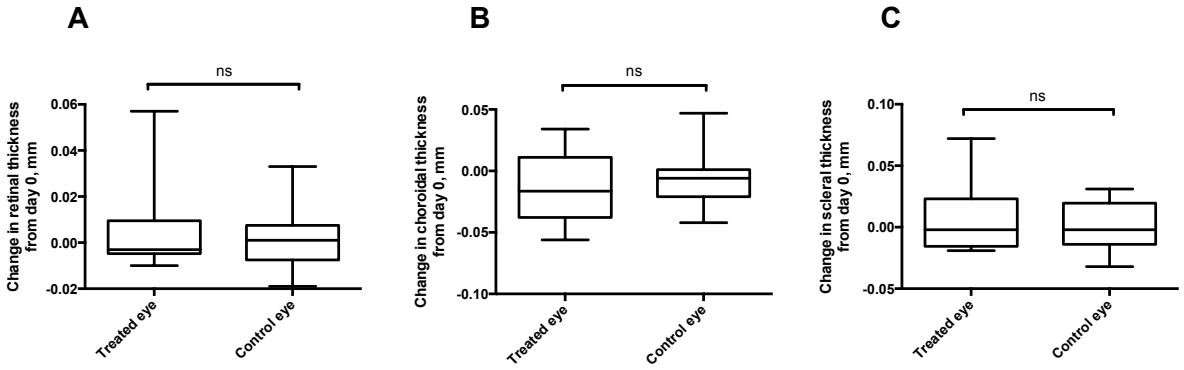

Figure 2.13. Change in retinal thickness (A), choroidal thickness (B), and scleral thickness (C) for treated and control eyes after 28 days of diffuser treatment in New Zealand guinea pigs. None of the differences between treated and control eyes are statistically significant (Wilcoxon test).

2.4.2.2 Visual acuity changes

Visual acuities measured on day 28 indicate that the New Zealand guinea pigs cannot see as well out of their diffuser-treated eye (Figure 2.14) (naturally, the experiment was performed without the diffuser in place) – the visual acuity of the treated eyes was on average 0.11 cycle/degree lower than that of the control eyes. These results suggest that the extent of eye elongation and concurrent

myopia development elicited after 28 days of form deprivation is sufficient to not only alter the eye's refractive state, but can also impact the animals' visual behavior. Because we did not see an equivalent decrement in visual acuity in the Elm Hill animals, we are tempted to ascribe this acuity decrement to optical defocus.

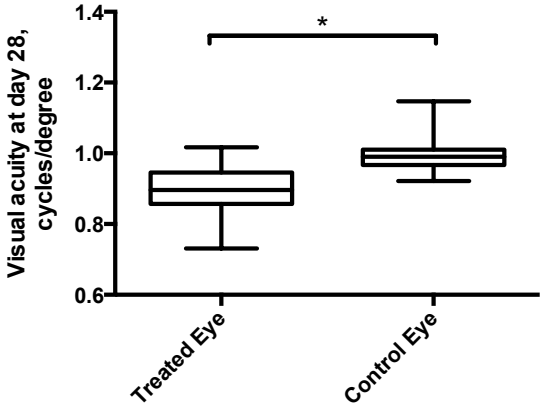

Figure 2.14. Visual acuity (VA) measurements of treated and control eyes of New Zealand guinea pigs after 28 days of diffuser treatment, acquired with an OptoMotry virtual cylinder. The difference between pairs was assessed with a Wilcoxon test, * represents $p<0.05$.

2.4.3 Comparing the form deprivation responses in New Zealand and Elm Hill guinea pigs

The refractive error and axial elongation responses to form deprivation of the Elm Hill and New Zealand guinea pig populations are contrasted below. Interocular changes in axial length and refractive error over the 28-day experiment are shown in Figures 2.15A and 2.15B, respectively, while interocular visual acuity data collected at day 28 are shown in Figure 2.16.

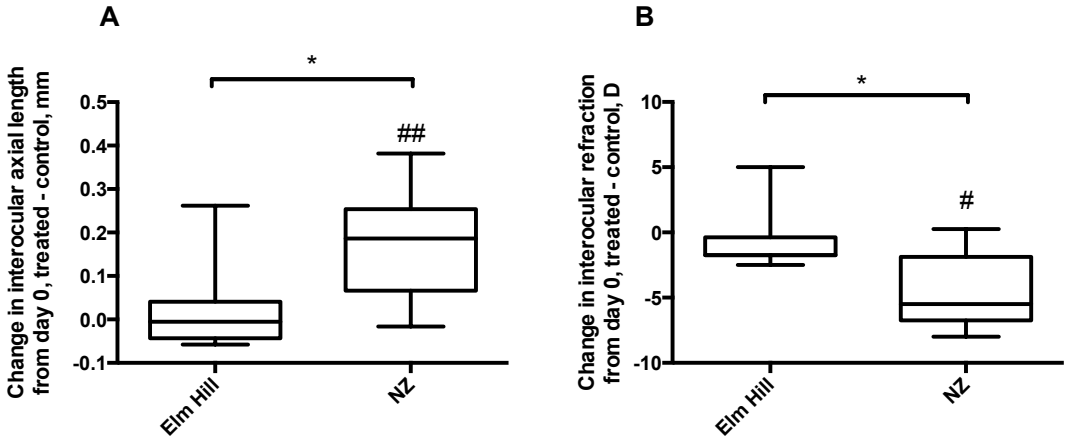

Figure 2.15. Changes in interocular differences (treated minus control), in axial length (A) and refractive error (B) for the Elm Hill and New Zealand (NZ) guinea pigs after 28 days of diffuser treatment. Intergroup differences assessed with Mann-Whitney test, * $p<0.05$. Differences between treated and control eyes assessed for each group with Wilcoxon test, # $p<0.05$, ## $p<0.01$.

As described previously, the New Zealand guinea pigs, but not in the Elm Hill guinea pigs showed the classic changes of form deprivation myopia in response to the applied 28 days of diffuser treatment. These differences stand out dramatically when graphically comparing the data for these two populations. After 28 days of form deprivation, the induced change in interocular differences in axial length for the New Zealand guinea pigs was approximately 0.17 mm larger than the equivalent value for the Elm Hill guinea pigs. The New Zealand animals were the only ones to show a significant myopic shift in refraction, becoming approximately 4 D more myopic than the Elm Hill group.

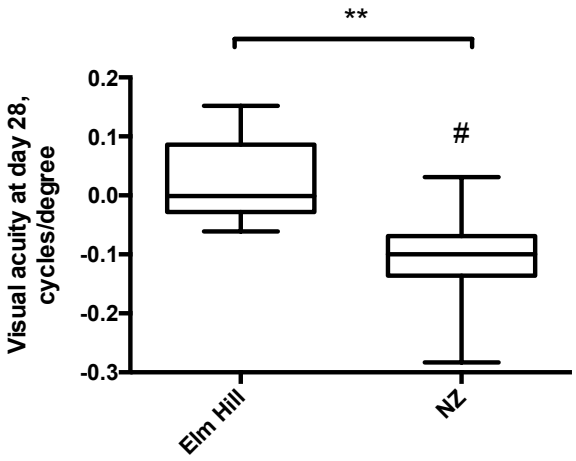

Figure 2.16. Interocular differences (treated minus control), in visual acuity measured in Elm Hill and New Zealand guinea (NZ) pigs after 28 days of diffuser treatment. Inter-group differences assessed with Mann-Whitney test. ** $p<0.01$. Differences between treated and control eyes assessed for each group with Wilcoxon test, # $p<0.01$.

Finally, the interocular difference in visual acuity for the Elm Hill guinea pigs was close to zero, compared to the negative value for the New Zealand guinea pigs (+0.02 vs. -0.11 cycles/degree, respectively). To understand the origin of the latter population difference, the visual acuities as well as axial lengths and refractive errors of the untreated control eyes of both groups were compared (Table 2.3). Although the eyes of the Elm Hill population were slightly longer and also relatively myopic on average compared to the New Zealand animals, the groups were not significantly different. Thus the more negative interocular difference in visual acuity recorded from the New Zealand can be attributed to a reduction in acuity of their myopic eyes.

Table 2.3. Comparison of axial lengths, refractive errors, and visual acuities of fellow (control) eyes of guinea pigs from the Elm Hill and New Zealand populations. Axial length and refraction data represent change over the 28-day treatment; visual acuity data represent measurements on day 28.

		Measurement of control eye, mean ± SD	p-value
Change in axial length, mm	New Zealand	0.52 ± 0.11	0.06
	Elm Hill	0.66 ± 0.18	
Change in refraction, D	New Zealand	0.17 ± 1.70	0.08
	Elm Hill	-1.21 ± 1.40	
Visual acuity, cycles/degree	New Zealand	1.00 ± 0.06	0.67
	Elm Hill	0.99 ± 0.04	

In summary, the New Zealand guinea pigs but not the Elm Hill animals showed robust responses to diffuser treatments, consistent with form deprivation myopia (increased axial length and myopic refractive errors for treated eyes), with the additional novel finding of reduced visual acuity in treated eyes. Because of the former population's proven sensitivity to myopia-inducing stimuli, it was also selected for the myopia-control experiments described later in this dissertation (Chapter 4).

2.5 Discussion

The experiments described in this chapter found markedly different responses to myopia-inducing stimuli between two pigmented guinea pig populations that would, at first inspection, be considered nearly identical. Guinea pigs from a commercial breeder (Elm Hill) and from a laboratory-maintained colony (originally sourced from University of Auckland, New Zealand) were treated with different myopia-inducing paradigms. The Elm Hill guinea pigs were treated with -10 D, -5 D, 0 D lenses and white plastic diffusers, while the New Zealand guinea pigs were treated only with the diffusers.

Minimal axial elongation was observed in the experimental eyes of Elm Hill guinea pigs treated with well-established myopia-inducing treatments – -10 D and -5 D lenses, and diffusers. Animals wearing 0 D lenses also showed minimal treatment-related changes. The latter treatment group served as a control for the Elm Hill study, against which to compare the groups wearing defocusing lenses. Despite the lack of axial elongation in the Diffuser group, there was a small myopic shift in refraction, perhaps reflecting a treatment effect on corneal curvature. The latter parameter was not measured, but future studies should include keratometry measurements to help clarify this question.

In contrast to the Elm Hill population, the New Zealand guinea pigs developed a significant amount of myopia over the 28-day treatment. Approximately half of the underlying axial growth changes occurs over the first week of treatment and reflected increased vitreous chamber elongation. Furthermore, in these animals the changes in anterior chamber, retina, and choroid of the diffuser-treated eyes were minimal, although trending towards being slightly thinner than their contralateral eye counterparts. In terms of the anterior chamber depth data, our results contrast with those reported by Howlett & McFadden[108], who noted an anterior chamber contribution to axial length increases over a short 16-day period of form deprivation in animals of a similar age at the start of their treatment to those in our study. In their study, the anterior chambers of treated eyes were slightly longer than those of control eyes by the end of the treatment (3.71 ± 0.02 vs. 3.67 ± 0.02 mm, respectively), though in both cases the anterior chamber contributes 15% to the total axial length. The pattern is similar for the vitreous chambers, which in both eyes constitute 39% of the total axial length and are slightly longer in the diffuser-treated eyes than in control eyes (3.15 ± 0.02 vs. 3.13 ± 0.01mm) [108]. The density of the diffusers used in Howlett & McFadden's study was not given. Another study with older animals (4 weeks at the start of the study) and lighter (60% transmission) diffusers than those use in our study[185] reported greater axial elongation, but a smaller myopic shift after 4 weeks of treatment compared to our finding for the New Zealand guinea pigs (treated minus control: 0.24 mm vs. 0.17mm; -2.66 D vs. -4.58 D). This mismatch between changes in axial length and refractive error changes likely reflects an optical artifact of ocular growth, and specifically the large eyes of older animals [186].

Unlike studies in rhesus monkeys, most guinea pig studies do not mention whether animals with a low/non-existent myopia response were excluded from reported results [98,99]. To our knowledge, no other studies have systematically examined the responses of different guinea pig populations to myopia development. Yet, the phenomenon of varying guinea pig responses is not unknown in the

guinea pig literature, having been noted by many authors who compare the myopia development of their animals with previously published work. In their study of the role of the FGF-2 gene on myopia development, An and colleagues[164] mention that they used "a different inbred line of guinea pigs from what [was] used in [a] previous study, which led to a more efficient induction of [Form Deprivation Myopia]". Long et al. also discuss the variability in the refractive status of normal guinea pigs [160], citing marked differences between their recorded refractive errors and those reported by Howlett and McFadden's study. They also mention similarities between the emmetropization patterns of their guinea pigs and those of Zhou et al. [187] and Lu et al. [185]. The similarities between the two latter studies is not surprising, given that their animals were sourced from the same colony

Guinea pig models for myopia are still relatively new and there is currently no general agreement in the community as to the ideal age to start lens/diffuser treatment, nor the ideal transmission of diffusers used for form deprivation treatment. For the purpose of better characterizing the myopia response profiles of guinea pigs and inter-study differences, the results of relevant studies published between 2003 and 2014 have been summarized in table form below (Table 2.4). Information about the source of the guinea pigs used is also included where available, as are the parameters measured and sample sizes (ranging from 5 to 40). Only those studies in which the guinea pigs were treated with myopia-inducing stimuli are included; where drugs and/or other optical treatments were also part of the study the related data are not mentioned. Interocular differences in axial length and refractive errors were calculated when not supplied (e.g., when treated and control eye data were reported separately). The data presented in this table points to significant apparent differences in sensitivity to myopia between different guinea pig populations.

Table 2.4. A sample of guinea pig myopia studies published between 2003 and 2013.
* Vitreous chamber depth, axial length not provided.

Authors, year of publication	Treatment (LIM: lens induced myopia. FDM: form deprivation myopia). Diffuser transmission reported when available	Source of guinea pigs ("n/a" when source is not mentioned)	Start age (sample size in parentheses)	Treatment duration	Mean axial length change in μm (interocular difference, treated-control)	Mean refractive error change in diopters (D) (interocular difference, treated-control).
[188]	LIM, -10D	n/a	4 weeks (7)	11 days	50	-2.45
[189]	FDM	n/a	4 weeks (5)	4 weeks	n/a	-6.25
[172]	FDM LIM, - 4D	Lab-maintained colony	5 days (13 for FDM, 5 for LIM)	16 days for FDM, 10 days for -LIM	FDM: 104 -4D LIM: 104	FDM: -6.64 -4D LIM: -5.78
[108]	FDM	Lab-maintained colony	5 days (15 for 6-day, 14 for 11-day, 19 for 16-day)	6, 11, or 16 days	6 day FDM: 106 11 day FDM: 146 16 day FDM: 110	6 day FDM: -4.80 11 day FDM: -6.60 16 day FDM: -6.60
[185]	FDM, 60% and lid suture	Animal Breeding Unit at Wenzhou	~3 weeks (6 for FDM,	2, 4, 6, 8 weeks	2 week FDM: 350 4 week FDM: 240	2 week FDM: -2.08 4 week FDM: -2.66

	(LS)	Medical College	24 for lid suture)		6 week FDM: 290 8 week FDM: 270 2 week LS: 70 4 week LS: 200 6 week LS: 320 8 week LS: 310	6 week FDM:- 3.28 8 week FDM: -4.25 2 week LS: -2.08 4 week LS: -2.20 6 week LS: -3.70 8 week LS: -4.45
173	FDM, 35% T	n/a	2 weeks (18 for each treatment group)	1, 2, and 3 weeks	1 week FDM: 101 2 weeks FDM: 171 3 weeks FDM: 232	1 week FDM: -1.64 2 weeks FDM: -2.32 3 weeks FDM: -2.83
187	FDM, 60% T	Animal Breeding Unit at Wenzhou Medical College	~3 weeks (11)	4 weeks	110	-3.77
149	LIM, -2 and -4D	Lab-maintained colony	2-3 days (6 for -2D, 12 for -4D)	10 days	-2D LIM: 20 -4D LIM: 70	-2D LIM: -4.10 -4D LIM: -4.70
190	LIM, -4D	Animal Breeding Unit at Wenzhou Medical College	3 weeks (16 for 2 wk treatment, 9 for 4 wk treatment)	2 and 4 weeks	2 weeks: 80* 4 weeks: -20*	2 weeks: -3.00 4 weeks: -2.50
152	FDM, 25% T	Lab-maintained colony	1 week (29)	2 weeks	169 ± 49*	−4.06 ± 0.35
175	FDM, 35% T	Animal Experiments Laboratory at Zhongshan Ophthalmic Centre	3 weeks (20)	3 weeks	470	-5.40 ± 1.08
191	FDM	Animals Laboratory Center (Zhongnan University)	3 weeks (40)	2 weeks	n/a	-7.00 ± 1.13D
155	FDM, 56%	Animal Center of Xiang-ya Medical College	4 weeks (10)	10 days	160	-4.46
174	-10D	Experimental Animal Center, China Medical University	4 weeks (34)	2 weeks	570	-8.45
180	FDM, 60%	n/a	3 weeks (16)	7 weeks	220*	−4.24
175	FDM, 35%	Animal Experiments Laboratory of Zhongshan Ophthalmic Centre (Sun Yat-sen University)	3 weeks (7)	3 weeks	470	-5.40 ± 1.08
166	FDM, 60% LIM, -4D	n/a	3 weeks (26 FDM, 23 LIM)	11 days	n/a	FDM: -3.24 LIM: -4.18
168	FDM LIM, -5D	n/a	2 weeks (30 FDM, 30 LIM)	2 weeks	FDM: 291 LIM: 173	FDM: -5.14 LIM: -3.64

[171]	FDM	Experimental Animal Center of Xiangya Medical College of Central South University	3 weeks (25)	2 weeks	250	-3.83
[164]	FDM	n/a	3 weeks (10)	2 weeks	160	-5.17
[153]	LIM, -10D	n/a	2 weeks (35)	6, 15, 30 days	6 days: 130 15 days: 1020 30 days: 1220	6 days: -2.09 15 days: -3.24 30 days: -5.43
[178]	LIM, -6D	Animal Department of the Central South University	3 weeks (15)	15 days	410	-5.9
[179]	LIM, -10D	Hebei Medical University	2 weeks (10 each group)	6, 15, 30 days	6 days: 130 15 days: 1020 30 days: 1220	6 days: -1.45 15 days: -3.24 30 days: -5.43
[170]	FDM	Animal Center of Xiangya Medical College	4 weeks (12)	2 weeks	240	-4.51

No other authors have reported that guinea pigs in their colony lack the ability to respond to myopia-inducing stimuli. However, a strain of spontaneously myopic guinea pigs has been identified and described. Ten animals, identified from a larger group of 220, exhibited binocular axial and refractive myopia [192].

Strain as well as sex differences in sensitivity to myopia-inducing stimuli have been extensively studied in chicks. While differences in sensitivity to myopia-inducing stimuli, rates of response, and features of the induced myopia have been uncovered, no reports of lack of sensitivity have appeared. Schmid and Wildsoet compared the form deprivation myopia responses in White Leghorn and Broiler chicks, starting at hatching and continuing until 2 weeks of age. While untreated (non-myopic) Broiler chicks exhibited faster eye growth than White Leghorns, they did not develop as much myopia after form deprivation treatment. That is, White Leghorn chicks had longer eyes and more myopic refractions than Broiler chicks after 2 weeks of form deprivation[193]. Troilo and colleagues further investigated species-specific differences by examining form deprivation responses of different strains of White Leghorn chick: Cornell-K and H&N. Anterior chamber and lens dimensions did not significantly differ between strains, while the vitreous chamber and refractive errors trended towards higher myopia in the H&N strain. The weaker myopic response in the Cornell-K strain was attributed to the significant corneal flattening measured in those animals [194]. In contrast, a recent study by Guggenheim et al. reports a different trend: in a study examining the susceptibility of three different chicken strains (White Leghorn, Broiler, and Brown Leghorn) to form deprivation myopia, the authors found that all three strains became somewhat equivalently myopic [195]. This is rather surprising, given previously published results and the fact that the three strains vary quite significantly in both body and eye growth, and could therefore be expected to also vary in their rate of eye growth and degree of developed myopia.

Sex as well as strain has been identified as an important factor in determining responses to myopiagenic stimuli. Male White Leghorn chicks have been found to have larger eyes on average,

and to be more reactive to form deprivation. In male chickens, form deprivation elicits a greater axial length increase, with a greater contribution from the anterior chamber[196,197].

A selective breeding study in chicks points to the possible directions that could be taken in guinea pig studies, now that both unreactive and spontaneously myopic strains have been reported. After two rounds of selective breeding of chicks with strongest and weakest responses to form deprivation, the progeny derived from the strongly responding chicks developed twice as much form deprivation myopia compared to those from the low susceptibility line[198].

While there are a number of potential sources for the inter-animal variability observed in our study and implied by the results summarized in Table 2.4, a genetic basis for the lack of susceptibility of the Elm Hill animals to myopia-inducing stimuli would seem the most reasonable explanation. When animals are sourced from the same colony, differences in the amount of induced myopia could be attributed to variations in diffuser transmission, light levels in the rooms, and animal behavior (hiding and burrowing in the corner as opposed to having more marked visual experiences). Also, as guinea pigs have a grooming ritual that includes running their front paws from their ears to their nose, it is possible for them to detach their diffusers in this process. Animals must therefore be monitored at frequent intervals to ensure that such treatments are not interrupted; it's been reported that as little as one hour of uninterrupted vision a day can reduce the amount of developed myopia by 50% [189]. The fact that both negative lenses and form deprivation failed to elicit a significant myopic response in the Elm Hill animals is interesting in of itself, as the visual conditions are quite different (closed-loop optical defocus and open-loop form deprivation), and it is generally assumed that different retinal signal pathways underlie the induced myopic responses [199]. The lack of sensitivity to both stimulus conditions may point to a mutation in the signal pathway beyond the retina. Further investigations are required to address this question.

2.6 Conclusion

Guinea pigs can vary dramatically in their sensitivity to myopia-inducing stimuli. This is exemplified by the "typical" form deprivation myopia responses in a population of guinea pigs sourced from the University of Auckland, New Zealand, and by the lack of responses to myopia-inducing stimuli in another guinea pig population (obtained from a commercial breeder, Elm Hill). These results provide documented evidence for observations quietly discussed among myopia research groups over the past few years: that the response of guinea pigs to myopia-inducing stimuli can markedly vary from population to population. The lesson for new researchers embarking on guinea pig studies is that they should carefully consider the source of their animals and, where possible, source their animals from colonies known to be sensitive to myopia-inducing stimuli.

Chapter 3. *In vitro* characterization of mammalian scleral fibroblast behavior on synthetic hyaluronic acid-based hydrogels

3.1 Introduction

Myopia (nearsightedness) is an ocular disease characterized by an elongated eye. This leads to a mismatch between the eye's length and it's refractive power, causing images of distant objects to form in front of the retina [2]. The worldwide prevalence of myopia has been steadily rising over the past few decades[6]; this trend is particularly evident in industrialized East Asia, where recent studies report levels as high as 96.5% for 19-year old Korean military conscripts [200] and 84% for Taiwanese children at the end of high school [201]. Recent increases in myopia prevalence are not limited to East Asia, having also been reported in the United States[202], Canada [203], and Europe [204]. Perhaps even more worrying is the fact that the age of myopia onset has significantly decreased [201], and thus with more time for their myopia to progress, many will have become high myopes (refractive error > -6 diopters) by adulthood.

The precise sequence of cellular signaling involved in myopia development remains unknown, but decades of research have revealed the effects of these signals on the sclera (white outer wall of the eye), namely a reduction in the synthesis rate of collagen, proteoglycans, and glycosaminoglycans, decreased scleral fibroblast proliferation, and increased expression of matrix metalloproteases. The combined effect of these biochemical changes is a decrease in scleral thickness and an increase in its creep response[34]. The risk of vision-threatening conditions such as retinal detachment, lacquer cracks, and chorioretinal atrophy [205] all increase with the amount of myopia[12]. In cases of high myopia, the extreme scleral thinning can also lead to localized ectasia and associated pathological changes in the retina, retinal pigment epithelium, and choroid [206,207]. It is important to stress, however, that even low levels of myopia increase the risk of vision loss[12,208,209].

Despite the increasing global prevalence of myopia and the risk it presents to the health and productivity of the world's working-age population, there are no widely adopted pharmacological treatments for myopia, with the exception of topical ophthalmic atropine drops, which has won some acceptance in Asia. Used off-label, it appears to be remarkably effective in the short term. Yet, in the most commonly used concentrations (1-2%), it carries undesirable ocular side effects such as mydriasis (pupil dilation) and cycloplegia (loss of accommodation, which prevents near focusing) [210]. Moreover, follow-up studies in children treated with atropine drops found that myopia progressed at an accelerated rate upon cessation of treatment [50].

Few myopia-control therapies have targeted the sclera. The ones that have mostly target highly myopic eyes with mechanically unstable scleras. Scleral reinforcement (buckling) surgery using strips of donor sclera is currently the only clinical treatment used to stabilize highly myopic eyes in the US, but its invasive nature, dependence on suitable donor tissue, and lack of published data on the long-term fate of the implant prevent it from being widely adopted in this country.

Crosslinking treatments adapted from keratoconus therapies – gluteraldehyde or riboflavin photoinitiators followed by UV treatment – have been trialed as an alternative approach for increasing the rigidity of the sclera and thus slowing myopia progression [211], but are both highly toxic and can lead to cellular death not only in the sclera, but also in inner ocular tissues [212]. In recent years, new studies have sought to develop less toxic crosslinking solutions based on genipin[213] and aliphatic β -nitro alcohols [214], with promising crosslinking results obtained from *ex vivo* tests. Mattson and colleagues employed Eosin Y in triethanolamine – a crosslinking solution that can be activated by visible light – to control eye growth in guinea pigs, and reported reductions in the rate of growth of the treated eyes [215].

The concept of using injectable hydrogels to modify scleral properties as an approach for rehabilitating highly myopic eyes and/or slowing early myopia progression has been explored previously in two different lines of research. The underlying premise was that an appropriate hydrogel, when implanted against the sclera, could serve as a scaffold into which scleral cells may migrate and lay down new matrix, thereby increasing scleral thickness (and decreasing associated creep). In this way, the changes characteristic of myopic scleras could be opposed or reversed; progression could be slowed or halted (in the case of childhood myopia) or myopic scleras could be rehabilitated (in the case of high myopia). The earliest report involved myopic children in Russia, but unfortunately the composition of the hydrogel was not disclosed, although it was reported to elicit significant immune responses in some patients [60]. In later studies in our lab, two different hydrogels were tested using the chick as an animal model [61,62]. One of the studies was conducted in collaboration with some of the Russian researchers involved in the work cited above, where an *in situ* polymerizing polyvinylpyrrolidone-based hydrogel was implanted over the external posterior sclera of myopic young chicks. The polymer caused dramatic thickening of the cartilage (innermost layer) of chick scleras, without any subsequent control of eye elongation. In a second follow-up study, a biomimetic thermoresponsive N-isopropylacrylamide (NIPAAm)-based hydrogel was used [62]. Advantage was taken of NIPAAm's thermoresponsive properties to synthesize a hydrogel that was a viscous liquid at room temperature and a gel at body temperature, allowing it to become injected and subsequently localized at the delivery site (external surface of the posterior sclera). The hydrogel was crosslinked with a peptide-based diacrylate crosslinker, degradable by MMP-2, -9, and -13. Furthermore, it contained an interpenetrating chain of linear acrylic acid grafted with the cell-binding peptide bsp-RGD(15). This hydrogel demonstrated good compatibility with chick scleral chondrocytes and fibroblasts *in vitro,* and also did not cause adverse inflammatory reactions *in vivo.* However, the implanted hydrogel had minimal inhibitory effect on myopic eye growth in chicks. This lack of effect was partly attributed to the stiffness of the chick sclera, which, as mentioned previously, has an inner cartilage layer that imparts significant rigidity to the tissue.

As a follow-up to the work described above, we sought to test the NIPAAm-based hydrogels as a potential myopia control therapy in a mammalian model with a fibrous-only sclera. As a first step, *in vitro* cytotoxicity and proliferation studies were conducted using primary guinea pig scleral fibroblasts. Unfortunately, the NIPAAm-based hydrogels did not support robust proliferation of these cells, necessitating a shift to a different material. Data for these preliminary *in vitro* studies are presented in Appendix 2.

The study described in this chapter covers the optimization of an alternative, hyaluronic acid-based hydrogel. We hypothesize that the hydrogel could be used either in the early stages of myopia, to slow eye elongation, or later in the disease process, to rehabilitate the scleras of highly myopic eyes. Hyaluronic acid (HyA) is a high molecular weight nonsulphated glycosaminoglycan, consisting of

repeating disaccharide units of D-glucuronic acid and N-acetyl-glucosamine. It is expressed by all mammals in its salt form (hyaluronate) and is highly abundant in connective tissues and many viscous fluids, including the ocular sclera and vitreous humor [21,216]. Thus it is not surprising that HyA is highly biocompatible; it is also biodegradable, and easily modifiable. Due to these properties, HyA has already been heavily exploited as a tissue engineering tool for applications as diverse as cartilage [217], white fat [218], intervertebral discs [219], skin[220], bone [221], brain [222], and vocal fold [223].

The tunable hydrogel employed in our studies allows for independent modulation of mechanical, cell-binding, and degradation properties [224]. The hydrogel contains two distinct macromers: acrylated hyaluronic acid (AcHyA) and acrylated hyaluronic acid conjugated to the cell-binding peptide bsp-RGD(15) (AcHyA-RGD), a 15-amino acid peptide derived from bone sialoprotein (CGGNGEPRGDTYRAY)[35]. The RGD-containing peptide was selected because to its known affinity for integrin subunits identified in the mammalian sclera [29]. Hyaluronic acid itself is degradable by the enzyme hyaluronidase; however, the inclusion of a matrix metalloprotease-degradable peptide (CQPQGLAKC) as a crosslinker allowed for additional control over the hydrogel's degradability. Thiol groups present in the terminal cysteines of the peptide allow for reactions with the acrylate groups in the HyA monomers through a Michael-type addition reaction [224]. The crosslinking peptide is degraded at different rates by MMP-9, MMP-2, and MMP-13, with enzyme selectivity k_{cat}/K_m of $2.1x10^4$, $1.8x10^4$, and $7.3x10^2$ $s^{-1}M^{-1}$, respectively [226]. Thus this peptide was also considered appropriate for our application, given that human and tree shrew scleral fibroblast have been reported to express mRNA for both MMP-2 and MMP-9 [24,25]. A microarray analysis of human sclera also reported gene expression of MMP-2 [26].

Our working model for this anti-myopia hydrogel therapy involved dual actions: (1) provide mechanical support to the vulnerable posterior sclera (region most vulnerable to excessive remodeling and thus ocular elongation), and (2) provide an environment into which scleral fibroblasts could migrate and deposit extracellular matrix that could eventually assume the characteristics of the native sclera, thereby increasing its overall thickness and counteracting the scleral thinning characteristic of myopic eyes. The results reported in this chapter are limited to the *in vitro* assays used to characterize the hydrogel's biocompatibility with guinea pig scleral fibroblasts. These included proliferation and live/dead assays – to determine cell compatibility and toxicity of the hydrogel – and a migration assay, developed to test the ability of scleral fibroblasts to migrate into the hydrogels. For the latter assay, we also developed an automated algorithm to analyze acquired images. *In vivo* myopia control studies using an optimized hydrogel formulation are described in Chapter 4.

3.2 Materials and methods

3.2.1 Establishment and maintenance of primary cultures of guinea pig scleral fibroblasts

Materials: Sodium pentobarbital (Euthasol) was purchased from Virbac Animal Health. All cell culture materials were purchased from Gibco® Life Technologies. The Dulbecco's Modified Eagle's Media (DMEM) used as part of the two cell culture media contained 4.5 g/L of glucose and 4 mM L-glutamine. The container used to freeze the primary cultures at a slow rate was purchased from Nalgene.

Two types of cell culture media were used in the establishment and maintenance of the scleral fibroblast cultures. Primary cell culture media consisted of Dulbecco's Modified Eagle's Media

(DMEM), 30% Fetal Bovine Serum (FBS), and 1% penicillin/streptomycin (pen/strep). Maintenance media consisted of DMEM, 10% FBS, and 1% pen/strep.

Sourcing scleral fibroblasts: Young pigmented guinea pigs (at most 7 days old) were euthanized with an intracardiac injection of sodium pentobarbital, delivered under anesthesia with 5% isoflurane in oxygen. Eyes were enucleated and cleaned of all extraorbital fat and muscle. For each eye, an incision was made at its equator using a sterile scalpel blade, then sharp scissors were inserted through the cut and the posterior eyecup was isolated. The retina, RPE, and choroid were gently scraped off using blunt forceps, then two scalpel blades were used to cut up the sclera into ~1 mm^2 pieces for use in the culture protocol.

Culture protocol: To establish primary cultures of guinea pig scleral fibroblasts**, t**he scleral pieces were first transferred to 24-well plates that had been pre-coated overnight at 37°C with 0.1% gelatin. Primary cell culture medium (300 μL) was pipetted into each well; to prevent the tissue from floating upon addition of medium, the plate was tilted forward ~45° and the medium then very slowly added. The pieces were allowed to attach overnight at 37°C/5%CO_2, after which an additional 500 μL of fresh primary cell culture medium were slowly added to each well. After 3 days, the medium was replaced with maintenance medium and thereafter replaced every other day. Significant scleral fibroblast outgrowth was observed after 10-14 days.

To isolate the primary cells, 250 μL of warm 0.25% trypsin-EDTA were added to each well and incubated for 1-2 minutes. Then, after adding 0.5 mL of maintenance medium to each well, the solution was agitated using a 1 mL pipette. Cell suspensions from all wells were pooled and the number of cells counted using a hemocytometer. Cells not used immediately were prepared for long-term storage by centrifuging for 6 minutes at 900 rpm. The supernatant was aspirated and an appropriate volume of freezing media (DMEM + 50% FBS + 10% dimethyl sulfoxide + 1% pen/strep) was used to resuspend the pellet at a concentration of $1x10^6$ cells/mL. One mL aliquots of the cell suspensions were transferred into cryovials and frozen overnight at 80°C in a freezing container. The cryovials were then transferred into liquid nitrogen for long-term storage. Cells obtained from different animals were never mixed, for we observed that this practice decreased their proliferation rate

Frozen cells were prepared for *in vitro* assays by first thawing them in a 37°C bath and very slowly diluting them (dropwise) into 10 mL of cell growth medium, in a T-75 cell culture flask (Falcon) that had been coated overnight with 0.1% gelatin. All subsequent cultures took place in gelatin-coated flasks, and cells were expanded in a 1:5 ratio at most. Cell passaging was performed by first washing cultured cells with warm Phosphate Buffered saline (PBS), then adding 1 mL of warm 0.25% trypsin-EDTA and incubating for 1-2 minutes. Four mL of cell culture medium was added to the flask and agitated to lift the cells from the surface, then 1 mL of the cell suspension was transferred to a new gelatin-coated T-75 flask containing 9 mL of cell culture medium. Only cells up to passage 5 were used for the *in vitro* assays.

3.2.2 Characterization of cell growth on hyaluronic acid-based hydrogels

3.2.2.1 Synthesis of hyaluronic acid-based hydrogels

Materials: All chemicals were used without additional purification. Hyaluronic acid (HyA sodium salt, 500kDa) was generously donated by Lifecore Biomedical. Adipic dihydrazide, 1-Ethyl-(3-dimethylaminopropyl)carbodiimide hydrochloride (EDC), 1-Hydroxybenzotriazole hydrate (HOBt),

sodium hydroxide (NaOH), hydrochloric acid (HCl), and triethanolamine buffer (TEA) were obtained from Sigma Aldrich. Dimethyl sulfoxide (DMSO), sodium chloride (NaCl), N-Acryloxysuccinimide, acetone, and ethanol were purchased from Fisher Scientific. Both sets of peptides used in the experiments – the MMP-degradable crosslinker peptide (CQPQGLAKC) and the cell-binding peptide bsp-RGD(15) (CGGNGEPRGDTYRAY) were synthesized by United Peptide Co. Tris(2-carboxyethyl) phosphine hydrochloride (TCEP) was purchase from Thermo Scientific. Dialysis membranes (10,000 MWCO, SpectraPor Biotech CE) were purchased from Spectrum Laboratories. Twenty-four well cell culture inserts (Millicell PICM01250) and centrifuge tubes fitted with a filter unit (Steriflip SCGP00525) were purchased from Millipore. The Live/dead staining kit containing Calcein AM and Ethidium Homodimer was purchased from Invitrogen. The water used in all synthesis steps was ultrapurified in a Milli-Q filtration system (Millipore).

Acrylated Hyaluronic acid (AcHyA) synthesis: Hyaluronic acid (HyA) was functionalized with acrylate groups to enable it to participate in polymerization reactions [224]. Functionalization involved a two-step process: adipic dihydrazide groups were first grafted onto the hyaluronic acid molecule, then modified with acryloxysuccinimide to yield acrylated hyaluronic acid.

A 3 mg/mL solution of HyA was prepared in ultrapure water, stirring overnight at 350 rpm – higher stirring rates must be avoided to prevent degradation. Thirty molar excess of adipic acid dihydrazide were slowly added to the HyA solution and the pH was adjusted to 6.8 using 0.1 M NaOH and 0.1 M HCl, with slow and constant stirring. Separate 3 mL, 3 mmol solutions of EDC and HOBt were prepared in 1:1 mixtures of DMSO: ultrapure water and added to the HyA solution. The reaction was allowed to proceed for 24 hours, with the pH being monitored and maintained at 6.8 for the first 6 hours. After 24 hours, the solution's pH was raised to 7.0 using 0.1 M NaOH, then the HyAADH was dialyzed for 3 days (1 day against 1g/L NaCl and 2 days against ultrapure water; dialysis solutions were changed twice a day). After the dialysis process was complete, NaCl was added to the HyAADH to yield a 5% w/v solution, which was then precipitated by adding it dropwise to 100% ethanol, with slow and constant stirring. The resulting precipitate was dissolved in ultrapure water and dialyzed once again as previously described. Acrylated hyaluronic acid (AcHyA) was prepared by reacting the HyAADH solution with acryloxysuccinimide (300 mg in 10 mL of ultrapure water) overnight at room temperature. The solution was dialyzed again for 3 days as previously described, sterilized through a 0.22 μm filter using 50 mL Steriflip tubes, lyophilized for 3 days, and stored at -20°C.

AcHyA-RGD synthesis: A monomer with the desired cell-binding functionality was prepared by reacting AcHyA with the peptide bsp-RGD(15) (CGGNGEPRGDTYRAY) (AcHyA-RGD). The peptide was first reduced by incubating it for 30 minutes at 4°C in a basic solution of TCEP – 10 mg bsp-RGD in 1 mL of 5.7 mg/mL TCEP and 3 mg/mL NaOH. Twenty-five mg of AcHyA were dissolved in 10 mL of ultrapure water. The reduced peptide was then added to the dissolved AcHyA and the resulting solution stirred continuously overnight at room temperature. Finally, the AcHyA-RGD was dialyzed, sterilized, lyophilized, and stored as previously described for AcHyA.

Hydrogel preparation: Hydrogels for the *in vitro* experiments were synthesized by reacting AcHyA and AcHyA-RGD with the crosslinking peptide CQPQGLAKC. A cartoon schematic of the final step involved in the hydrogel synthesis is shown in Figure 1. Crosslinking involves a Michael-type addition reaction between the acrylate groups on the HyA precursors and the thiol groups present on the terminal cysteines of the crosslinking peptide [224].

In preparation for the synthesis of the hydrogels, triethanolamine (TEA) buffer was purged of oxygen by bubbling it with dry nitrogen gas for 30 minutes. The purged TEA was used to dissolve AcHyA and AcHyA-RGD, then the solution was incubated at 37°C for ~20 minutes to aid dissolution of the hyaluronic acid precursors. Once the precursors were dissolved, the solution was slowly but thoroughly mixed through pipetting to ensure that no clumps of HyA remained. Thiol-terminated MMP-degradable peptide was dissolved in TEA buffer and added to the dissolved HyA precursors, after which the solution was thoroughly mixed, briefly spun in a microcentrifuge to eliminate bubbles, pipetted into 24-well inserts, and allowed to polymerize at 37°C for 30-45 minutes. Hydrogels were used immediately after synthesis.

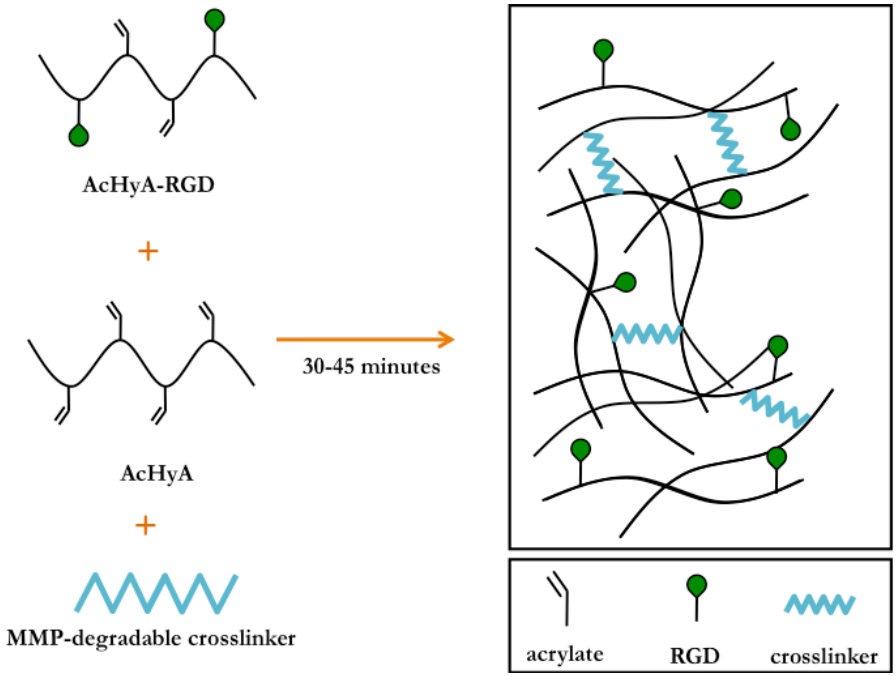

Figure 3.1. **Schematic for hydrogel synthesis.** HyA hydrogels were synthesized by reacting the functionalized HyA precursors AcHyA (hyaluronic acid functionalized with acrylate groups) and AchyA-RGD (AcHyA decorated with the cell-binding peptide bsp-RGD(15)) with a cysteine terminated MMP-degradable peptide crosslinker, which was linked to the acrylate groups on the HyA precursors via a Michael-type addition reaction.

Hydrogels of two different monomer contents were selected for this study: 2.0 and 3.3 % weight/volume, both with 100% crosslinking ratios (defined as a 1:1 molar ratio of the crosslinker cysteines and the acrylate groups on the HyA precursors). Their selection was partly based on their mechanical properties, which were characterized by measuring their complex shear moduli through dynamic oscillatory parallel plate rheology, using 15 mm-diameter sanded parallel plates and a gap height of 1 mm. A humidity chamber was placed around the sample plate to prevent the hydrogels from drying during the measurements. Samples were tested at 0.1-10 Hz, 10% strain, and 22°C. Only formulations with 380 μM RGD were tested. Since the ratio of acrylate groups in the monomers to cysteine groups in the crosslinker was always kept constant (1:1, as described above), we did not expect the modulus to vary with RGD concentration[224]. Note that because a marked softening of the hydrogels was noticed at the end of the proliferation experiments (see section 3.2.2.2 below), their mechanical properties (post cell-culture moduli) were reevaluated after the last proliferation time-point.

3.2.2.2 Cell viability and proliferation on hyaluronic acid-based hydrogels

Cytotoxicity assay: To assess the early cytotoxicity of the synthesized hydrogels, primary guinea pig scleral fibroblasts were seeded over the surface of polymerized hydrogels at a density of $10x10^3$ cells/cm^2 and cultured for 2 days. Hydrogels were then stained for 30 minutes at 37°C with a calcein AM/ethidium homodimer solution in PBS. Images were acquired using a swept field confocal microscope (Prairie Technologies).

Alamar Blue proliferation assay: To quantify cell proliferation in the hydrogel surfaces and to determine whether it is dependent on the concentration of cell-binding peptide, a 14-day proliferation assay was performed with the non-toxic reagent Alamar Blue, which allows for repeated testing of the same cell population. For this cell proliferation assay, guinea pig scleral fibroblasts were seeded on the hydrogels (synthesized in 24-well Millipore inserts) or on tissue culture polystyrene (TCPS) plates alone at a density of $5x10^3$ cells/cm^2, for a total of $3x10^3$ cells and $9.5x10^3$ cells seeded onto the hydrogel and TCPS surfaces, respectively. Five replicates were tested for each condition. Cell numbers were assessed on days 7 and 14 using Alamar Blue (Life Technologies), according to the manufacturer's instructions. The reagent was first sterilized by filtering through a 200 μm-pore syringe filter. The reagent was incubated with the samples for 2 h at 37°C, then the solution was carefully removed and its fluorescence determined at excitation/emission of 570 nm/600 nm.

3.2.2.3 Migration through hyaluronic acid-based hydrogels

As part of our migration assay, we established a stable cell monolayer before exposing the cells to the migration "stimulus", i.e., the hydrogels. This design more closely represent the *in vivo* situation to which the scleral cells would be exposed to the implants, and so better predicts their preference of one environment over another. Three hydrogels each of 200 Pa 0 μM RGD and 380 μM RGD were synthesized for the migration assay. A schematic of the assay setup is shown in Figure 3.2.

Cell culture migration assay set-up: Primary guinea pig scleral fibroblasts were first seeded onto 8 mm-diameter glass coverslips (Fisher Scientific) at a density of $20x10^2$ cells/cm^2 and allowed to attach overnight. The cell-seeded coverslips were transferred (cell side facing up) to the bottom of 24-well inserts using fine forceps (Erem Eropssa Straight Ultra Fine Point Tweezer). Any liquid remaining around the edges of the coverslips was pipetted off. Hydrogel solutions (200 Pa, 0 and 380 μM RGD) were polymerized over the cell-seeded coverslips and the system was incubated for 2 days at 37°C, 5% CO_2. The hydrogels were then washed in PBS, fixed in 4% paraformaldehyde for 30 minutes, incubated with 0.2% Triton for 8 minutes, and stained to label the cell nuclei (NucBlue Fixed Cell Stain Ready Probes, Molecular Probes). Z-stacks (10 μm-thick slices) were acquired using an inverted confocal microscope (Zeiss LSM 710 AxioObserver), with a 405 nm laser set at 2.65 mW power. Each insert was placed over a coverslip # 1.5 (Zeiss), and positioned on a stage above a 10X objective. Images were acquired at every other field of view along the surface of the hydrogel, with laser power and exposure kept constant.

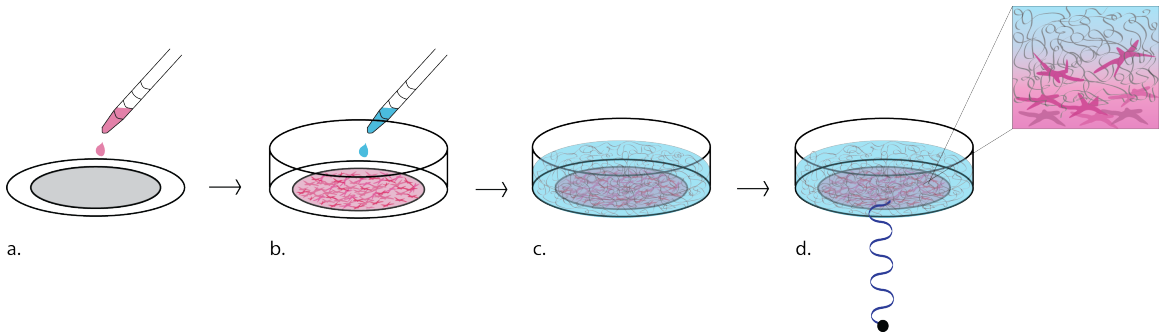

Figure 3.2. Setup for migration assay through hyaluronic acid hydrogels. Guinea pig scleral fibroblasts were seeded on a glass coverslip (A) and allowed to attach overnight. Coverslips were transferred to a 24-well insert, then a solution of hyaluronic acid macromers was polymerized over the cell surface (B). Maintenance cell culture media was added to the system, which was then cultured for 2 days (C). After the culture period, the migration assay setups were fixed, stained, and imaged (D). Z-stacks (10 μm-thick steps) were acquired through the entire surface of the hydrogel (skipping every other field of view).

Z-stack automated image analysis: The number of cells in each captured Z-stack image was counted using an automated analysis script. The software first processed each image with Source Extractor (http://www.astromatic.net/software/sextractor), a source detection algorithm used to identify galaxies in astronomical images. Source Extractor was designed to recognize continuous light sources, a situation akin to fluorescent cell nuclei in a hydrogel. Every single image was subjected to the following processing steps, which are also illustrated in Figure 3.3. The raw images (Figure 3.3A) underwent background measurement and subtraction (background depicted in Figure 3.3B). Detections were separated from neighboring sources through thresholding, deblending, and segmentation (Figure 3.3C). The shape, brightness, and position of all detections were measured (Figure 3.3D), generating a detection database.

Since cells spanned multiple stacks, the images were analyzed with a custom association algorithm that iteratively searched through all detections to find the center of each cell nucleus – that is, the position where the nucleus was most in focus. Once the nuclei center were identified, we determined their distance to the reference starting position (glass coverslip). The algorithm was optimized to account for crowded sources, associations (one or more cells that seem to form a single object, but likely separate further down into the stack), and spurious detections. A verification image is generated for each slice in the stack (Figure 3.3E), labeling each nucleus with a number. Non-equivocal detections are labeled in blue, associations are labeled in yellow, spurious detections (small, non-spherical bright spots that are too small to be a cell nucleus) are labeled in red, and nuclei in close proximity to each other (but still able to be identified as two separate bright spots) are indicated with a dotted circle.

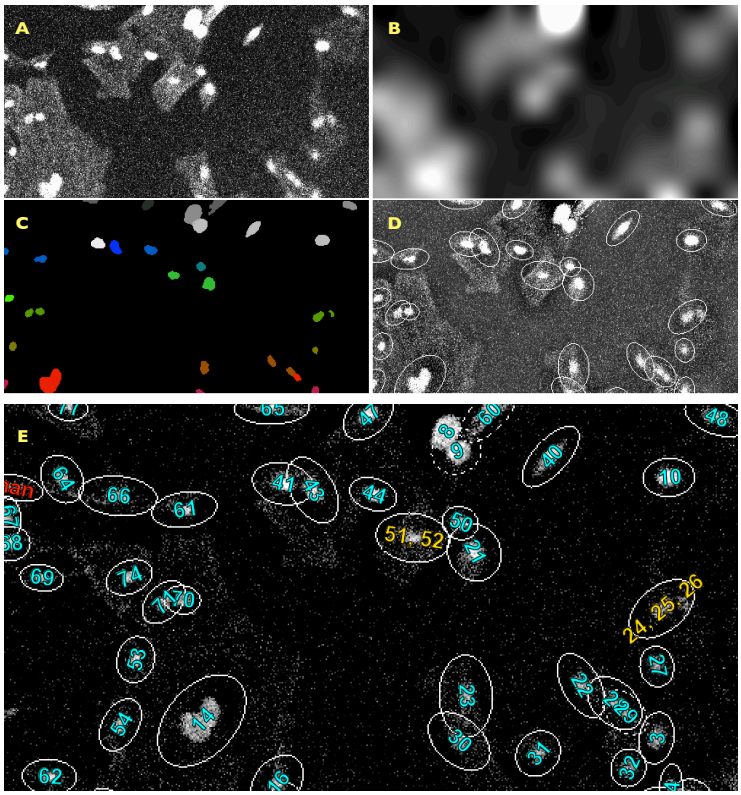

Figure 3.3. Steps in the image processing algorithm used to analyze images acquired in the migration assay. Each raw image (A) undergoes background measurement (B) and subtraction. Detections are further highlighed through thresholding, deblending and segmenting (C). The shape, brightness, and position of each identified object are measured (D). An association algorithm both determines the center of each nucleus and generates verification images that highlight all identified objects in the Z-stack (E).

The coverslip generally does not occupy a single slice in the Z-stack. We took advantage of the autofluorescence of the glass coverslip to generate a reference surface for each stack: the mean pixel brightness of each image was measured and plotted as a function of distance. The peak was fitted to a Gaussian function using least squares regression, then its mean was treated as the reference location for the nuclei identified in that stack (Figure 3.4).

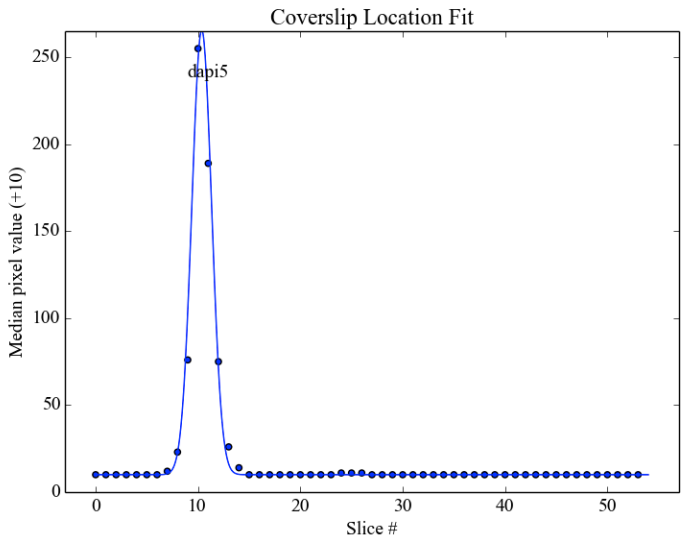

Figure 3.4. Graph of pixel brightness versus slice number, with fitted Gaussian function, used to identify the reference position for the Z-stack. Since the background brightness of the coverslip was so much higher than that of the rest of the stack, the coverslip's position was easily identified by a peak in the graph.

All the code used to process these images (developed by Adam Morgan) along with documentation to aid its implementation, is available at https://github.com/qmorgan/qsoft/tree/master/Software/Cell.

3.3. Results

The hydrogels tested here were intended for *in vivo* injections through a 19G sub-Tenon's capsule needle. The 2.0 and 3.3 weight percent solutions were selected because they represented the maximum amount of macromer that could easily be diluted (3.3 weight percent), along with a softer formulation tested to cover the possibility of post-implantation deformation of the scleral shell with the stiffer hydrogel, a clearly undesirable surgical outcome. The 100% crosslinking ratio was chosen to control the extent of hydrogel swelling upon contact with culture media (in the case of *in vitro* work) and tissue fluids, including blood and aqueous outflow (in the case of *in vivo* work).

3.3.1 Rheological characterization of hyaluronic acid - based hydrogels

Hydrogel moduli remained relatively constant during the frequency-sweep measurement, with a slight increase at higher testing frequencies, perhaps suggesting a shear-thickening effect. This behavior has implications for applications relying on injections, as in the current case; specifically, such hydrogels must be injected very slowly to ensure adequate delivery. The average complex moduli of 2 and 3.3 weight percent hydrogels were 177.0 ± 36.1 and 852.1 ± 42.2 Pa, respectively. For the sake of simplicity, these moduli will be approximated as 200 and 800 Pa in later discussions. These measured moduli indicate that the synthesized hydrogels are significantly softer than the guinea pig sclera, whose modulus has been reported as 2.09 ± 0.99 MPa for guinea pigs[227].

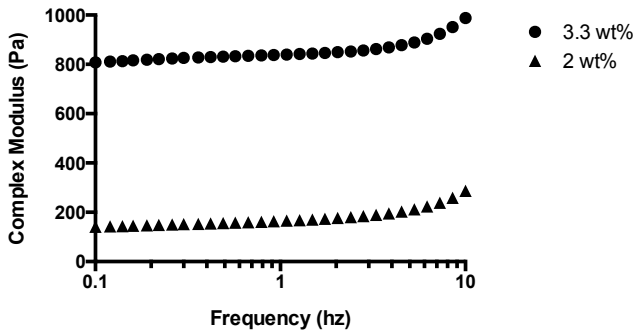

Figure 3.5. Rheological characterization of polymerized 2 and 3.3 wt% hyaluronic acid hydrogels with 380 μM RGD, plotted as complex shear modulus as a function of frequency, measured by oscillatory parallel plate rheology.

3.3.2 Cell viability and proliferation on hyaluronic acid - based hydrogels

To compare the biocompatibility of hydrogels for guinea pig scleral fibroblasts, cultures were stained with calcein AM (green stain, labels live cells) and ethidium homodimer (red stain, labels dead cells). Composite images of 3D stack projections are shown in Figure 3.6. The very low proportion of dead cells after 2 days of culture strongly suggests that the hydrogels are not toxic to scleral fibroblasts. However, the concentration of RGD did affect cell morphology; specifically, cells seeded onto hydrogels with 0 μM RGD retained a rounded shape, while cells seeded with RGD-containing hydrogels start to exhibit a spindle-like shape. Also, cell counts were consistently lower for the 0 μM gels, perhaps pointing to poor initial attachment to the hydrogel, and their subsequent loss in the process of replacing media with dye solution. Note also that during this optimization phase of this project, scleral fibroblasts were observed to take ~2-3 days to form strong attachments to the matrix, even where they displayed a more fibroblast-like (stellate) phenotype.

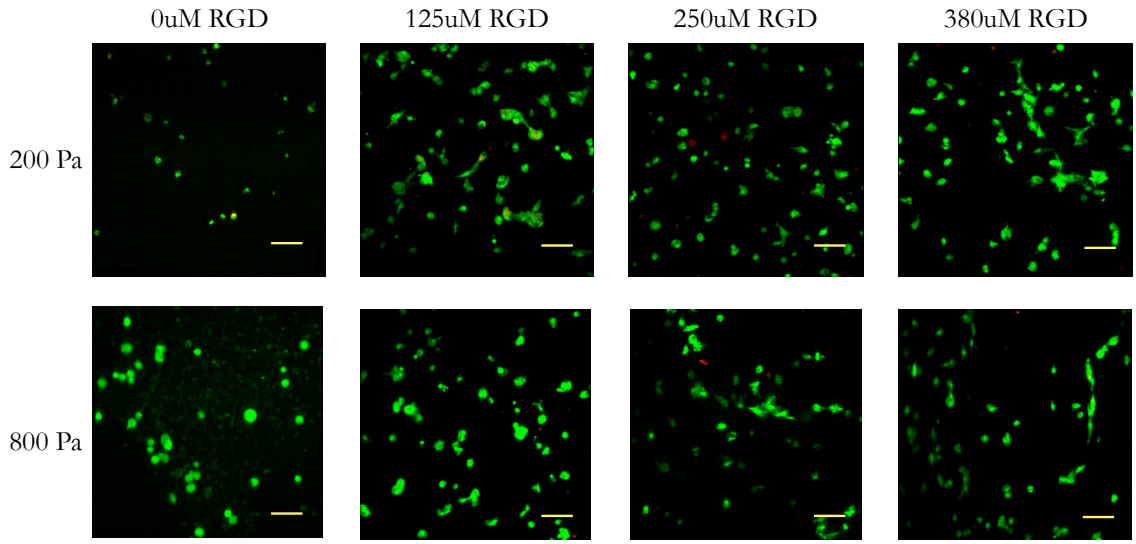

Figure 3.6. Z-stack projections of guinea pig scleral fibroblasts stained with calcein AM (indicator of live cells, green) and ethidium homodimer (indicator of dead cells, red), acquired after 2 days of 2D culture on 200 and 800 Pa hydrogels with varying RGD (cell-binding peptide) concentration.
Scale bars represent 100 μm.

To measure cell proliferation over a more extended time period, primary guinea pig scleral fibroblasts were seeded in 2D over polymerized hydrogels of varying moduli (200 & 800 Pa) and RGD concentrations (0-380 μM), and cell numbers assessed after 7 and 14 days of culture using Alamar Blue. To accurately relate the number of cells to the measured fluorescence, a standard curve was prepared with cells sourced from the same animal and same passage as used in the proliferation assay. Graphs of time-dependent proliferation for both hydrogels and control (tissue culture polystyrene) culture conditions are shown in Figure 3.7. There was a lag period before the cells entered their exponential growth phase; over this initial 7 day culture period, the number of cells on the HyA hydrogels remained relatively constant (or perhaps slightly decreased, as observed for the 125 μM hydrogels of both moduli), after which numbers substantially increased. However, at both 7 and 14 time points, cell numbers recorded with all 8 hydrogels were significantly lower than those recorded with tissue culture polystyrene.

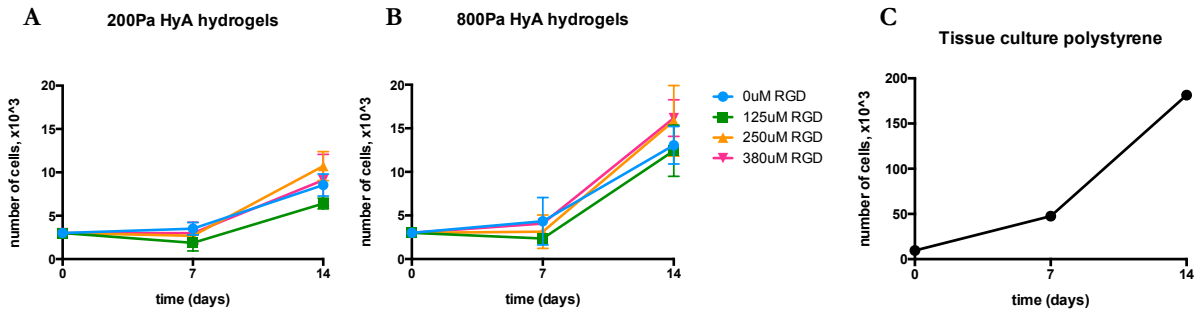

Figure 3.7. Guinea pig scleral fibroblast counts derived from cultures over 14 days on 200 Pa (A) and 800 Pa (B) hyaluronic acid hydrogels, with RGD concentrations varying from 0-380 μM, and tissue culture polystyrene (C, control). In all, cases, there is lag before cells began to proliferate. Note the different y-axis scale used in panel C. Data points represent mean ± standard deviation (SD) for 5 samples/condition.

A more detailed analysis of cell numbers at day 14 is shown in Figure 3.8. The influences of both gel modulus and RGD concentration were assessed with a two-way ANOVA and Tukey's multiple comparisons test (Figure 3.8C) using Graphpad Prism 6. The influence of RGD concentration was further analyzed for each of the two sets of hydrogels (200 & 800 Pa respectively), with a one-way ANOVA and Tukey's multiple comparisons test (Figures 3.8A and 3.8B). After 14 days in culture there was no statistically significant difference between the number of cells grown on hydrogels with 0, 125, 250, or 380 μM RGD, both for 200 and 800Pa hydrogels. Furthermore, irrespective of the stiffness of the hydrogel (200 or 800 Pa), proliferation rates for the hydrogels were consistently and significantly lower than that found for tissue culture polystyrene (Figures 3.8A and 3.8B). Hydrogel stiffness (modulus) had an inconsistent effect on cell proliferation, with stiffer compared to softer gels yielding significant higher cell numbers for the 125 and 380 μM RGD concentrations only (Figure 3.8C).

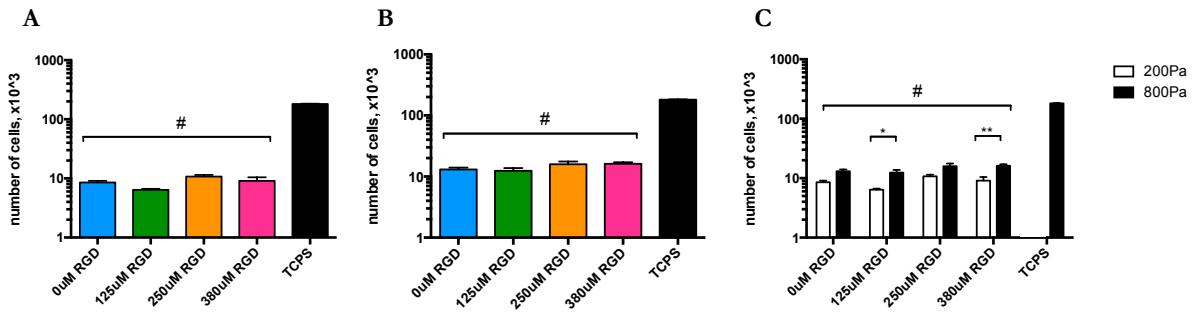

Figure 3.8. Guinea pig scleral fibroblast numbers after 14 days of culture on 200 Pa (A) and 800 Pa (B) hyaluronic acid hydrogels, with RGD concentrations varying from 0-380 μM, or on tissue culture polystyrene (TCPS, control). Columns represent mean + SD for 5 samples/condition. In panel C, the effect of modulus is compared, for each RGD concentration. * $p<0.05$, ** $p<0.01$, # significant difference from TCPS, $p<0.05$.

Over the course of the proliferation experiment, it was evident that the hydrogels became significantly softer, particularly those with the highest (380μM) RGD concentration. This was easily observed at days 7 and 14 of culture, when the media in the cell culture inserts was being replaced with Alamar Blue assay solution (the gels tended to "jiggle", like soft Jello, on slight movement). At day 14, in particular, some of the hydrogels were so soft that extreme care had to be taken not to aspirate them along with the media. These qualitative observations were verified with additional rheology measurements applied to the hydrogels at the end of the proliferation experiment. The post-cell culture results (complex shear modulus) for three hydrogels per condition are shown in Figure 3.9 and Table 3.1. For both 2.0 and 3.3 wt% conditions, the 380 μM RGD hydrogels had the softest moduli after 14 days of cell culture, having changed from 200 and 800 Pa to ~4.5 and 20.4 Pa, respectively.

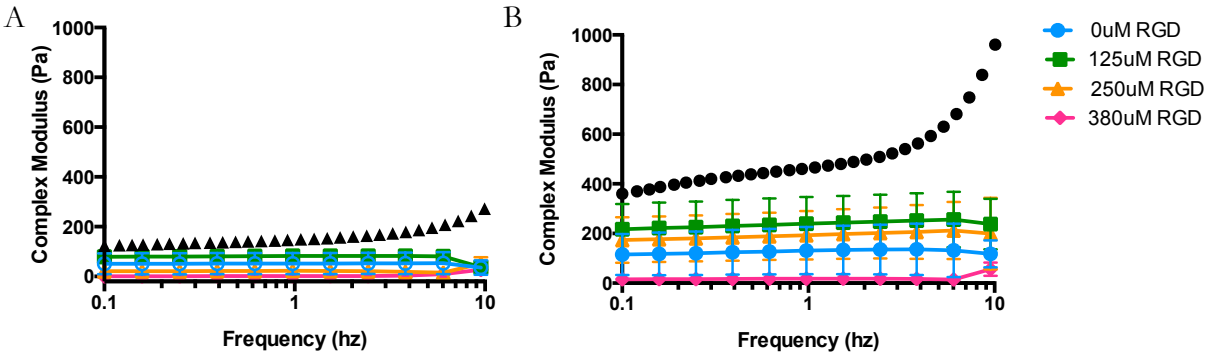

Figure 3.9. Results of rheological measurements on 2.0 (A) and 3.3 (B) wt% hydrogels of varying RGD concentrations after 14 days of cell culture (original moduli ~200 and ~800Pa, respectively). The complex modulus is plotted against frequency, ranging from 0.1 to 10 Hz. Points represent mean ± SD for 3 samples/condition. The black data points represent the moduli as measured immediately after synthesis (also shown in Figure 3.5).

[RGD], μM	Hydrogel modulus (Pa)	
	2.0 wt%	3.3 wt%
0	50.41 ± 4.88	126.40 ± 7.70
125	77.13 ± 13.15	237.00 ± 12.50
250	23.50 ± 9.57	192.3 ± 12.32
380	4.56 ± 7.86	20.39 ± 12.06

Table 3.1. Average moduli of hydrogels after 14 days of cell culture. Mean ± standard deviation. Original moduli immediately after synthesis: ~200Pa for 2.0 wt% and ~800Pa for 3.3 wt%.

3.3.3 Migration through hyaluronic acid -based hydrogels

Histograms of cell numbers ("Counts") versus slice number (position into the hydrogel, each slice is 10 μm-thick and the coverslip represents slice 0) for cells tracked during migration over two days through 200 Pa hydrogels with either 0 μM or 380 μM RGD are shown in Figure 3.10. The results for each of three samples of each type are represented by different colors (red, blue, and green), and the fields of view imaged for each hydrogel are distinguished as variations in the shade of each of the colors. The figure also contains a line representing the cumulative percentage of migrating cells; a dotted line indicates the 50th location percentile of the hydrogel. Note that the x-axis cuts off at slice number 80, beyond which there was only 1 cell per slice. The truncation of the x-axis allows for easier comparison of the two tested hydrogel conditions, and gives focus to the histograms representing the last gel location (slice), which contain relatively large numbers of cells.

Over 2 days in culture, scleral fibroblast migration through the 0 μM RGD hydrogels follows a somewhat bimodal shape, with an early tall narrow peak centered around slice 12 (~120 μm into the gel), followed by a more spread out distribution from slices 20-50 (200-500 μm into the gel). A very small number of cells remain attached to the coverslip (see bars near slice # 0). The peak number of migrating cells occurs near the fiftieth percentile, which is located at around slice 15 (~150 μm into the gel) (Figure 3.10A). With the 380 μM RGD hydrogels, many more cells remained attached to the coverslips compared to their 0 μM RGD counterparts (Figure 3.10B). Nonetheless, the migration patterns in these hydrogels can also be considered bimodal, but with a broader early peak in a similar location to that of the 0 μM RGD gels (slice 15 vs. slice 12). The other main difference observed with the 380 μM RGD gels compared to 0 μM RGD gels is that more cells were located deeper into the gels, with small but consistent numbers recorded 600-700 μm into the gel (slices 60-70). Thus while cells appeared to be more reluctant to migrate into the 380 μM RGD hydrogels than into the 0 μM RGD hydrogels, the subpopulation that did, migrated further.

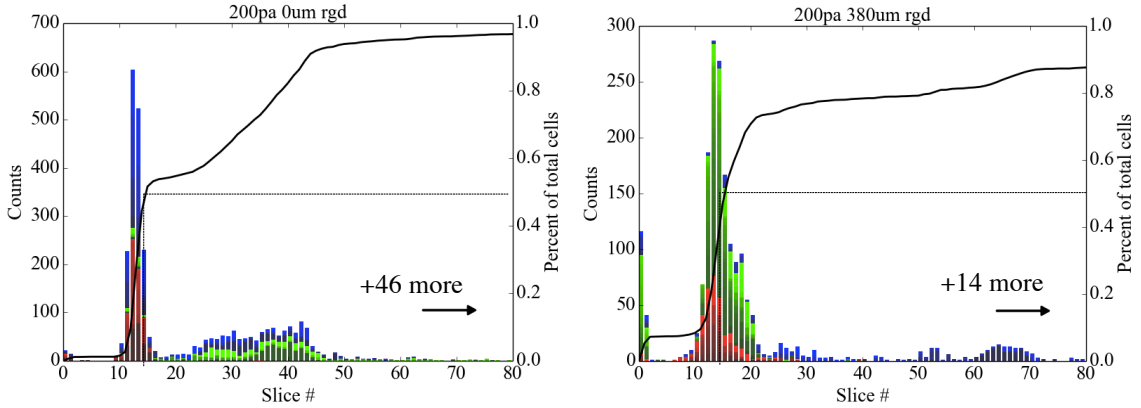

Figure 3.10. Graph of scleral fibroblast migration through 0 μM RGD (left panel) and 380 μM RGD (right panel) hydrogels, both 200 Pa, after 2 days of culture (n=3). Each color represents the results for different samples (n=3) of each of the tested hydrogels. The inserted text refers to the number of single cells counted after slide 80.

3.4 Discussion

The experiments in this chapter were designed to characterize the interactions between guinea pig scleral fibroblasts and HyA hydrogels *in vitro*, to assess their toxicity and ability to foster proliferation and migration. Such testing plays an important role in the development of new tissue engineering therapies, as they can aid in the optimization of hydrogel composition and shed light onto the behavior of cells under simpler, more controlled conditions.

The HyA hydrogels tested in this study were quite soft - significantly softer than guinea pig sclera, and thus cannot be considered suitable scleral buckling materials. They have a relatively long crosslinking time (30-45 minutes), which proves beneficial – they are relatively easy to inject and can be then manipulated in situ, into a shell conforming with the potential space between Tenon's capsule and a wide area of the posterior sclera. Thus the hydrogel implants can be positioned well to support cell migration from adjacent tissues, at the same time minimizing the risk of mechanical distortion of the globe.

Overall the results of the toxicity and proliferation assays suggested that the hydrogels exhibited good biocompatibility with the scleral fibroblasts. The use of an extended culture duration (14 days) in combination with the Alamar Blue assay also proved very informative, as the scleral fibroblasts did not enter an exponential growth phase until after 7 days of culture, with very little change in cell numbers being observed for all hydrogels tested at this early time-point. Such delays in entering an exponential growth phase is not entirely unexpected, as soft substrates have been shown to inhibit spreading and migration not only of scleral fibroblasts, but of other cell types as well [62,228,229]. Nonetheless, after 14 days in culture, the number of migrating cells had significantly increased, by 184±43, 113±21, 257±56, and 204±99% for 200 Pa - 0, 125, 250, and 380 μM RGD hydrogels respectively. For the 800 Pa hydrogels, the percent increases were 335±72, 314±98, 428±125, and 429±70% for 0, 125, 250, and 380 μM hydrogels. Expression of the cell migration data in this way also highlighted the potential benefit of using a stiffer hydrogel.

The RGD concentration had no significant effect on cell numbers, as assessed at the end of the 14-day culture period, with similar RGD-concentration independence recorded with 200 Pa and 800 Pa

gels. This result allows for two points of discussion. First, it is of interest that the guinea pig scleral fibroblasts survived well in hydrogels with no added RGD peptides, suggesting that in the absence of RGD-binding integrins the cells were able to engage with other elements of the hydrogels, possibly through CD44 receptors. Although CD44 receptors have not yet been characterized in mature scleral fibroblasts, they have been identified in multipotent stem cells resident in mouse scleras [230]. Second, increasing the RGD to concentrations as high as 380 μM had no deleterious effects on cell numbers, implying that cell-matrix engagement was not so extensive as to impair cytoskeletal cell changes necessary for mitosis. However, despite the apparent homogeneity in cell proliferation behavior for hydrogels of different RGD concentrations, their moduli were measurably different at the end of the 14 day culture period, most notably for the 380 μM RGD gels, which became significantly softer. These changes offer further evidence that the scleral fibroblasts were actively interacting with the hydrogels, in this case degrading these matrices, presumably through secretion of MMPs and hyaluronidase. Note, however, that the reduction in modulus did not show a dose-dependent relationship with RGD concentration.

These results, in conjunction with those from the proliferation assays, indicate that scleral fibroblasts are able to survive and proliferate in HyA hydrogels of moduli 200 and 800 Pa, with RGD concentrations ranging from 0-380 μM. Proliferation was evident even in the absence of added cell-binding motifs and on soft hydrogels. This finding is of itself interesting, given that the modulus of the cells' native environment is much higher, in the range of 2.09 ± 0.99 MPa for guinea pig sclera[227]. These are not the first reported cases of fibroblasts surviving on soft matrices, yet the scleral cell morphology and behavior observed with our HyA hydrogels suggests a more normal phenotype than reported in some other studies. For example, while scleral fibroblasts seeded on 1.5 mg/mL collagen matrices (modulus ~10 Pa) were able to survive, they maintained a rounded morphology, unlike primary fibroblasts isolated from Tenon's capsule and corneas [231,232]. In another series of studies, the ability of human foreskin fibroblasts to migrate and generate traction on soft (4 Pa) collagen matrices, was dependent on the addition of Platelet Derived Growth Factor to the culture medium[231,233].

In addition to being able to proliferate in 0 μM RGD hydrogels, scleral fibroblasts were also able to migrate through them, in a manner quite similar to that observed with the 380 μM RGD hydrogels. In the design of the migration assay described in this chapter, the cells were allowed to form a stable monolayer on a glass coverslip before being exposed to the hydrogel, and therefore could "choose" to remain on the coverslip instead of migrating into the soft synthetic matrix. This assay method has the additional advantage of avoiding potential confounding effects that can arise when cells do not readily attach to the substrate; unattached cells are expected to die, distorting early cell counts, but under the current assay conditions this problem was avoided by allowing cells to first attach to the more rigid glass coverslips. As hyaluronic acid is a key component of scleral extracellular matrix [16], it is not surprising that scleral fibroblasts can thrive in a hydrogel composed primarily of this glycosaminoglycan. However, given that fibroblasts exhibit a strong preference for stiffer substrates[234], it is surprising that cells migrated into the hydrogel so promptly, when they could have remained on the significantly stiffer glass coverslip. Thus our migration data argue for influences beyond matrix stiffness, perhaps tied to more compatible binding sites offered by the hydrogel, imparting a chemotactic property to it.

3.5 Summary & conclusion

Synthetic hyaluronic acid-based hydrogels were synthesized by combining acrylated hyaluronic acid with and without the cell-binding peptide bsp-RGD(15) to a thiol-terminated peptide crosslinker that is amenable to degradation by MMPs expressed by scleral fibroblasts. Varying the monomer content altered the modulus of the gels; the 2.0 wt% and 3.3 wt% had moduli of 200 Pa and 800Pa, respectively. Yet both gels could be easily injected through a 19G needle, the gauge used for the injections in guinea pigs. Proliferation assays indicated that cells were able to proliferate in these hydrogels even in the absence of RGD-containing peptides. These results were reinforced by those from migration assays: though cells migrated slightly further in the RGD-containing gels, the 50^{th} percentile migration distance (i.e. distance in the gel at which 50% of the cells have migrated) was similar for the 0 and 380 μM RGD hydrogels.

The results from the *in vitro* studies reported in this chapter indicate that the HyA-based hydrogels are highly compatible with guinea pig scleral fibroblasts, as judged by their ability to both migrate and proliferate in these gels. Based on these promising results, the decision was made to proceed with *in vivo* myopia-control experiments in guinea pigs. Based on the *in vitro* performance profiles of the hydrogels tested and the specific requirement for our *in vivo* application that the hydrogel be injectable, we chose for the follow-up experiments to limit testing largely to a 200 Pa hydrogel formulation. This formulation was slightly easier to inject than the stiffer 800 Pa hydrogels and exhibits proven compatibility with both cell migration and proliferation.

Chapter 4. Myopia control in guinea pigs through hydrogel-mediated scleral support and regeneration

4.1. Introduction

As discussed in Chapter 1, treatments for myopia have been mostly limited to pharmacological and optical strategies. A few studies have investigated the intriguing possibility of myopia control through scleral support[60–62], opening research path towards a therapy that could be implemented at the early stages of myopia development in high-risk cases, such as children from families with a history of high myopia. This early intervention could prevent excessive eye elongation, restraining myopia to levels that carry a lower risk of vision-threatening conditions.

Though there is a dearth of research in the field of biomaterial-based myopia control, a variety of biomaterials have been tested for other ocular applications such as drug delivery. In the area of trans-scleral drug delivery, a few examples include the use of scleral plugs[235], adhesive ocular inserts [236], and biodegradable inserts[237–240]. A nail-like poly(lactic-co-glycolic) (PLGA)-based drug-eluting scleral plug has been developed for treatment of endophthalmitis (intraocular inflammation) as an alternative to the frequent intravitreal injection of antibiotics and steroids currently used to treat this disease [235]. Gilhotra and colleagues formulated an anti-inflammatory drug, piroxicam, into bioadhesive ocular inserts consisting of poly(vinylpyrrolidone), 0.5% carboxymethylcellulose, and 1% hydroxypropylmethylcellulose [236]. In a similar application, episcleral implants loaded with a chemotherapeutic drug, topotecan, were developed for treatment of advanced intraocular retinoblastoma [237]. This study employed a 7x3 mm double-faced polymeric disc of poly(caprolactone), with separate drug-loaded and blank faces; this design was intended to isolate the drug from the conjunctiva, instead directing drug release towards the interior of the eye, and so decreasing drug loss to systemic circulation. Along the same lines, a two-sided poly(D,L-lactide) implant loaded with the corticosteroid triamcinolone was developed for ophthalmic use [239,240].

Hyaluronic acid has a long history of being used for ophthalmic applications. In fact, the first isolation of hyaluronic acid was performed from bovine vitreous humor in 1934 [241]. In the realm of ophthalmic surgery, hyaluronic acid been studied extensively as a vitreous substitute[242,243]. It is also a critical tool in other surgical procedures, where it is used to protect cells and to maintain spacing of relevant ocular tissues, as required during such surgeries as cataract removal, intraocular lens implantation, and corneal transplants[244,245].

In Chapter 3, we described *in vitro* developmental studies undertaken to establish a suitable hyaluronic acid-based hydrogel that was capable of supporting scleral cell migration and proliferation while also being injectable, in keeping with our desire to develop a relatively noninvasive treatment.

In Chapter 2, we showed that we could successfully induce myopia in one strain of young guinea pigs using form deprivation. This chapter makes use of the findings described in Chapters 2 and 3. It

recounts experiments in which we tested the ability of the hyaluronic acid-based hydrogel scaffold to control myopia in our animal model. The hydrogel was injected under Tenon's capsule at the posterior pole of guinea pig eyes in the early stage of myopia development (after one week of form deprivation). The myopia-inducing stimulus (form deprivation) was continued for three more weeks to simulate continued disease progression, as one would expect to encounter in myopic children. We hypothesized that when the hydrogel is injected *in vivo*, scleral fibroblasts would migrate into it and remodel it as they secrete matrix, degrading the surrounding material and over time replacing the implanted hydrogel with a new layer of scleral matrix that would thus thicken and strengthen the native sclera. Recall that the hydrogel is crosslinked with peptide-based crosslinkers degradable by matrix metalloproteases. When injected adjacent to the sclera *in vivo*, these hydrogels can be expected to be degraded by MMPs and hyaluronidase, both of which are secreted by scleral cells [26].

Envisaged as an injectable treatment, our approach is less invasive than current scleral buckling surgeries used to treat high myopia [57,58] and does not rely on availability of donor tissue. Because the protocol does not rely on *in situ* chemical reactions, as with scleral cross-linking treatments currently under investigation by others, the possibility of toxic reactions is also avoided. As discussed in section 3.1, the latter treatments make use of potentially toxic photoinitiators and in some cases, UV activation [211]. If proven effective and safe, our proposed treatment could therefore become a viable myopia-control alternative that could be implemented in young patients still in the early stages of myopia progression.

4.2. Materials and methods

4.2.1. Animals

Male and female pigmented English Short hair guinea pigs were generously provided by Prof. John Phillips (University of Auckland, NZ) and housed in breeding pairs or harems (1 male and a maximum of 3 females), in oval-shaped breeding tubs. Pups were weaned at 5 days of age and housed as single sex pairs in transparent plastic wire-top cages, in a room with 12h/12h light/dark cycle. Cages measured 16 inches wide by 20 inches long and had a layer of low-dust aspen shavings as bedding. The animals had free access to water and vitamin C-supplemented food, and received fresh fruit and vegetables three times a week as diet enrichment. All animal care and treatments in this study conformed to the ARVO Statement for the Use of Animals in Ophthalmic and Vision Research. All experimental protocols were approved by the Animal Care and Use Committee of the University of California-Berkeley.

4.2.2. Experimental design

A schematic of the experimental design for the work described in this chapter can be seen in Figure 4.1. Guinea pigs were fitted with diffusers at 7 days of age, after baseline A-scan ultrasonography and refraction measurements. Diffusers were worn for 7 days, then the animals in which the diffuser-treated eye grew at least 50 μm more than its contralateral control were assigned into one of three groups: Diffuser only (Group I), Diffuser + HyA (Group II), or Diffuser + Sham (Group III). Group I continued to wear the diffusers for an additional 21 days. Group II received a sub-Tenon's capsule injection of 200 Pa 380 μM RGD hyaluronic acid hydrogel on experimental day 7 (14 days of age), while Group III received a sub-Tenon's capsule injection of the same buffer used to dissolve the HyA precursors (0.2 M triethanolamine buffer, TEA). Both groups II and III were re-fitted with diffusers immediately after surgery; as with Group I, they were worn for an additional 21 days. Ultrasonography measurements were made twice a week, at experimental days 0, 3, 7, 14, 17,

21, 24, and 28. Cycloplegic refraction measurements were made on experimental days 0, 14, and 28 (7, 21, and 35 days of age). On the last day of the monitoring period (experimental day 28; 35 days of age), retinal activity, visual acuity, and intraocular pressure were measured using electroretinography, an Optomotry device, and a rebound tonometer, respectively. After the final measurements, the guinea pigs were euthanized and their eyes were processed for histology. An additional animal was imaged in a 7 T small animal MRI, for *in vivo* visualization of the implanted polymer.

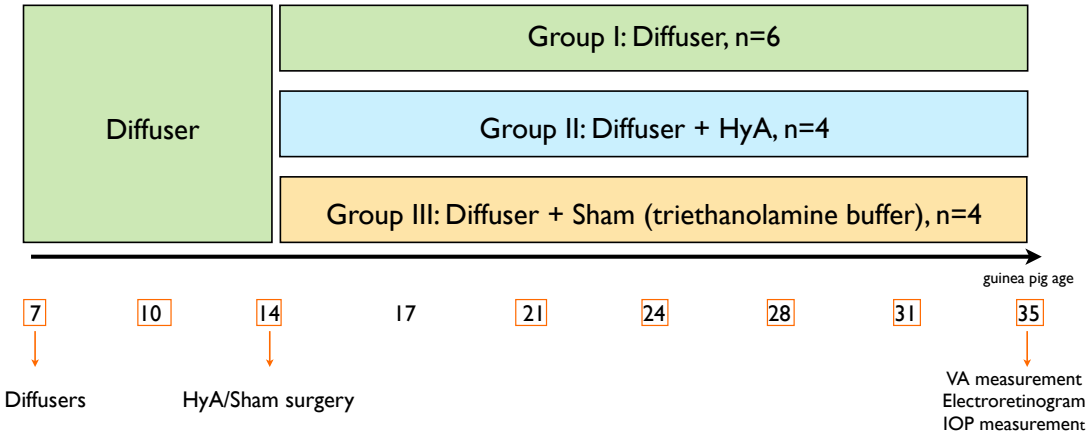

Figure 4.1. Schematic representation of experimental design and measurements. Guinea pigs were 7 days old at the start of the experiment. After 7 days of diffuser wear (simulating early stages of myopia development), guinea pigs with a minimum interocular difference in elongation of 50 μm (treated minus control) were divided into 3 groups: Diffuser-only, Diffuser + HyA, and Diffuser + Sham. The latter two groups received a sub-Tenon's capsule injection of either HyA or TEA buffer. Axial eye length of all animals was measured using A-scan ultrasonography 8 times, on the days marked by the orange squares. Cycloplegic refractions were measured at experimental days 0, 14, and 28 (7, 21, and 35 days of age).

4.2.3. Diffusers

The diffuser manufacture and attachment protocols were adapted from those implemented in chicks [103]. All treatments were monocular, the untreated eye serving as a contralateral control (Figure 4.2). Diffusers were mounted on Velcro ring supports, made by punching a 1.8 cm central hole through a 3.5 cm circular hook Velcro® disc (part # 192346, Velcro Industries). Diffusers were prepared by hot-molding white styrene (Midwest Products Co, Part # 701-01) and fitting them onto the hook Velcro® surround with UV-curing glue (Norland Optical Adhesion 68, Part # 6801, Norland Products). Before fitting the diffusers, their transmittance was measured using a light meter (ILT1700, International Light Technologies). Only diffusers with transmittance of 15±1% were used for the study.

To attach the diffusers to the guinea pigs, rings of loop Velcro were made first prepared from discs using a 1.8 cm punch; four 1/8 sections of the circles were symmetrically affixed to the fur surrounding one of the guinea pig's eyes using a small amount of gel cyanoacrylate glue (SureHold® Plastic Surgery) [108].

Figure 4.2. Representative guinea pigs used as animal models in this study, showing the position of the hook Velcro segments (left panel) and a fitted diffuser (right panel). The right eye is left uncovered as a contralateral control (often referred to as "fellow eye").

4.2.4. Sub-Tenon's capsule surgery

Sub-Tenon's capsule injections of 200 Pa 380 μM RGD HyA hydrogels (synthesized as described in Chapter 3) or 0.2 M triethanolamine (TEA) buffer (Sham) were performed at the posterior pole of guinea pig eyes after 7 days of diffuser treatment. The surgeries were performed with the aid of a surgical microscope and conformed to the UC Berkeley Animal Care and Use Committee guidelines for sterile surgery. Guinea pigs were anesthetized with a ketamine/xylazine cocktail (0.45/0.045 mg/kg body weight), placed over a warming pad, and covered with a sterile surgery blanket with an opening cut out for the eye. After cleaning the fur surrounding the eye with an alcohol pad, an eyelid retractor was positioned to increase visibility to the upper eye. A drop of local anesthetic was instilled onto the surface of the eye (0.5% Proparacaine Hydrochloride, Bausch & Lomb). An anchor suture (Reli® Plain Gut 5-0, Myco Medical Supplies) was threaded through the upper conjunctiva, secured with a hemostat, and gently pulled downwards in a nasal direction to roll the eye and facilitate access to the posterior sclera. Using surgical micro-scissors, an incision (5-10 mm wide) was made through the conjunctiva, episclera, and Tenon's capsule, exposing the sclera. The sclera was separated from its overlying tissues using blunt forceps and the incision was loosely closed using a loop suture (6-0 or 7-0 silk suture, Ethicon) – note that the incision was not sutured off completely – that is, the silk suture was not tightened and knotted. At this point, the injection solution was prepared by mixing diluted HyA precursors with diluted crosslinker (for Diffuser + HyA group). 80 μL of hydrogel (for Diffuser + HyA group) or TEA buffer (for Diffuser + Sham group) were drawn through a zero-dead-volume syringe fitted with a curved 19G retrobulbar injection needle (Beaver-Visitec), which was then threaded through the loop suture to reach the posterior pole of the ocular globe. The hydrogel/buffer was injected very slowly into the sub-Tenon's space (note that at this stage a variable amount of the hydrogel leaked back out of the incision; thus the volume of solution remaining at the injection site is also subject to variation, being as low as ~50 μL). The speed of injection is critical in this process, as too rapid injections can lead to the formation of bubbles and expulsion of much larger amounts of the hydrogel/buffer through the surgical incision. The loop suture was gently closed as the same time as the needle was retracted from the incision, to minimize escape of solution from the injection site. At this point, the incision was fully closed and the suture tied off. Topical moxifloxacin hydrochloride solution (Vigamox, Alcon) was applied to the surface of the eye, the lid retractor was removed, any blood or fluid was

very gently cleared away with sterile gauze. Diffusers were replaced and guinea pigs were kept on a warming pad until completely recovered from anesthesia. Topical moxiflocaxin was instilled once daily for two days following the surgery. For the remainder of the study, the operated eyes were closely examined for signs of inflammation (redness, swelling, discharge, eyelid ptosis).

It must be noted that a relatively soft (200 Pa) hydrogel was selected for the *in vivo* myopia control experiments after preliminary *in vivo* experiments using a stiffer (800 Pa) formulation revealed evidence of scleral indentation and distortion. An example of this phenomenon can be seen in Figure 4.3 (which also features a larger injection volume, ~100 μL). These early experiments also helped to optimize the volume of hydrogel that should be injected into the sub-Tenon's space.

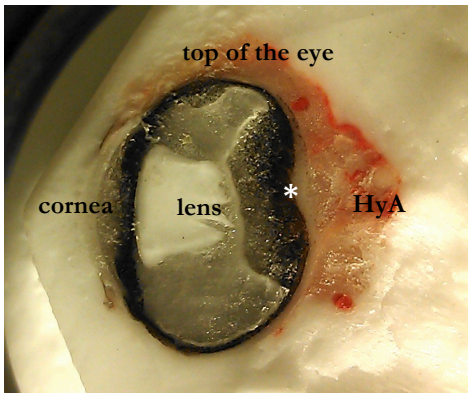

Figure 4.3. Guinea pig eye enucleated 2 weeks after a ~100 μL sub-Tenon's capsule injection of 800 Pa, 380 μM RGD HyA hydrogel and embedded in Optimal Cutting Temperature (OCT) compound. The asterisk marks the region of scleral indentation resulting from by the implantation of a relatively stiff (800 Pa) hydrogel.

4.2.5. Magnetic Resonance Imaging (MRI)

A two week-old pigmented NZ guinea pig received a sub-Tenon's capsule injection of HyA hydrogel (200 Pa, 380μM RGD) as described above. After a two-day recovery period, it was transported to the 7 T Small Animal MRI Facility at the University of California – San Francisco, China Basin. T2-weighed images were acquired using a spin-echo multislice imaging sequence.

The imaging made use of an additional surface coil positioned over the eye. All aspects of the imaging procedure, including the preparation of the animal, were performed by an experienced MRI technician. No contrast agents were used. The guinea pig was anesthetized with 3% isoflurane in oxygen and placed on the MRI imaging platform. Body temperature was kept at 37°C with heated air jets; body temperature and respiration were continuously monitored through a rectal probe and pressure pad, respectively. Artificial tear gel was applied to the corneas to prevent them from drying during imaging.

4.2.6. Measurements

4.2.6.1. Refractive errors and ocular biometry

Both refractive error and axial ocular dimensional data were collected over the experimental period. Cycloplegic refractions were measured using streak retinoscopy on awake animals, 30 minutes after

instillation of 1% cyclopentolate hydrochloride (Bausch & Lomb). Refractive errors are reported as Spherical Equivalent Refractions (average of the results for the two principal meridians).

As described above, axial length measurements were made more regularly, twice a week, over the 28-day duration of the experiment. The only exception was the measurement at experimental day 10 (3 days after surgery); a few animals died following this measurement when we were undertaking pilot studies to optimize the surgery and follow-up procedures. One possible explanation is that animals were more likely to die when they were anesthetized twice in short succession. When we experimented with skipping the day 10 measurement, no more animals died during the post-surgery phase of the experiment, and we therefore adopted this modified measurement schedule in all subsequent guinea pig experiments.

High frequency A-scan ultrasonography was performed using a custom-built system comprising a Panametrics ultrasound probe (P725-025-SU-R100) driven by a Panametrics amplifier (5072PR). For this procedure, animals were first placed under gaseous anesthesia (2.5-3% isoflurane in oxygen), with eyelid retractors inserted to hold eyes open during measurement [183]. Each measurement comprised an average of at least 7 recordings. Measurements on individual animals were conducted at the same time of day to prevent any possible confounding effects of circadian rhythms in eye growth [184]. The ultrasonography system has a resolution of 10 μm and outputs peaks representing the front of the cornea, front of the lens, back of the lens, vitreous/retina interface, retina/choroid interface, choroid/sclera interface, and back of the sclera. Optical axial length, otherwise referred to as axial length, was calculated by adding the axial dimensions of the anterior chamber, lens and vitreous chamber.

4.2.6.2. Functional testing and IOP measurement

Three measurements were performed at the end of the 28-day study to address concerns that the hydrogel and/or implantation surgery itself might be impacting ocular health.

Retinal function was assessed in guinea pigs from the Diffuser + HyA and Diffuser + Sham groups through flash electroretinograms (ERGs), using an Espion small animal unit (Diagnosys). ERGs can help to detect damage to the optic nerve and thus retinal ganglion cells sustained during or after the surgery, as well as retinal toxicity resulting from the hydrogel and/or buffer. They are a reliable tool – used both in animals and in human patients – that can detect altered retinal function with relatively high sensitivity. In addition, ERGs can distinguish between functional changes in the photoreceptor layer (origin of the a-wave), inner nuclear layer (origin of the b-wave), and ganglion cell layer (origin of photopic negative response).

Guinea pigs were anesthetized with a subcutaneous injection of 0.45/0.045 mg/kg of ketamine/xylazine, respectively; pupils were dilated with two drops of 1% cyclopentolate. Once the animals were completely anesthetized, they were placed in a prone position over a warming pad and the eyelids of both eyes were held open with lid retractors. A DTL electrode (Diagnosys) was placed over the lower cornea of each eye, close to the lower lid margin, and secured at the nasal and lateral canthi. One or two drops of 2.5% hydroxypropyl methylcellulose (EyeGel, Eyesupply USA) were used to further secure the electrode and to prevent the cornea from drying during the ERG measurement. Reference and ground electrodes (subcutaneous platinum needles, Diagnosys) were placed in the mouth (over the tongue and behind the incisor teeth) and under the neck skin, respectively. Flash ERG stimuli were delivered bilaterally through two Ganzfeld stimulators (50 mm internal diameter, Diagnosys ColorBurst), which were positioned such that each eye looked into the

center of the Ganzfeld dome. After 10 minutes of light adaptation at 3 cd/m^2, retinal light responses were recorded with stimuli comprising 20 4 ms-long white light flashes of intensity 3cd.s/m^2, each separated by a 1 second-long dark interval.

Amplitudes and implicit times (i.e. time from baseline to wave peak) for the a-wave, b-wave, and photopic negative response (PhNR) components were reported as indices of retinal function. A representative ERG wave illustrating each of the ERG components can be seen in Figure 4.4.

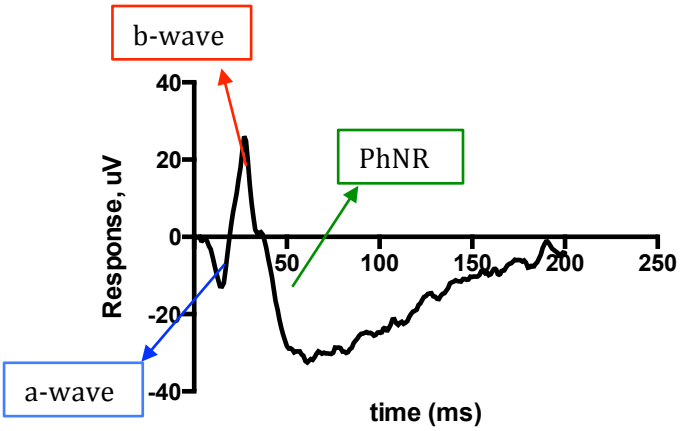

Figure 4.4. Representative guinea pig ERG response. The a-wave, b-wave, and photopic negative response (PhNR) components are highlighted in blue, red, and green, respectively. Amplitudes were measured as the voltage difference from the baseline to peak (for a-wave), peak of a-wave to peak of b-wave (for b-wave), and peak of b-wave to lowest subsequent trough (for PhNR). Implicit time was measured as the time (in milliseconds) from onset of stimulus to wave peak.

Behavioral measures of visual acuity were determined using an OptoMotry device (Cerebral Mechanics), which takes advantage of the optokinetic reflex (moving/revolving stimuli elicit involuntary eye and/or head and body movements). Guinea pigs were positioned at the center of its virtual cylinder and presented with drifting (12 degrees/second) sine wave grating stimuli that reversed in direction five times per tested frequency. The contrast of the gratings was set to 100%. Testing made use of built-in software driving a staircase test method, with each spatial frequency tested five times.

Finally, intraocular pressures (IOPs) were measured in awake animals using a small animal rebound tonometer (Tonolab, iCare). To avoid potentially confounding effects of circadian variations in IOP and elevated pressure due to stress, all measurements were performed at the same time of day, in a quiet room, once the animals had at least 3 minutes to calm down after being removed from their cage.

4.2.6.3. Statistical analyses and data representation

Statistical analyses were performed with Graphpad Prism 6. Much of the data are reported as interocular differences (treated eye minus control eye) or changes in the interocular differences (CID) over the 28-day treatment, i.e. normalized to baseline values. For all treatment groups, the differences between treated and contralateral (fellow) eyes were determined for all measured parameters and subsequently analyzed using a Wilcoxon Matched Pairs Test. To compare the

responses of the three treatment groups, interocular differences or changes therein were compared using a Mann Whitney or Kruskal-Wallis test with Dunn's multiple comparisons post-hoc test, as appropriate. P values lower than 0.05 were considered statistically significant. Data are also graphically represented as box-and-whisker plots, with the middle line indicating the median value of the data set, the box encompassing the 25^{th}-75^{th} percentiles, and the whiskers reaching the minimum and maximum data values. Whenever numerical values are given in the text, they represent means ± standard deviations (SDs).

4.2.7. Histological studies

At the end of the 28-day treatments, guinea pigs were euthanized with an intracardiac injection of sodium pentobarbital (Euthasol, Virbac Animal Health), delivered under anesthesia with 5% isoflurane in oxygen. Eyes were carefully enucleated and cleaned of excess extraorbital fat and muscle. Extreme care was taken not to disturb any remnants of hydrogel implant.

Eyes were fixed overnight in 4% paraformaldehyde and stored in 70% ethanol for up to 7 days. Paraffin embedding and sectioning was performed at the Histology Core of the Gladstone Institute (University of California – San Francisco). Eyes were placed in a cassette and dehydrated using the extended protocol for a Thermoshandon Excelsior tissue automated processor. Each eye was sliced in half using a microtome blade, and then embedded using a paraffin mold, with the cut surface facing down, taking care to avoid bubbles. Five μm-thick sections were cut using a microtome and then stained with either hematoxylin and eosin, to visualize overall morphology, or alcian blue, to highlight the HyA hydrogel. For both sets of stains, sections were rehydrated by serial incubations with xylene followed by decreasing concentrations of ethanol, from 100-0%. After the samples were stained (incubation for 3-5 minutes in hematoxylin followed by 30 seconds in eosin, or 10 minutes in hematoxylin followed by 30-45 minutes in 1% alcian blue in 3% acetic acid), they were then dehydrated with increasing concentrations of ethanol followed by washes in xylene. Finally, sections were mounted in DPX mounting medium (Fluka) and imaged under brightfield microscopy in an Axioplan 2 microscope (Zeiss) fitted with an Axioplan HRc camera (Zeiss).

4.3. Results

4.3.1. Effect of hydrogel/sham surgeries on axial components and refractive error

To ensure that every guinea pig participating in the study had a minimum amount of developed myopia, a selection criterion of 50 μm interocular difference in axial elongation after 7 days of form-deprivation was imposed onto the study. That is, if after 7 days of form-deprivation the treated eye did not elongate by at least 50 μm more than its fellow (control), that guinea pig was excluded from the study. The data below relates only to guinea pigs completing the entire experiment.

After 7 days of myopia induction with form deprivation, guinea pigs were randomly assigned to either continued diffuser treatment alone (Diffuser group), or diffuser treatment combined with either a sub-Tenon's capsule injection of HyA-based hydrogels (Diffusers + HyA) or TEA buffer (Diffuser + Sham). Diffusers were left in place and animals were monitored for an additional three weeks. Slight redness was initially observed around the surgical site in operated eyes, but no swelling or other signs of inflammation occurred.

The net CID for axial length over 28 days of treatment is shown for all three groups in Figure 4.5A. Changes in axial length for treated and control eyes in each group are plotted separately in Figure

4.5B. As expected, the diffuser-treated eyes of the Diffuser group, elongated significantly more than their contralateral control eyes over the 28-day treatment, by an average of 0.75±0.09 mm compared to 0.51±0.11 mm, respectively (p=0.03, Wilcoxon test), corresponding to a mean axial length CID of 0.24±0.08 mm. In contrast, for both the Diffuser + HyA and the Diffuser + Sham groups there were no statistically significant differences between the amount of elongation of treated and control eyes (0.63±0.03 vs. 0.61±0.06 mm for the Diffuser + HyA group and 0.62±0.06 vs. 0.62±0.02 mm for the Diffuser + Sham group). In terms of CIDs, the difference between the Diffuser and Diffuser + HyA groups was statistically significant, as was the difference between the Diffuser and Diffuser + Sham groups (Kruskal-Wallis test).

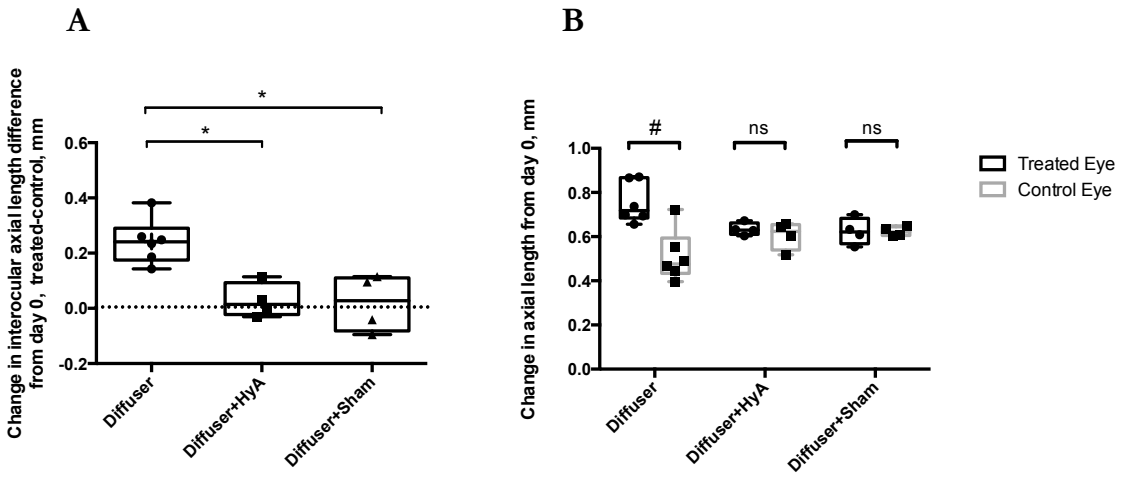

Figure 4.5. Axial length data for NZ guinea pigs after 28 days of Diffuser, Diffuser + HyA, or Diffuser + Sham treatment. Data for individual animals are included in both graphs. Panel A depicts total changes in interocular differences (treated minus control), with a dotted line at zero, the value at which the change in the treated eye is equal to the change in the control eye. Values above this line indicate that the treated eyes elongated more than the control eye. The axial length CID for the Diffuser group was significantly different from that for both Diffuser + HyA and Diffuser + Sham groups (Kruskal-Wallis test, * $p<0.05$). Panel B shows changes in axial lengths of treated (black bars) and control (gray bars) eyes. A significant difference in changes in axial length was found between treated and fellow eyes of animals in the Diffuser group (Wilcoxon Pairs test, # $p<0.05$), but not for the animals in the Diffuser + HyA or Diffuser + Sham groups.

Most of the axial length elongation in the Diffuser group occurred over the first 7 days of diffuser wear (0.166 mm out of the total 0.242 mm interocular elongation) (Figure 4.6). For both Diffuser + HyA and Diffuser + Sham groups, the CID measured at the first time point following the surgery (experimental day 14) is already nearly zero. That is, at this point the treated eyes are almost the same size as the control eyes, despite the fact that all treated eyes continued to receive an optical stimulus (form deprivation) to elongate.

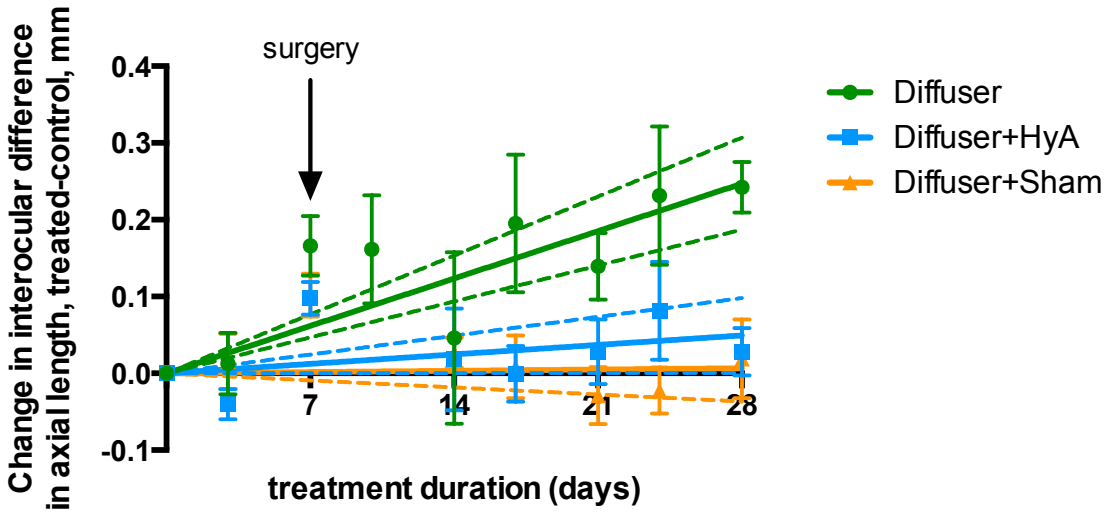

Figure 4.6. Change in interocular axial length difference over time for all treated groups, mean ± SD. The arrow indicates date of surgery, which was performed after 7 days of diffuser treatment (14 days of age). Axial length data has been fit with a linear regression curve and includes 95% confidence interval bands (dotted lines).

The different elongation patterns of the three treatment groups were further examined by comparing the elongation of treated and control eyes before the surgery (from treatment days 0-7), with the elongation that occurred after surgery (from treatment days 7-28) (Figure 4.7). The dotted line in the figure has a slope of 1; therefore mean values above the line indicate that change in treated eyes is greater than the change in control eyes. In the first cluster (days 0-7), the treated eyes of all three groups grew by approximately the same amount and more than their fellows, with the fellow eyes of the Diffuser + HyA and Diffuser + Sham groups growing, on average, slightly more than those of the Diffuser group. For the post-surgery cluster, treated eyes in the Diffuser group are the only ones to grow more than their fellow (control) eyes. However, notice that once again the fellow eyes of the Diffuser + HyA and Diffuser + Sham groups elongated slightly more than the fellow eyes of the Diffuser group.

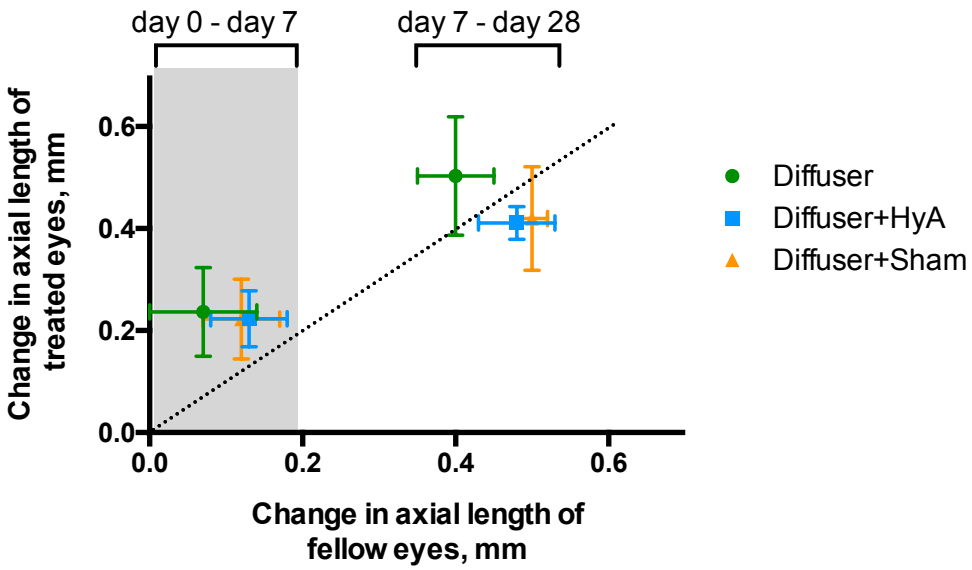

Figure 4.7. Change in axial length in treated eyes plotted against change in axial length in fellow (control) eyes. Data form two clusters, reflecting the different durations of the monitoring periods before the surgery (days 0-7) and after surgery (days 7-28). The dotted line, with a slope of 1, represents equal elongation in treated and fellow eyes. The pre-surgery period is shaded in gray.

To understand the origin of the changes in axial lengths described above, the changes in interocular differences over the 28-day treatment period for individual ocular components were analyzed. For the anterior segment components - anterior chamber depth (ACD) and lens thickness (LT), there were no statistically significant differences between the treated and control eyes for either component, even within the Diffuser group (Wilcoxon test) (Figure 4.8). Also, no significant intergroup differences were detected for either of the ocular components (Kruskal-Wallis test), although there are some interesting trends. Specifically, the mean change in interocular difference of ACD was more positive for the Diffuser + Sham group than either the Diffuser and Diffuser + HyA groups were (0.122±0.10 vs. 0.00±0.09 vs. -0.05±0.05 mm, respectively). In contrast, the mean change in interocular difference in LT was negative for the Diffuser + Sham group, contrasting with the positive means recorded for the other two groups (-0.06±0.12 vs. 0.07±0.07 vs. 0.09±0.07 mm, respectively). Because these differences in ACD and LT were in opposite directions, the changes in interocular differences in the combined ACD+LT varied little between the three groups (0.06±0.16 vs. 0.04±0.09 vs. 0.07±0.08, respectively; p=0.92).

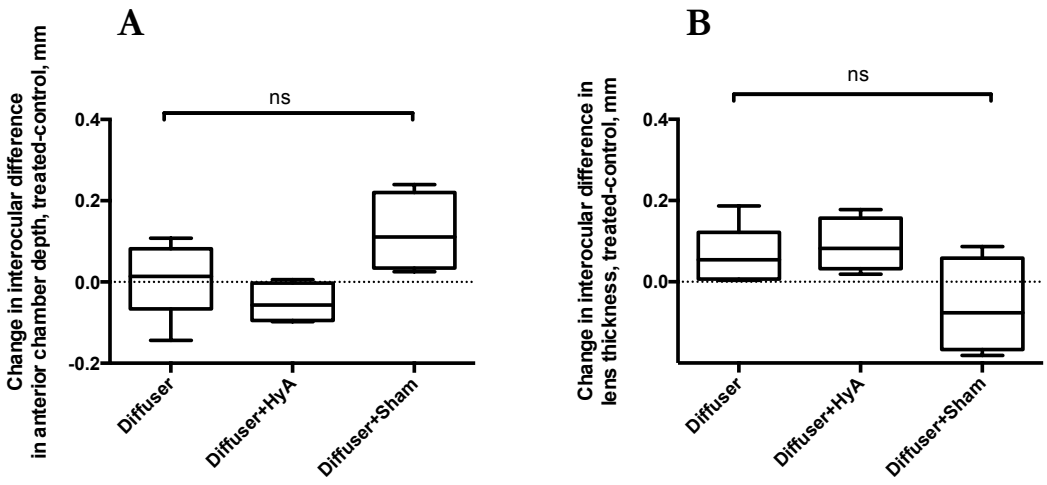

Figure 4.8. Change in interocular differences of anterior chamber depth (A) and lens thickness (B) for guinea pigs treated with Diffusers, Diffusers+HyA, and Diffusers+Sham. Changes in intergroup differences assessed with Kruskal-Wallis test and in treated vs. control eye differences assessed with a Wilcoxon test.

Typically, the axial length increases in myopia reflect increased elongation of the VCD. Changes in interocular VCD differences and their relationship to changes in interocular axial length differences changes are shown in Figure 4.9. The mean CIDs of vitreous chamber depth for Diffuser + HyA and Diffuser + Sham groups were approximately zero (-0.01 ± 0.10 and -0.02 ± 0.09 mm, respectively), compared to the larger positive value for the Diffuser group (0.17 ± 0.14 mm). Nonetheless, the changes in vitreous chamber depth for treated eyes were not significantly different from those of control eyes for any of the groups. Intergroup differences also did not reach statistical significance (Figure 4.9B). This lack of significance in the difference of VCD between treated and control eyes can be attributed to the large standard deviation in the control eye data (Table 4.1). In further analyses, the relationship between CID of axial length and CID of vitreous chamber depth were analyzed graphically (Figure 4.9A) and a regression line fitted to all data points (i.e., from all three groups). The two parameters proved to be strongly correlated (r^2= 0.76, p <0.001). Nonetheless, the CIDs for axial length and vitreous chamber depth appear to be better correlated for the Diffuser and Diffuser + Sham groups than for the Diffuser + HyA group. Given that form deprivation was shown to significantly increase the VCDs of treated eyes relative to the VCDs of control eyes in the same line of New Zealand guinea pigs (Chapter 2, Figure 2.11), it is likely that increasing the sample size would also yield a significant difference between the VCDs of treated and control eyes.

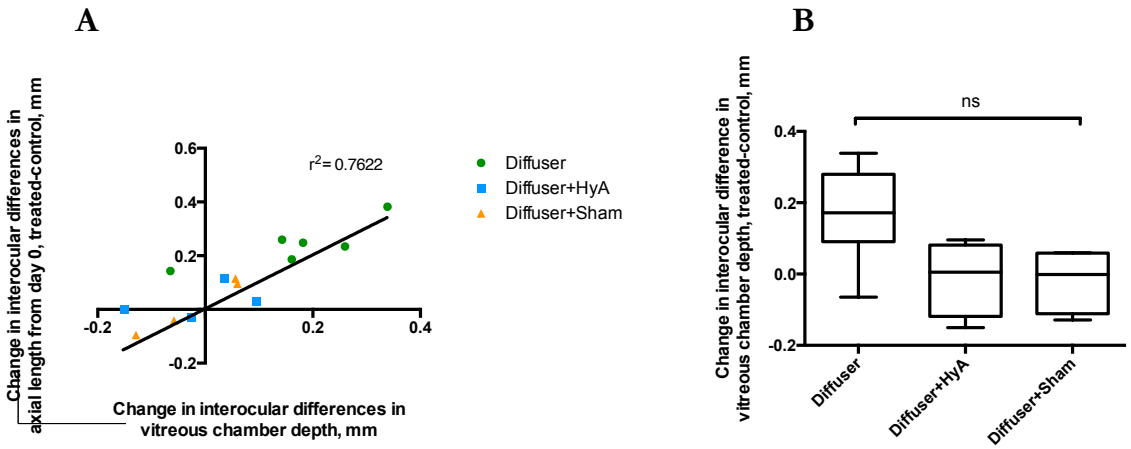

Figure 4.9. Panel A: CID in axial length plotted against CID in vitreous chamber depth after 28 days of treatment with Diffusers, Diffusers + HyA, or Diffusers + Sham. Panel B: Change in interocular differences of Vitreous Chamber Depth for guinea pigs treated with Diffusers, Diffusers+HyA, and Diffusers+Sham. Changes in intergroup differences assessed with Kruskal-Wallis test and in treated vs. control eye differences assessed with a Wilcoxon test.

Scleral thickness (ST) is another metric of interest, given that with our hydrogel injections we hoped to trigger cellular events (i.e., cell migration and matrix deposition) to thicken the sclera. However, no significant CID of scleral thickness was observed for any of the treatment groups (Figure 4.10C), the changes being negligible in all cases (0.00 ± 0.01 mm for Diffuser group, -0.02 ± 0.04 for Diffuser + HyA group, and -0.01 ± 0.03 mm for Diffuser + Sham group). Nonetheless, it is also not clear whether the ultrasonography technique used would have detected recently added tissue due to likely differences in impedance [62]. Note also that there were no significant differences in the CID in the other components making up the wall of the eye (choroid and retina; Figure 4.10A and B). In the case of these tissues, decreases in thickness may be used as a crude index of toxicity, and so by this measure, no toxicity related to the surgery was detected.

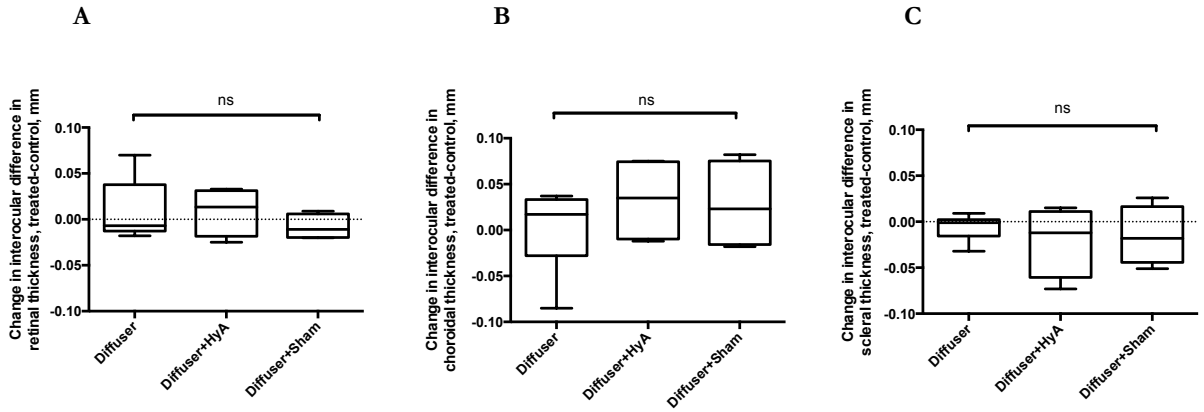

Figure 4.10. Change in interocular differences of retinal thickness (A), choroidal thickness (B), and scleral thickness (C) for guinea pigs treated with Diffusers, Diffusers+HyA, and Diffusers+Sham. Changes in intergroup differences assessed with Kruskal-Wallis test and in treated vs. control eye differences assessed with a Wilcoxon test.

Table 4.1. Change in dimensions of ocular components over the 28-day treatment.

Diffuser Group			
Ocular component	**Change in treated eye (mm) mean ± SD**	**Change in control eye (mm) mean ± SD**	**p value (Wilcoxon test)**
Anterior chamber depth	0.118 ± 0.146	0.114 ± 0.130	0.844
Lens thickness	0.430 ± 0.109	0.243 ± 0.187	0.062
Vitreous chamber depth	0.205 ± 0.082	0.035 ± 0.140	0.0625
Retinal thickness	0.010 ± 0.027	-0.003 ± 0.012	0.812
Choroidal thickness	-0.004 ± 0.030	-0.004 ± 0.032	0.812
Scleral thickness	-0.002 ± 0.020	0.005 ± 0.014	0.375
Axial length (Anterior chamber + Lens + Vitreous chamber)	0.754 ± 0.092	0.512 ± 0.115	0.031
Diffuser + HyA Group			
Ocular component	**Change in treated eye (mm) mean ± SD**	**Change in control eye (mm) mean ± SD**	**p value (Wilcoxon test)**
Anterior chamber depth	0.099 ± 0.019	0.150 ± 0.057	0.250
Lens thickness	0.448 ± 0.024	0.357 ± 0.058	0.125
Vitreous chamber depth	0.087 ± 0.046	0.098 ± 0.063	> 0.999
Retinal thickness	0.011 ± 0.017	0.002 ± 0.014	0.375
Choroidal thickness	0.024 ± 0.016	-0.009 ± 0.040	0.625
Scleral thickness	-0.054 ± 0.007	-0.034 ± 0.033	0.375
Axial length (Anterior chamber + Lens + Vitreous chamber)	0.606 ± 0.063	0.634 ± 0.028	0.750
Diffuser + Sham Group			
Ocular component	**Change in treated eye (mm) mean ± SD**	**Change in control eye (mm) mean ± SD**	**p value (Wilcoxon test)**
Anterior chamber depth	0.210 ± 0.077	0.086 ± 0.027	0.125
Lens thickness	0.327 ± 0.083	0.415 ± 0.011	0.125
Vitreous chamber depth	0.104 ± 0.093	0.122 ± 0.034	0.875
Retinal thickness	-0.008 ± 0.015	0.002 ± 0.011	0.375
Choroidal thickness	0.035 ± 0.023	-0.006 ± 0.028	0.250
Scleral thickness	-0.023 ± 0.025	-0.022 ± 0.015	>0.999
Axial length (Anterior chamber + Lens + Vitreous chamber)	0.624 ± 0.021	0.624 ± 0.06	>0.999

The net changes in interocular refractive errors over 28 days of treatment are shown for all three groups in Figure 4.11A. Due to the length of time over which these experiments were conducted, the refraction measurements collected for the Diffuser group and those collected for the Diffuser + HyA and Diffuser + Sham groups were performed by different retinoscopists. To account for biases in measurements, a correction factor was applied to measurements in the Diffuser group. A full account of the calculation of the correction factor can be seen in Appendix A.

While the axial length data clearly indicates that the eyes receiving either HyA or Sham injections elongated less than the eyes treated only with Diffusers, the corresponding refractive error data are

less clear in terms of the effects of the three treatments. On one hand, the difference between treated and control eyes reflects the trends observed for axial length (significant for Diffuser group, but not for Diffuser + HyA and Diffuser + Sham groups; Wilcoxon test). On the other hand, the CIDs for refractive errors of the three treatment groups were not significantly different (-3.92±3.37 vs. -6.37±2.31 vs. -2.06±2.89 D for the Diffuser, Diffuser + HyA, and Diffuser + Sham groups, respectively). Nearly all the treated eyes of the animals in the Diffuser group exhibited relative myopia (negative change in interocular differences; 4 out of 6). Interestingly, despite the lack of significant CIDs in axial length for the Diffuser + HyA and Diffuser + Sham groups, the treated eyes of animals in the Diffuser + HyA group were all relatively myopic (4 out of 4) as were nearly all of the treated eyes of the animals in the Diffuser + Sham group (3 out of 4). These data suggest a significant refractive contribution to the guinea pigs treated with HyA and Sham injections, rather than an axial origin to their myopia. In support of this interpretation, a plot of CIDs for refractive error versus axial length (Figure 4.12), shows a strong correlation between these parameters for the Diffuser group (Panel A, p=0.01), but a poor correlation when these data are combined with the equivalent data for the other two treatment groups (Panel B, p=0.26).

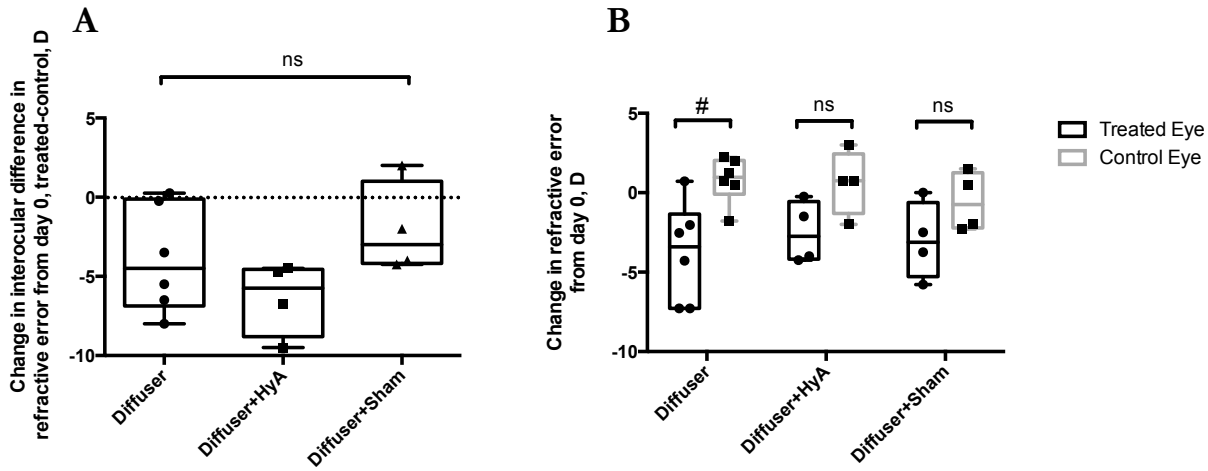

Figure 4.11. CIDs for refractive errors (Panel A) and changes in refractive error for treated and control eyes (Panel B) of guinea pigs treated with Diffusers, Diffusers+HyA, and Diffusers+Sham. Changes in intergroup differences assessed with Kruskal-Wallis test and in treated vs. control eye differences assessed with a Wilcoxon test (#p<0.05).

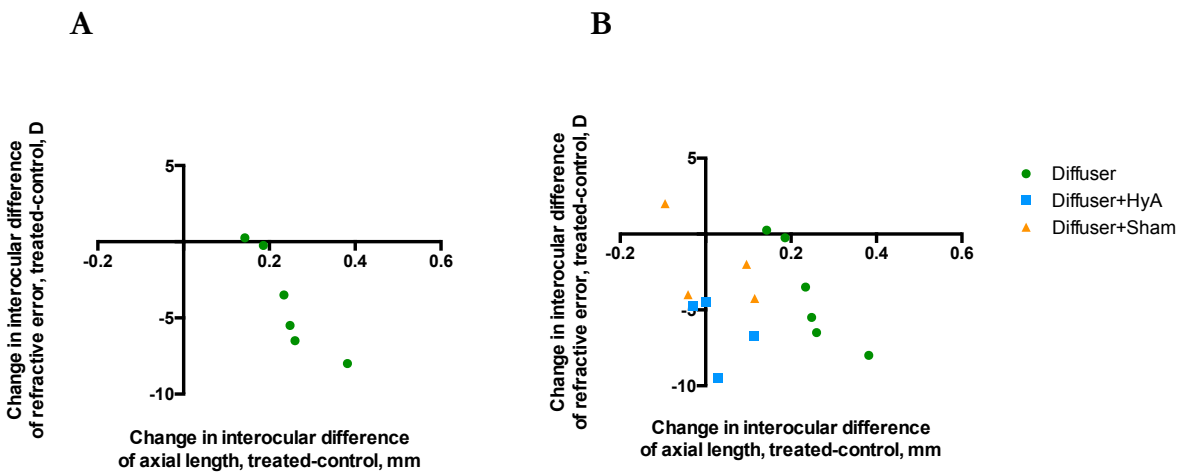

Figure 4.12. CID in axial length plotted against CID in refractive error for the Diffuser group alone (A) and all three treatment groups (B). These parameters are strongly correlated for the Diffuser group (A, p=0.01). However no significant correlation was found when data from all three groups was considered together (p=0.26).

For all three treatment groups, most of the changes in refractive errors, as measured in terms of interocular differences, took place by experimental day 14. (Figure 4.13)

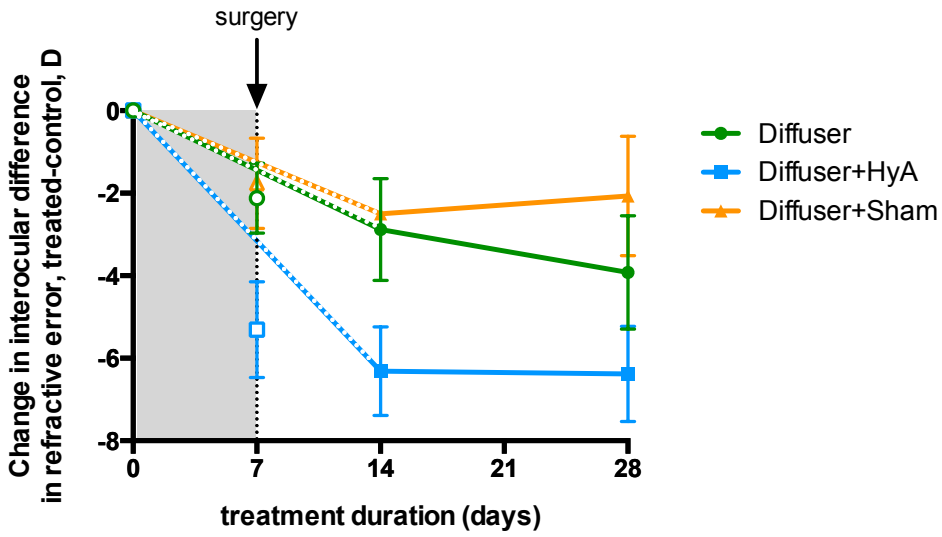

Figure 4.13. Changes in interocular differences for refractive errors over time for all treated groups, all measured under cycloplegia (mean ± SD). Open symbols at day 7 represent *non-cycloplegged* refractive errors (measured before the surgeries in the case of Diffuser + HyA and Diffuser + Sham groups).

4.3.2. Retinal function and visual acuity in guinea pigs after hydrogel/sham surgery

Retinal function: Electoretinograms were measured in guinea pigs from the Diffuser + HyA and Diffuser + Sham groups. Note that the ERGs were recorded simultaneously from treated and fellow control eyes of individual animals, thereby ensuring that any variables related to the experimental set-up (such as those related to depth of anesthesia) are expected to similarly affect the recordings from both eyes. The interocular differences in amplitudes and implicit times (time from stimulus onset to wave peak) for the a-wave, b-wave, and photopic negative responses are shown in Figure 4.14. The mean values for the treated and control eyes for each of the two groups are also summarized in Table 4.2.

Interocular differences in a-wave amplitudes for both Diffuser + HyA and Diffuser + Sham groups were centered near zero and not significantly different ($p=0.83$, Mann-Whitney test), although the data collected from the former group had a larger standard deviation (interocular differences were -1.67±11.83 and -1.65±3.87 μV, respectively). Similar trends were observed for the b-waves and for the photopic negative responses. Recorded interocular differences in b-wave amplitudes were -2.31±16.22 μV for the Diffuser + HyA group and -3.72±9.43 μV for the Diffuser + Sham group ($p=0.83$). Interocular differences in the photopic negative response amplitudes were -6.89±11.50 μV for the Diffuser + HyA group and -3.14±11.87 μV for the Diffuser + Sham group ($p=0.83$).

As with amplitudes, for each of the ERG components and each of the groups there was no difference in the implicit times between treated and control eyes. Furthermore, there were no inter-group differences in the interocular differences in implicit times. The interocular differences in implicit times for the a-waves were -0.25±0.50 ms for the Diffuser + HyA group and -0.25±3.40 ms for the Diffuser + Sham group ($p=0.63$, Mann-Whitney test). Interocular differences in implicit times for the b-waves were 0.00 ± 0.00 and 0.00 ± 0.82 ms for the Diffuser + HyA group the Diffuser + Sham respectively ($p>0.99$, Mann-Whitney test). The mean interocular differences in implicit times for the photopic negative responses were 2.25±22.14 ms for Diffuser + HyA and 6.75±7.18 ms for Diffuser + Sham ($p=0.66$, Mann-Whitney test), the discrepancy between the two groups being apparently large but not significant because of the large standard deviations for this parameter.

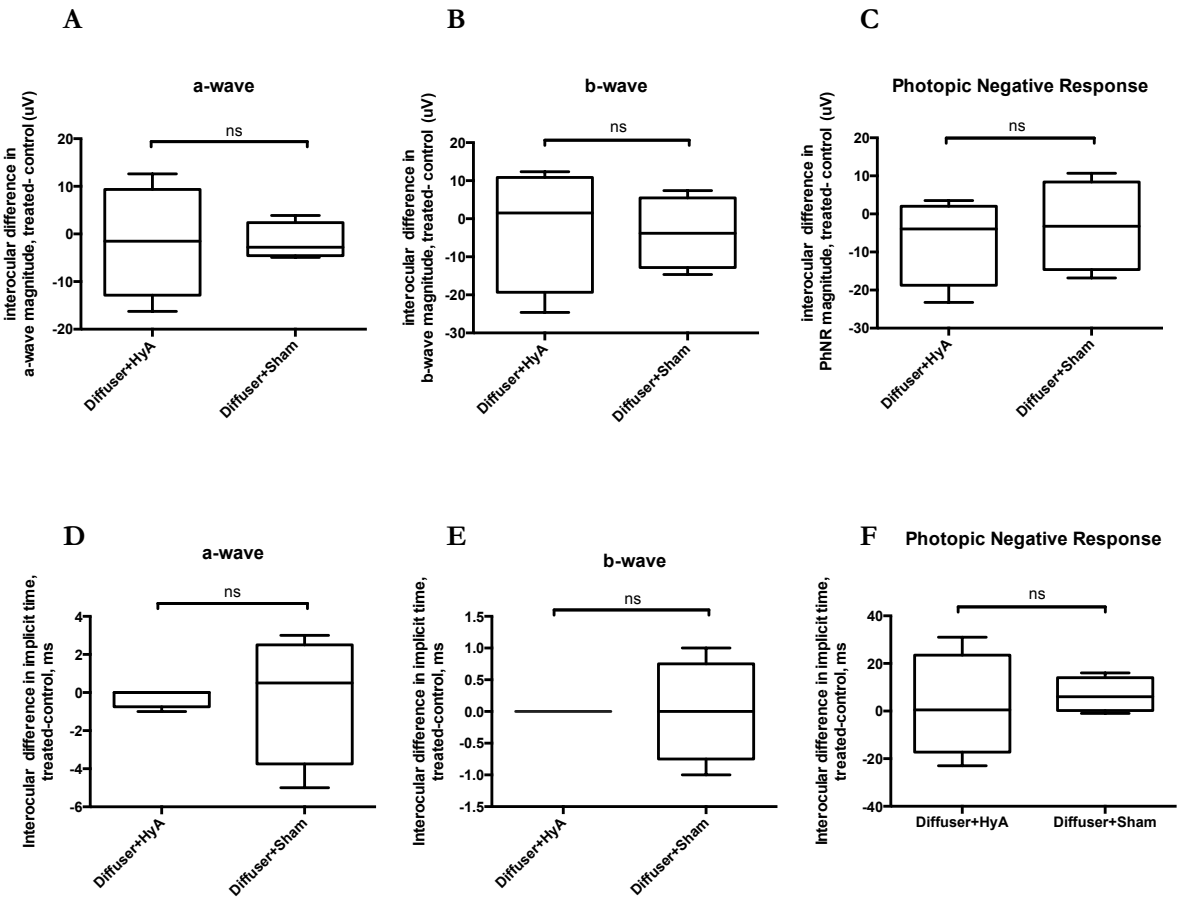

Figure 4.14. Interocular differences in wave amplitudes (A-C) and time-to-peak (implicit times) (D-F) obtained from ERG recordings from treated and control eyes from guinea pigs in the Diffusers + HyA and Diffusers + Sham groups. ERG measurements were performed at the end of the 28-day study (7 days Diffuser only + 21 days Diffuser + HyA/Sham). Intergroup differences assessed with Mann-Whitney test and differences between treated vs. control eyes assessed with Wilcoxon test.

Table 4.2. Mean and standard deviation values for amplitude and implicit time (time-to-peak) of three ERG waves, measured in the treated and control eyes of Diffuser + HyA and Diffuser + Sham guinea pigs.

	Wave amplitude (μV) mean ± SD			Implicit time (ms) mean ± SD		
	a-wave	b-wave	PhNR	a-wave	b-wave	PhNR
Diffuser + HyA Treated eye	16.40±7.62	18.38±8.53	31.52±7.52	15.50±0.57	27.75±0.50	72.50±15.29
Diffuser + HyA fellow eye	18.07±4.83	20.70±9.28	38.41±6.51	15.75±0.96	27.75±0.50	70.25±14.15
Diffuser + Sham treated eye	13.63±2.26	18.55±4.58	35.51±8.62	14.75±1.89	27.75±0.96	79.00±12.91
Diffuser + Sham fellow eye	15.28±3.22	22.27±6.04	38.65±4.94	15.00±1.83	27.75±0.96	72.25±11.03

Visual acuity: Results of the visual acuity measurements are shown in Figure 4.15. In animals treated only with diffusers (i.e. Diffuser group), the visual acuities of the treated eyes were not significantly different from those of control eyes (0.94±0.06 vs. 1.00±0.10 cycles/degree, p=0.25). There were also no significant differences between treated and control eyes in the two groups receiving injections (1.00±0.06 vs. 1.02±0.06 respectively for Diffuser + HyA and 0.95±0.04 vs. 0.95±0.04 respectively for Diffuser + Sham). Furthermore, there were no statistically significant intergroup differences (interocular differences in visual acuities:
-0.02±0.10, 0.00±0.03, & -0.06±0.07, for Diffuser + HyA and Diffuser + Sham, and Diffuser groups respectively, p=0.50).

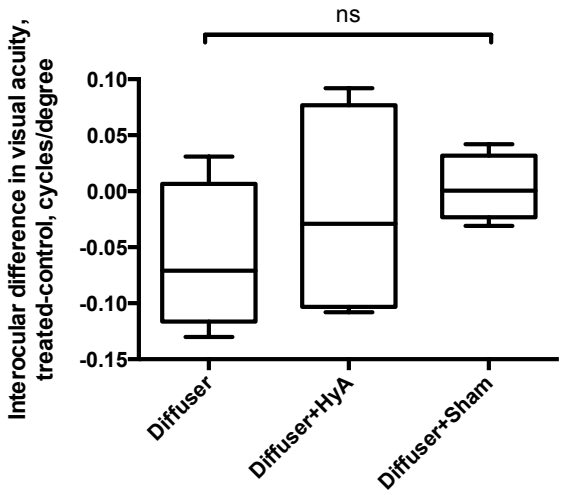

Figure 4.15. Interocular difference in visual acuity measured at the end of the 28-day study in guinea pigs treated with Diffusers, Diffuser + HyA, and Diffuser + Sham. Intergroup differences assessed with Kruskal-Wallis test and treated vs. control eye differences assessed with a Wilcoxon test.

4.3.3. Intraocular pressure in guinea pigs after hydrogel/sham surgery

Because the implantation surgery involved deposition of a hydrogel mass behind the eye, it was important to verify that intraocular pressure was not adversely affected. To this end, IOPs were measured in both groups of animals that underwent surgery (Diffuser + HyA and Diffuser + Sham groups) at the end of the 28-day experiment (Figure 4.16).

No difference in IOP between treated and control eyes were observed for either treatment group: 14.92±8.52 vs. 14.89±7.58 mmHg respectively for the Diffuser + HyA group (p>0.99) and 20.41±7.23 vs. 19.59±7.65 mmHg respectively for the Diffuser + Sham group (p=0.63). The interocular differences in IOPs for these two groups were also not significantly different from each other, 0.03±2.05 and 0.83±2.01 MmHg, Diffuser + HyA and Diffuser + Sham respectively; p=0.74, Mann-Whitney test).

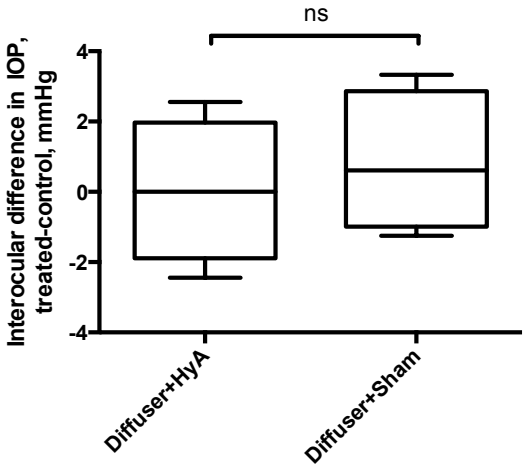

Figure 4.16. Intraocular pressure (reported as interocular difference, treated-control) measured at the end of the 28-day study in guinea pigs from the groups Diffuser + HyA, and Diffuser + Sham. Interocular differences for the two groups compared with a Mann-Whitney test and treated vs. control eye differences assessed with a Wilcoxon test.

4.3.4. MRI localization of implant and histology analyses

The T2-weighed MRI acquisition parameter highlights water-rich structures, making it ideal to visualize our implanted hydrogel. Figure 4.17 shows an axial view of the eye of the guinea pig imaged after receiving a sub-Tenon's capsule injection of HyA hydrogel. The hydrogel implant can clearly be seen encasing the posterior pole of the eye, with some "escape" into the superior orbit. Even though the needle used to inject the hydrogel was slowly withdrawn from the surgical site, it is inevitable that some hydrogel is drawn into the needle track, as evidenced by its presence in the superior orbit.

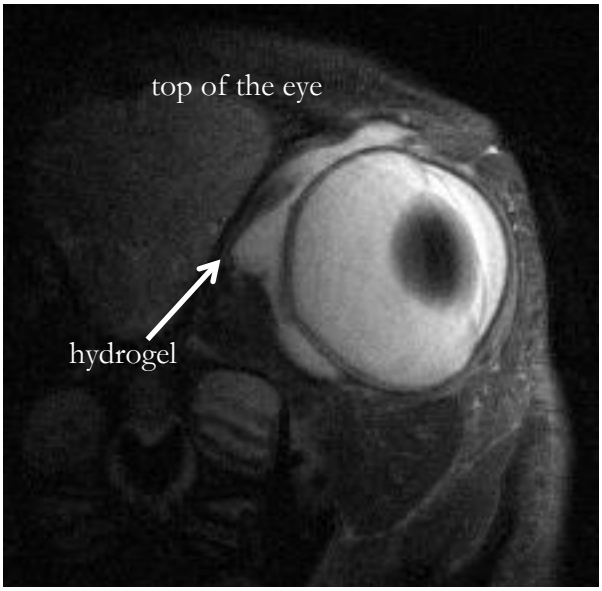

Figure 4.17. Image of an eye and surrounding orbital structural, recorded with a 7 T MRI after injection of HyA hydrogel under Tenon's capsule. The hydrogel can clearly be seen surrounding the posterior pole and over the superior surface of the eye, reflecting hydrogel drawn into the

needle track during the surgery.

To visualize the effects of the surgeries on the morphology of the posterior eye wall, eyes were embedded in paraffin at the end of the treatment and stained with Hematoxylin & Alcian blue (a glycosaminoglycan stain) or Hematoxylin & Eosin (Figure 4.18). For eyes receiving the hydrogel implant, remnants of the implant were clearly visible between the sclera and Tenon's capsule and exhibited extensive cell infiltration (demonstrated by staining of cell nuclei inside the hydrogel). Tenon's capsule also appeared to be thickened. Interestingly, similar thickening of Tenon's capsule was also evident in eyes receiving the sham injection, and in both cases the capsules appeared structurally more disorganized than normal (compare middle & right panels with left panel in Fig. 4.18).

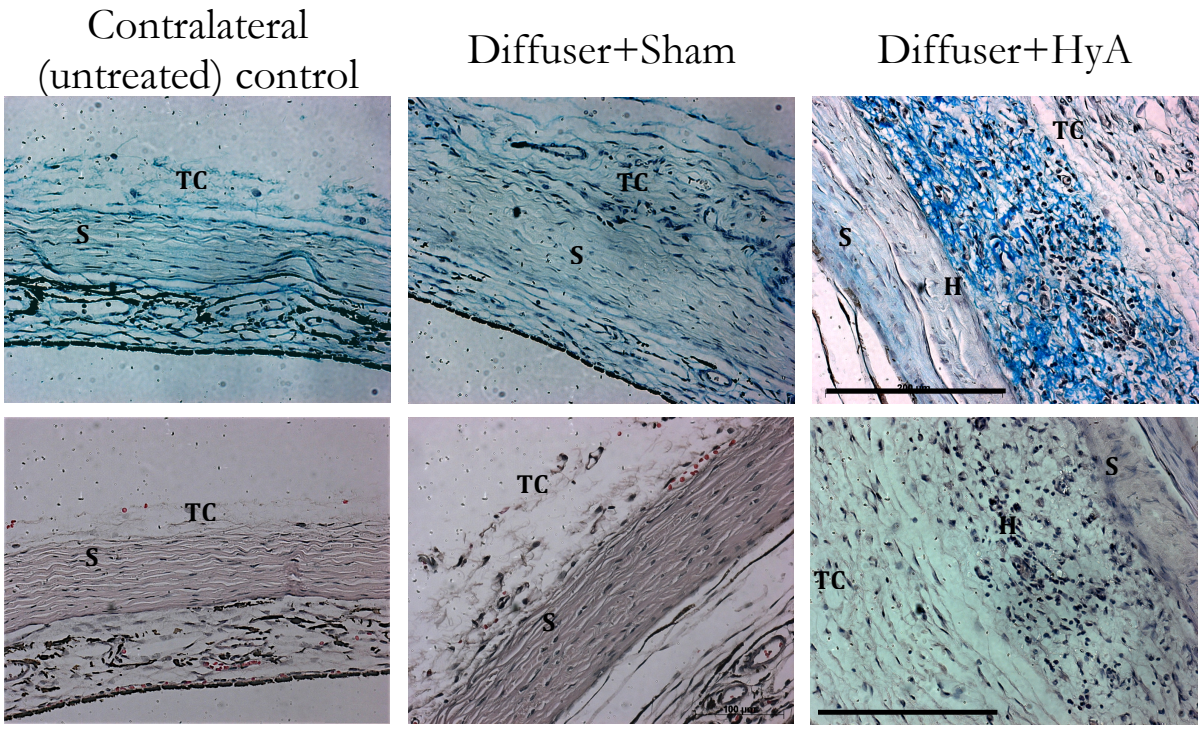

Figure 4.18. Guinea pig eyes stained with Hematoxylin & Alcian Blue (top row) and Hematoxylin & Eosin. Scale bars represent 200 μm. S = sclera, TC = Tenon's capsule, H = hydrogel. Note the thicker Tenon's capsules in both the Diffuser+ HyA and Diffuser + Sham eyes.

4.4. Discussion

This chapter presents the results of the *in vivo* trial of a HyA hydrogel, intended as a scleral-based therapy for the early stages of myopia. The working hypothesis underlying this therapy and thus framing the research described in this dissertation is that a degradable scaffold amenable to cell infiltration and proliferation, implanted adjacent to the sclera, would allow fibroblasts to lay down a new layer of matrix that would serve to thicken and strengthen the native tissue. This would thereby provide a degree of protection against the increased elongation underlying myopia development and progression. The testing described in this chapter was limited to an optimized formulation, as determined through *in vitro* testing (Chapter 3). The hydrogel (or buffer in the control group) was

injected under Tenon's capsule at the posterior pole of guinea pig eyes after a short period of form deprivation to induce myopia.

At the end of the 28-day experiment, the total elongation of the treated eyes in the Diffuser + HyA group was nearly identical to that of their fellow untreated controls, despite the continued presence of the diffusers as a myopia-inducing stimulus. The results of post-mortem histological analysis of the implant and adjacent tissues (sclera and Tenon's capsule) confirmed the biocompatibility of the hydrogel, as evidenced by extensive cell infiltration, providing further validation of our choice of a HyA-based hydrogel for our myopia-control studies. As discussed previously, hyaluronic acid is abundantly present in the eye, not only in the sclera but also as part of the vitreous and aqueous humors. Interestingly, the nuclei of the cells – as shown through hematoxylin staining – in the implanted hydrogel were more rounded than the nuclei of fibroblasts in the native sclera, perhaps suggesting that despite the ability of the hydrogel to support cell migration, it was lacking some critical feature of the native sclera required for the retention of the cells' normal phenotype. This result is consistent with those observed for the 200 Pa gels in our *in vitro* studies (Chapter 3), in which cells cultured over those hydrogels had more rounded morphology than those cultured on the stiffer (800 Pa) formulation. Apart from the differences in stiffness of the gel and sclera environments, the more rounded shape of the cells may also partly reflect differences in the ultrastructure of their environment. Specifically, in the native sclera cells are enclosed in a dense collagen scaffold, leaving them little room to "round up". However, there are also differences in the biomechanical forces experienced in each environment, which may also contribute to the differences in cell shape. Scleral fibroblasts in their native ocular environment experience constant stress, resulting from intraocular pressure and tension from attached extraocular muscles[246]. As cells migrate into the hydrogel, these influences are likely to decrease significantly, although some residual influences may be expected given the location of implants, sandwiched between Tenon's capsule and the sclera. The importance of such influences has been demonstrated in *in vitro* studies of isolated human and chick scleral fibroblasts, which are reported to show differential expressions of MMPs and matrix components after being exposed to mechanical stretch[25,247,248]. In future work, protein array studies of recovered hydrogels (i.e. removed from the eye at certain time points after implantation) might help shed light onto how these new environments affect cell behavior [224].

Histological analyses revealed the implants to still be present 3 weeks after the implantation surgery. This is exemplified in Figure 4.19, in which a thick band of hydrogel is clearly visible between the sclera and Tenon's capsule. Recall that in Chapter 3 we reported that scleral fibroblasts heavily degraded the hydrogels (particularly the formulation with 380 μM RGD), turning them nearly into a liquid by the end of the two-week proliferation period. Two possible scenarios could explain this difference in apparent degradation rates under *in vitro* and *in vivo* conditions. One possibility for the apparent resistance of the hydrogel to degradation *in vivo* is that under this condition the scleral fibroblasts secrete matrix at a similar (or faster rate) than they degrade the surrounding hydrogel, therefore allowing the implant to retain its shape for a longer period. Such differences in behavior under *in vivo* and *in vitro* conditions are plausible, given that in the latter situation cells are cultured under very controlled conditions, while in the former cells may be exposed to a variety of growth factors secreted by neighboring cells. Alternatively, it is possible that the cells migrating into the hydrogel *in vivo* do not represent a homogenous group. Although none of the cells exhibited the characteristic multinucleated feature of macrophages, which are an expected feature of any accompanying inflammatory response, it is possible that the conditions triggered the transformation of some fibroblasts into myofibroblasts, showing altered MMP secretion[249].

We currently do not know how long it takes for the polymer to be completely degraded *in vivo*. We can report that the degradation time is beyond 5 weeks, the longest experiments conducted to date. As shown in Figure 4.19 below, the implant was still visible around the posterior pole of the enucleated eye. However, sections of the same eye stained with Alcian Blue revealed a considerable amount of empty space within the implant, suggesting extensive hydrogel degradation. Similar histological results were observed in a previous study conducted by our group, in which myopic chicks received posterior sclera injections of a degradable NIPAAm-based hydrogel that also contained cell-binding motifs and degradable crosslinkers[62]. However, note that for both studies we cannot rule out histological artifacts as the origin of some of the holes, as both made use of frozen sections, which do not preserve tissue morphology as well as sections prepared from paraffin-imbedded tissue (compare Figures 4.19 and 4.18).

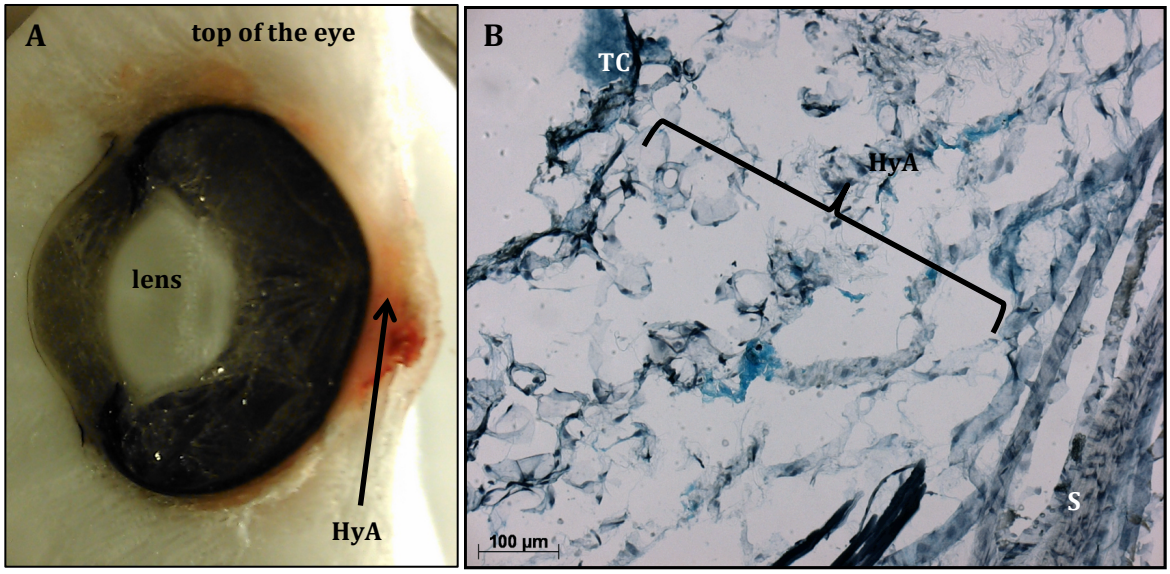

Figure 4.19. Bisected enucleated eye embedded in OCT (A) and Alcian Blue-stained frozen section from the same eye (B), 5 weeks after HyA hydrogel implantation. TC: Tenon's capsule. S: Sclera. HyA: Hyaluronic acid-based hydrogel.

Despite the apparent lack of scleral thickening as determined by A-scan ultrasonography, the overlying Tenon's capsule became thicker and less organized in the areas manipulated during the surgery. Of note is that fact that such changes were evident in the eyes from both the Diffuser + HyA and Diffuser + Sham groups. This thickening of Tenon's capsule in both groups offers a potential explanation for some of the myopia-control effects observed with both types of surgeries – that the thickened Tenon's capsule increased the mechanical stability of the posterior scleral wall. This effect on Tenon's capsule (and eye growth) could represent a wound-healing response, given that the initial surgical incision through the conjunctiva and Tenon's capsule unavoidably results in some disruption of these tissues and of local vascular networks [250]. Even a mild inflammatory/wound-healing reaction may be sufficient to alter the mechanical properties of the posterior sclera, if the affected area of scar formation is sufficiently large. Consistent with this model, histological sections from an eye subjected to the Diffuser + Sham treatment (Figures 4.20A and B) revealed the presence of scar-like tissue and possibly an infiltrating blood vessel in regions directly affected by the surgery; no such changes are apparent in the regions of the same eye that are not

manipulated during the surgery (Figure 4.20C and D). The net effect of mechanical stabilization of the posterior sclera would be slowed eye growth, as observed. But note that these changes were not sufficient to prevent eyes from growing altogether.

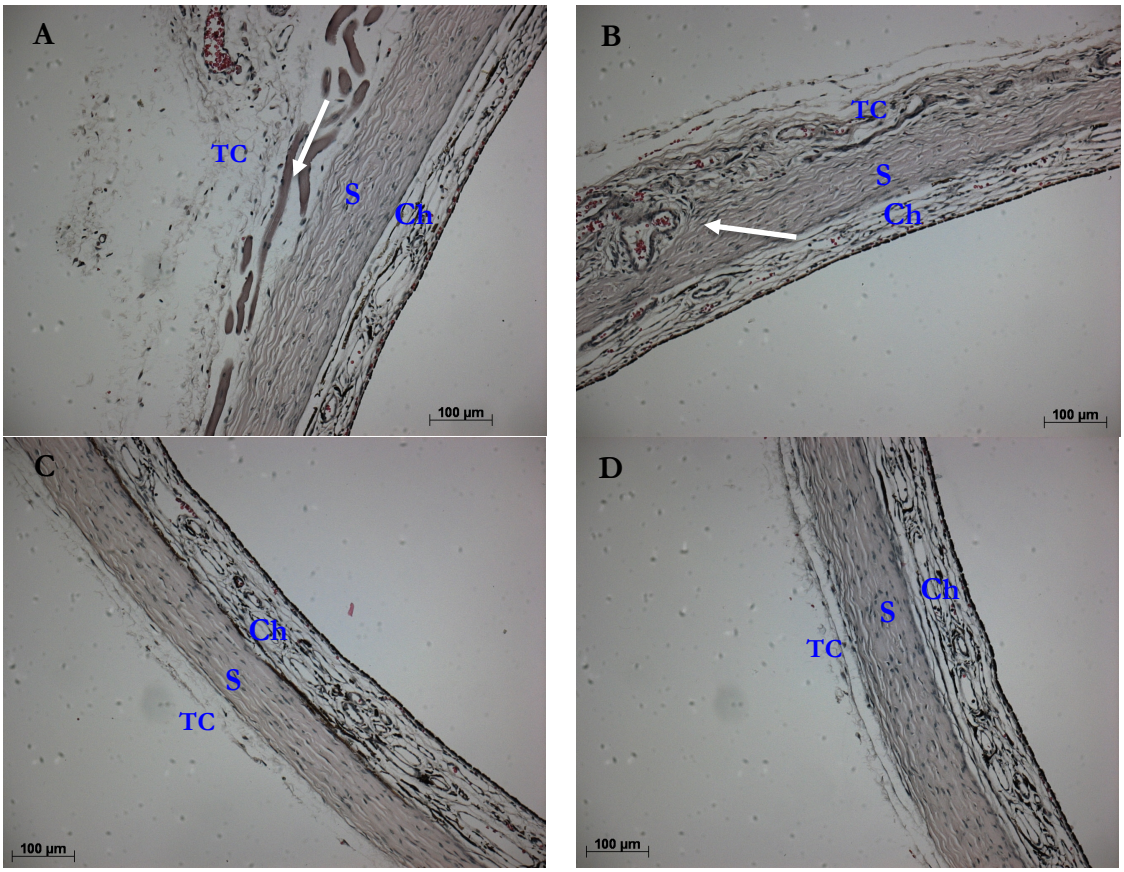

Figure 4.20. Hematoxylin & Eosin-stained sections of Diffuser + Sham eyes. Panels A and B highlight the surgical site, with the arrow in panel A indicating possible presence of blood and the arrow in panel B highlighting thickened scar-like tissue. Panels C and D show the "underside" of the same eye, the area inferior to the optic nerve that is not penetrated by the blunt sub-Tenon's needle. Note that the sclera and Tenon's capsule appear tightly affixed, implying that the buffer injection did not permanently separate these two layers. S: sclera. Ch: choroid. TC: Tenon's capsule.

The response observed in the Diffuser + Sham group, which was similar to that of the Diffuser + HyA group in terms of both reduced ocular elongation and thickening of Tenon's capsule, was unexpected. Above, we offered a potential explanation for this effect - the product of a wound healing response. While we cannot rule out the possibility that our hydrogel implants themselves had an inhibitory effect on axial elongation, the similarity of results for the Diffuser + HyA and Diffuser + Sham groups point to additional influences on axial elongation related to the surgery itself. From our results it is not possible to distinguish between effects of the surgery alone, potential effects of the injected triethanolamine buffer alone, or the two acting in concert to control eye elongation. Interestingly, triethanolamine was an ingredient of a crosslinking cocktail used in another related study, which employed the guinea pig myopia model to investigate the efficacy of scleral cross-linking as a myopia-control treatment [215]. In an attempt to develop a crosslinking solution that could be activated by visible light – as an alternative to the UV-activated solutions previously studied – different doses of Eosin Y in triethanolamine were injected subconjunctivally over the sclera of

guinea pigs. The eyes were then proptosed and the crosslinking solution activated with 525 nm light. The Eosin Y treatment was found to decrease the rate of vitreous chamber elongation, at least when injected as a more concentrated solution. Although the injections are described as "sub-conjunctival", published histology figures show Eosin Y staining over "the entire sclera surface". Unfortunately this study did not include a triethanolamine-only group, but the lack of effects on eye growth observed in the animals treated with a low concentration of Eosin Y predict that the buffer alone would have minimal effect on eye growth. Although our commercially-purchased buffer contained a higher concentration of triethanolamine than the solution used by Mattson (200 mM vs. 90 mM), we are inclined to rule out buffer-induced crosslinking as the explanation for the reduced rate of eye growth in our Diffuser + Sham group, favoring instead the proposed wound healing explanation. Nonetheless, resolution of this question can only be reached with an additional study in which guinea pigs are subjected to the same surgical manipulations – in which the blunt needle in pushed underneath Tenon's capsule to the posterior pole of the eye – but no buffer is injected.

In contrast to the control of axial elongation observed in the Diffuser + HyA and Diffuser + Sham groups, the Diffuser-only group showed the characteristic increased axial elongation of myopic eyes. This result was expected, given that our guinea pig colony was sourced from a larger population shown to respond reliably to form deprivation [152]. However, the story told by the refractive error measurements is less straightforward – as none of the three groups were significantly different from each other in terms of changes in interocular differences. Two factors likely contributed to this outcome: first, the more subjective nature of retinoscopy, which was used to determine refractive errors. Compared to the high precision of our ocular biometry setup, which offers 10 μm resolution, retinoscopy can lead to operator-dependent biases. Unavoidably, due to the long time frame over which our work was conducted, two different retinoscopists were involved in data collection for this study. This also leads to increased variability in the refraction data, even though we attempted to control for operator-specific biases as described in the methods section. Second, because of the small sample sizes involved (n= 6 for the Diffuser group, n=4 for both Diffuser + HyA and Diffuser + Sham groups) and the large variability in the refractive error data, the study lacks statistical power. The small sample sizes reflect two constraints under which we were operating - the small size of our breeding colony and the relatively long gestation period of guinea pigs (59-72 days) – together they resulted in relatively few animals being available for this research. Furthermore, to ensure some consistency in the disease phenotype of animals included in the study, a minimum elongation criterion in response to form deprivation was imposed. Specifically, treated eyes must have elongated at least 50 μm more than their fellows after 7 days of form deprivation. This condition further reduced the number of animals entering the study.

Our results of strong ocular growth inhibition after the surgery logically lead to questions about retinal health, and whether the surgery, hydrogel and/or buffer caused damage to the retina, perhaps even contributing to the observed ocular growth inhibition. Flash electroretinograms (ERGs) are a commonly used tool for assessing retinal function. It allows the health of different subgroups of retinal cells to be separately evaluated through analysis of the components making up the recorded waveform, itself a recording of the retina's response to a flash of light. Of the components making up the waveform, the properties of the b-wave are likely to be most insightful, as it is reported to be attenuated in eyes undergoing disruption to retinal blood flow in humans[251] and animals (rabbits)[252]. Thus any damage to the external vasculature feeding the retina, incurred either during the surgery, or resulting from mechanical compression by the implant, might be expected to similarly affect the b-wave. Another potential complication of the surgery and/or implant is compromise to choroidal blood flow resulting from mechanical compression. While this possibility would seem unlikely, given

the high blood flow rates of the choroid, it can be ruled out by analyzing the magnitudes and implicit times of both a- and b-waves, both of which have been shown to be affected by impaired choroidal blood flow [253,254]. While recordings from treated eyes exhibited, on average, slightly lower wave amplitudes and longer implicit times than those from their fellow controls, in no cases were these differences statistically significant (Table 4.2). Importantly, the lack of differences in a- and b-wave amplitudes and implicit times between recordings from the treated and control eyes, in conjunction with the results of other ERG components, suggests that neither surgery (with buffer or hydrogel) adversely affected the retina.

Visual acuity testing provides yet another set of information about retinal function. It relies on spatial contrast processing, mostly at the level of the inner retina. It also has the advantage of being sensitive to optical defocus, while flash ERGs are relatively robust against it. Nevertheless, our OKN method of evaluating visual acuity was not without potential flaws. Due to its behavioral nature, it is dependent on the temperament of each animal. In the wild, guinea pigs are prey animals that react to frightening stimuli by "freezing" and refusing to move, so loud noises and floor tremors during visual acuity measurements can affect the results. Despite initial difficulties, we were able to refine our measurement techniques to obtain reliable data and thus report no significant differences between treated and control eyes for any of the three groups, which were also not different in terms of their interocular differences. These visual acuity findings are consistent with our ERG results, from which we conclude that the implantation surgery is without adverse effects (due to toxicity or mechanical trauma) on the retina.

An additional perspective on potential side-effects of the surgery is provided by intraocular pressure (IOP) data. The decision to collect these data was made to rule out the possibility that the surgeries resulted in increased IOP, due either to direct mechanical pressure on the globe or to disruption of aqueous flow out of the eye. Once again, we found no evidence of adverse effects. Specifically, for both the Diffuser + HyA and Diffuser + Sham groups no differences were found between the treated and control eyes. In all cases, measured IOPs were also similar to those recorded with the same tonometer in an independent study of untreated (non-myopic) guinea pigs previously conducted in our lab (19.1 ± 4.9 mmHg, n=15, unpublished data, Ostrin 2012).

Despite the control of myopia progression exhibited by the surgery alone, i.e., in the absence of a hydrogel implant (in the Diffuser + Sham group), the use of hydrogel itself is not without merit, especially since its biocompatibility has been demonstrated both *in vitro* and *in vivo* (as least for guinea pig scleral fibroblasts). For example, the hydrogel could be leveraged as a drug delivery depot, not only for anti-myopia drugs such as atropine, but also for drugs targeting other posterior segment diseases such as retinal and/or choroidal neovascularization and inflammation. For such applications, the composition of the hydrogel may need to be further optimized to cover the desired treatment period, given that the current formulation degraded significantly over 5 weeks *in vivo*. In relation to its application for the control of myopia progression, additional studies are also warranted to confirm the results reported here and to determine just how long the implants remain. In addition to the above anti-myopia application of our hydrogel, it is plausible that it could also be used, after further optimization, in place of available hydrogel-based scleral buckles. In widest use currently are ones based on the non-degradable polymer poly(methyl acrylate-*co*-2-hydroxyethyl acrylate) (MIRA-gel), with reported complications of fragmentation and subsequent foreign body giant cell granulomatous reactions [65]. Given their lower modulus, injectable HyA-based hydrogels are less likely to present fragmentation issues and could also be adapted for delivery of novel therapeutic drugs as they become available. For such applications, the hydrogel could be modified with non-

degradable crosslinkers (such as thiolated polyethylene glycol) to slow the rate of degradation and thus prolong its life *in situ*.

4.5 Conclusion

The results presented in this chapter suggest that a sub-Tenon's capsule injection of hyaluronic acid-based hydrogel can control myopia progression without causing adverse effects to retinal health and intraocular pressure. Likewise, an injection of 0.2 M triethanolamine buffer was also found to have a myopia-control effect. Animals in both treatment groups exhibited no significant interocular difference in the axial elongation of their treated and fellow eyes, despite their treated eyes being continuously subjected to form deprivation, a myopia-inducing stimulus. Histology revealed extensive cell infiltration into hydrogel implants, as well as the presence of scar-like tissue contributing to a thickening of Tenon's capsule at the incision sites of eyes receiving hydrogel and those injected only with buffer.

This work raises the possibility of new and relatively noninvasive surgical methods to control myopia progression. Future studies are warranted to better understand the myopia-control effects of the sham surgery itself, and to ascertain whether sufficient myopia control may be achievable with its refinement.

Chapter 5 – Summary and future directions

5.1 Dissertation summary

The experiments described in this dissertation presented a novel sclera-based therapy that can control axial myopia progression in a mammalian model.

Chapter 2 described our efforts to develop a guinea pig myopia model. The sclera-based nature of our intended therapy necessitated the development of a reliable mammalian model, which, like humans, has a fibrous-only scleral structure. Our first attempts to establish a guinea pig myopia model involved purchasing animals from a commercial breeder and applying well known myopia-inducing paradigms: negative lenses and diffusers. Interestingly, in a phenomenon never before reported in the literature for the guinea pig, none of the animals involved in the study developed myopia. As an alternative source of suitably responsive animals, we thus obtained breeding pairs from a myopia research laboratory at the University of Auckland (New Zealand), which were used to establish our own breeding colony. As expected, animal sourced from this colony proved responsive to form deprivation. Nonetheless, our experience calls attention to the wide variability in guinea pig responses to myopia-inducing stimuli.

The work detailed in Chapter 3 concerns the synthesis and *in vitro* characterization of a hyaluronic acid-based hydrogel as a myopia-control tool. Hyaluronic acid was modified with acrylate groups, decorated with the peptide, bspRGD(15) (which binds integrins (α_V, $\alpha_5\beta_1$, $\alpha_8\beta_1$, or $\alpha_{IIb}\beta_3$), and crosslinked with an MMP-degradable peptide-based crosslinker, to generate an artificial matrix to which scleral fibroblasts could adhere and eventually degrade. Through cell proliferation assays, we found that primary guinea pig scleral fibroblasts can proliferate in hydrogels with moduli of 200 and 800 Pa, independent of the concentration of the cell-binding peptide. A similar peptide concentration-independence was observed with migration assays: cells exhibited similar migration patterns, even when the hydrogel contained no cell-binding peptide. The latter results imply that scleral fibroblasts can engage with the hydrogels through receptors other than the RGD-binding integrins. Overall, the HyA-hydrogels proved highly compatible with scleral fibroblast mitosis and migration.

Lastly, *in vivo* myopia-control experiments in our established guinea pig model were presented in Chapter 4. Myopia was induced through form deprivation for one week, after which guinea pigs received sub-Tenon's capsule injections of 200 Pa 380 μM RGD hydrogels (Diffuser + HyA) or triethanolamine buffer (Diffuser + Sham). An additional group received no injection (Diffuser group) and acted as a further control. We observed significant inhibition of the typical form deprivation-induced increased axial elongation in both the Diffuser + HyA and Diffuser + Sham groups over a 3 week monitoring period. This result suggests that the injection surgery (perhaps in combination with the buffer) can itself serve as a myopia control treatment, independent on any effect of the hydrogel. Histology performed on eyes from both treatment groups revealed a thickened Tenon's capsule in treated eyes, possibly secondary to a wound-healing response. It was speculated that these changes, by improving the mechanical stability of the sclera, may underlie the slowed axial elongation of treated eyes. Neither the hydrogel nor the sham surgery, which involved

injection of the buffer solution used to prepare the hydrogel, adversely affected retinal electrical function (as measured with ERGs), visual acuity, or intraocular pressure.

5.2 Future directions

We have related results pertaining to the response (and lack thereof) of different guinea pig populations to myopia-inducing stimuli. The successful development of a guinea pig myopia model enabled us to pursue our proposed hydrogel-mediated therapy, but important questions still remain as to the curious lack of responses observed in the "myopia-resistant" animals. What is different about that population? Can be it narrowed down to a few sets of attributes? Pursuit of these questions – possibly using DNA microarrays – could open the doors to further understanding the genetic factors contributing to myopia development in humans.

We have also presented data suggesting that a sub-Tenon's capsule injection of buffer can have significant myopia-control effects. Many questions remain as to the mechanism underlying this phenomenon and whether these effects are sustained long-term. While these studies open the doors to exciting new directions for myopia control therapies, much work must be done before any such therapy can be considered for translation to humans. Important follow-up questions to be addressed include:

1) **What underlies the myopia control effect observed in the Diffuser + HyA and Diffuser + Sham groups?**

a. **Are the mechanical properties of the sclera altered at the surgery site?** One hypothesis offered in explanation for the control of myopia progression observed in the Diffuser + Sham groups is an improvement in the mechanical stability of the posterior sclera – large enough to prevent the scleral creep characteristic of myopic eyes, yet not so large as to prevent normal eye growth. The observed thickening of the Tenon's capsule overlying the surgical site supports the hypothesis that the biomechanical stability of the posterior eye wall is altered by the surgery. Whole eye creep tests, such as those previously described by our laboratory[43], could be an effective tool to address this hypothesis.

b. **Are myopia-related genes differentially regulated in the sclera as a result of the surgery?** Several research groups, including ours, have identified bidirectionally-regulated genes involved in ocular growth regulation. These genes are differentially regulated, depending on whether the eye is exposed to stimuli that accelerate or slow down eye growth. Examples in chick myopia models include ZENK in the retina [255] and Bone Morphogenic Protein-2 in the retinal pigment epithelium [256]. Recent studies in a tree shrew myopia model have identified other bidirectionally-regulated genes, including collagen 6A6 and the metallopeptidase ADAMTSL3 in the sclera[123]. As another strategy for elucidating the scleral mechanism underlying the myopia control elicited by our surgical manipulations, expression levels of candidate bidirectional genes could be studied in guinea pig scleras. Such a study would first require the establishment of scleral profiles for guinea pig eyes undergoing form deprivation treatment alone.

2) **Can the myopia control effect be elicited through surgery alone?**
As a logical follow-up experiment to our work, it is important to test the effect of the surgical manipulation in isolation. That is, guinea pigs should undergo sub-Tenon's capsule surgery in which nothing is injected. All surgery procedures must be followed - the sclera from Tenon's

capsule separated from each other to create a potential space into which a needle pushed and subsequently a suture inserted to close the incision.

3) **How long does the myopia-control effect last?**
   Our experimental protocol included a relatively short post-surgical follow-up period (3 weeks). A key question to pursue is whether the observed myopia control effect is maintained beyond 3 weeks if form deprivation is extended for longer. As our myopia control treatment is intended for use in young children, we must assume that the stimulus for myopia progression in enduring, at least into adolescent years.

4) **How long does the hydrogel last *in vivo*?**
   Though a significant myopia-control effect was observed in the Diffuser + Sham group, the good biocompatibility observed for the HyA hydrogel potentially makes it a better therapeutic candidate, as it can be used as a drug/growth factor depot for long-term drug delivery. Before such applications can be considered, however, a better understanding of the life span (degradation timeline) of the hydrogel *in vivo* must be obtained. Our use of MRI imaging, albeit limited in the current studies, revealed its potential utility for longitudinal, long-term monitoring to address this type of question. For example, guinea pigs could be scanned every 1-2 weeks for a period of several months, until the hydrogel is no longer visible.

5) **Can the sub-Tenon's capsule injection prevent myopia development if it is conducted before the form deprivation is established?**
   In the experimental protocol used in this dissertation, myopia was generated in guinea pigs before the surgical intervention. As a companion to question 2, we pose the question of whether the extent of myopia developed as a consequence of form deprivation could be decreased if the surgery is performed *before* the diffusers are fitted to the guinea pigs. If so, this could open the doors to a relatively simple preventative surgery that could be implemented in patients with family histories of very high myopia.

6) **Can the myopia control effect be reproduced in a primate model?**
   Before translation to human therapy, a logical next step would be to ascertain whether the myopia-control effect observed in guinea pigs can be reproduced in a primate myopia model, either the rhesus macaque or marmoset model.

As the prevalence of myopes continues to grow around the world, and the need for an early intervention correspondingly rises, more effective myopia control therapies will remain a high public health priority. Thus further refinement and characterization of the myopia control therapy described in this dissertation could benefit millions of people around the world.

References

1. Stone R, Khurana T. Gene profiling in experimental models of eye growth: Clues to myopia pathogenesis. Vision Res. 2010. doi:10.1016/j.visres.2010.03.021.

2. Curtin B. The myopias: basic science and clinical management. Philadelphia: Harper & Row; 1985.

3. Holden B, Sankaridurg P, Smith E, Aller T, Jong M, He M. Myopia, an underrated global challenge to vision: where the current data takes us on myopia control. Eye. 2014;28:142–146.

4. Resnikoff S, Pascolini D, Mariotti S, Pokharel G. Global magnitude of visual impairment caused by uncorrected refractive errors in 2004. Bull World Health Organ. 2008;86:63–70.

5. Rein D, Zhang P, Wirth K, et al. The economic burden of major adult visual disorders in the United States. Arch Ophthalmol. 2006;124(12):1754–60. doi:10.1001/archopht.124.12.1754.

6. Morgan I, Ohno-Matsui K, Saw S. Myopia. Lancet. 2012;379(9827):1739–48. doi:10.1016/S0140-6736(12)60272-4.

7. Saw S-M, Tong L, Chua W-H, et al. Incidence and progression of myopia in Singaporean school children. Invest Ophthalmol Vis Sci. 2005;46(1):51–7. doi:10.1167/iovs.04-0565.

8. Curtin B. The posterior staphyloma of pathologic myopia. Trans Am Ophthalmol Soc. 1977;75:67–86.

9. Jones D, Luensmann D. The prevalence and impact of high myopia. Eye Contact Lens. 2012;38(3):188–96. doi:10.1097/ICL.0b013e31824ccbc3.

10. Grossniklaus H, Green W. Pathologic findings in pathologic myopia. Retina. 1992;12(2):127–33.

11. Iwase A, Tomidokoro A. Prevalence and causes of low vision and blindess in a Japanese adult population: the Tajimi study. Ophthalmology. 2006;113:1354–1362.

12. Flitcroft D. The complex interactions of retinal, optical and environmental factors in myopia aetiology. Prog Retin Eye Res. 2012;31(6):622–60.

13. Sorsby A. Refraction and its components in twins. London: HM Stationary Office; 1962.

14. Wiesel T, Raviola E. Myopia and eye enlargement after neonatal lid fusion in monleys. Nature. 1977;266(3):66–68.

15. Rada J, Shelton S, Norton T. The sclera and myopia. Exp Eye Res. 2006;82(2):185–200. doi:10.1016/j.exer.2005.08.009.

16. Watson P, Young R. Scleral structure, organisation and disease. A review. Exp Eye Res. 2004;78(3):609–623. doi:10.1016/S0014-4835(03)00212-4.

17. Miller J, Wildsoet C, Guan H, Limbo M, Demer J. Refractive error and eye shape by MRI. In: Association for Research in Vision and Ophthalmology. Fort Lauderdale, FL; 2004.

18. Bailey A. Structure, function and ageing of the collagens of the eye. Eye. 1987;1:175–183.

19. Zorn M, Hernandez M, Norton T, Yang J, Ye H. Collagen mRNA expression during scleral maturation. In: X International Congress of Eye Research.; 1992:S110.

20. Rada J, Achen V, Perry C, Fox P. Proteoglycans in the human sclera. Evidence for the presence of aggrecan. Invest Ophthalmol Vis Sci. 1997;38(9):1740–1751.

21. Trier K. The sclera. Adv Organ Biol. 2006;10(05):353–373. doi:10.1016/S1569-2590(05)10013-5.

22. Kuc I, Scott P. Increased diameter of collagen fibrils precipitated in vitro in the presence of decorin from various connective tissues. Connect Tissue Res. 1997;36:287–296.

23. Spitznas M. The fine structure of human scleral collagen. Am J Ophthalmol. 1971;71:68.

24. Siegwart J, Norton T. Selective Regulation of MMP and TIMP mRNA Levels in Tree Shrew Sclera during Minus Lens Compensation and Recovery. Invest Ophthalmol Vis Sci. 2005;46(10):3484–3492.

25. Shelton L, Rada J. Effects of cyclic mechanical stretch on extracellular matrix synthesis by human scleral fibroblasts. Exp Eye Res. 2007;84(2):314–22. doi:10.1016/j.exer.2006.10.004.

26. Young T, Scavello G, Paluru P, Choi J, Rappaport E, Rada J. Microarray analysis of gene expression in human donor sclera. Mol Vis. 2004;10:163–176.

27. Rada J, Thoft R, Hassell J. Increased aggrecan (cartilage proteoglycan) production in the sclera of myopic chicks. Dev Biol. 1991;147(2):303–312.

28. Møller-Pedersen T, Ledet T, Ehlers N. The keratocyte density of human donor corneas. Curr Eye Res. 1994;13(2):163–169.

29. Metlapally R, Jobling A, Gentle A, McBrien N. Characterization of the integrin receptor subunit profile in the mammalian sclera. Mol Vis. 2006;12(December 2005):725–34.

30. Jobling A, Nguyen M, Gentle A, McBrien N. Isoform-specific changes in scleral transforming growth factor-beta expression and the regulation of collagen synthesis during myopia progression. J Biol Chem. 2004;279(18):18121–6. doi:10.1074/jbc.M400381200.

31. Marshall G. Human scleral elastic system: an immunoelectron microscopic study. Br J Ophthalmol. 1995;79(1):57–64. doi:10.1136/bjo.79.1.57.

32. Guggenheim J, McBrien N. Form-deprivation myopia induces activation of scleral matrix metalloproteinase-2 in tree shrew. Invest Ophthalmol Vis Sci. 1996;37(7):1380–95.

33. Frost M, Norton T. Alterations in protein expression in tree shrew sclera during development of lens-induced myopia and recovery. Invest Ophthalmol Vis Sci. 2012;53(1):322–36. doi:10.1167/iovs.11-8354.

34. McBrien N, Jobling A, Gentle A. Biomechanics of the Sclera in Myopia: Extracellular and Cellular Factors. Optom Vis Sci. 2009;86(1):23–30.

35. Moring A, Baker J, Norton T. Modulation of glycosaminoglycan levels in tree shrew sclera during lens-induced myopia development and recovery. Invest Ophthalmol Vis Sci. 2007;48(7):2947–56. doi:10.1167/iovs.06-0906.

36. Rada J, Nickla D, Troilo D. Decreased proteoglycan synthesis associated with form deprivation myopia in mature primate eyes. Invest Ophthalmol Vis Sci. 2000;41(8):2050–8.

37. McBrien N, Gentle A. Role of the sclera in the development and pathological complications of myopia. Prog Retin Eye Res. 2003;22:307–338.

38. Campbell I, Coudrillier B, Ethier C. Biomechanics of the posterior eye: a critical role in health and disease. J Biomech Eng. 2014;136.

39. Siegwart J, Norton T. Regulation of the mechanical properties of tree shrew sclera by the visual environment. Vision Res. 1999;39(2):387–407.

40. Phillips J, Khalaj M, McBrien N. Induced Myopia Associated with Increased Scleral Creep in Chick and Tree Shrew Eyes. Invest Ophthalmol Vis Sci. 2000;41(8):2028–2034.

41. Avetisov E, Savitskaya N, Vinetskaya M, Iomdina E. A study of biochemical and biomechanical qualities of normal and myopic sclera in humans of different age groups. Metab Pedriatric Syst Ophthalmol. 1984;7(4):183–188.

42. McBrien N, Cornell L, Gentle A. Structural and ultrastructural changes to the sclera in a mammalian model of high myopia. Invest Ophthalmol Vis Sci. 2001;42(10):2179–2187.

43. Lewis J, Garcia M, Rani L, Wildsoet C. Intact globe inflation testing of changes in scleral mechanics in myopia and recovery. Exp Eye Res - Press. 2014.

44. McBrien N, Metlapally R, Jobling A, Gentle A. Expression of collagen-binding integrin receptors in the mammalian sclera and their regulation during the development of myopia. Invest Ophthalmol Vis Sci. 2006;47(11):4674–82. doi:10.1167/iovs.05-1150.

45. Ganesan P, Wildsoet C. Pharmaceutical intervention for myopia control. Expert Rev Ophthalmol. 2010;5(6):759–787.

46. Gwiazda J, Hyman L, Hussein M, et al. A randomized clinical trial of progressive addition lenses versus single vision lenses on the progression of myopia in children. Invest Ophthalmol Vis Sci. 2003;44(4):1492–500.

47. Aller T, Wildsoet C. Results of a one-year prospective clinical trial (CONTROL) of the use of bifocal soft contact lenses to control myopia progression. Ophthalmic Physiol Opt. 2006;26(S1):8–9.

48. Cho P, Cheung S, Edwards M. The longitudinal orthokeratology research in children (LORIC) in Hong Kong: a pilot study on refractive changes and myopic control. Curr Eye Res. 2005;30(1):71–80.

49. Walline J, Lindsley K, Vedula S, Cotter S, Mutti D, Twelker J. Interventions to slow progression of myopia in children. Cochrane Database Syst Rev. 2011;(12). doi:10.1002/14651858.CD004916.pub3#sthash.mWe5zHZQ.dpuf.

50. Tong L, Huang X, Koh A, Zhang X, Tan D, Chua W. Atropine for the treatment of childhood myopia: effect on myopia progression after cessation of atropine. Ophthalmology. 2009;116(3):572–9. doi:10.1016/j.ophtha.2008.10.020.

51. Chia A, Chua W, Wen L, Fong A, Goon Y, Tan D. Atropine for the treatment of childhood myopia: changes after stopping atropine 0.01%, 0.1% and 0.5%. Am J Ophthalmol. 2014;157(2):451–457.e1. doi:10.1016/j.ajo.2013.09.020.

52. Dorje F, Wess J, Lambrecht G, Tacke R, Mutschler E, Brann M. Antagonist binding profiles of five cloned human muscarinic receptor subtypes. J Pharmacol Exp Ther. 1991;256(2):727–733.

53. Siatkowski R, Cotter S, Miller J, Scher C, Crockett R, Novack G. Safety and Efficacy of 2% Pirenzepine Ophthalmic Gel in Children With Myopia - A 1-Year, Multicenter, Double-Masked, Placebo-Controlled Parallel Study. Arch Ophthalmol. 2004;122(11):1667–1674.

54. Trier K, Ribel-Madsen S, Cui D, Christensen S. Systemic 7-methylxanthine in retarding axial eye growth and myopia progression: a 36-month pilot study. J Ocul Biol Dis Infor. 2008;1:85–93.

55. Cui D, Trier K, Zeng J, et al. Effects of 7-methylxanthine on the sclera in form deprivation myopia in guinea pigs. Acta Ophthalmol. 2011;89(4):328–334.

56. Nie H-H, Huo L-J, Yang X, et al. Effects of 7-methylxanthine on form-deprivation myopia in pigmented rabbits. Int J Ophthalmol. 2012;5(2):133–137.

57. Curtin B, Whitmore W. Long-term results of scleral reinforcement surgery. Am J Ophthalmol. 1987;103(4):544–8.

58. Ward B, Tarutta E, Mayer M. The efficacy and safety of posterior pole buckles in the control of progressive high myopia. Eye. 2009;23(12):2169–2174.

59. O'Brien PG. Scleral bioreactor: design and use for evaluation of myopia therapies. 2011.

60. Avetisov E, Tarutta E, Iomdina E, Vinetskaya M, Andreyeva L. Nonsurgical and surgical methods of sclera reinforcement in progressive myopia. Acta Ophthalmol Scand. 1997;75(6):618–23.

61. Su J, Iomdina E, Tarutta E, Ward B, Song J, Wildsoet C. Effects of poly(2-hydroxyethyl methacrylate) and poly(vinyl-pyrrolidone) hydrogel implants on myopic and normal chick sclera. Exp Eye Res. 2009;88(3):445–457. doi:10.1016/j.exer.2008.10.029.

62. Su J, Wall S, Healy K, Wildsoet C. Scleral reinforcement through host tissue integration with biomimetic enzymatically degradable semi-interpenetrating polymer network. Tissue Eng Part A. 2010;16(3):905–16. doi:10.1089/ten.TEA.2009.0488.

63. Lloyd A, Faragher R, Denyer S. Ocular biomaterials and implants. Biomaterials. 2001;22(8):769–785. doi:10.1016/S0142-9612(00)00237-4.

64. Remulla H, Rubin P, Shore J, et al. Complications of porous spherical orbital implants. Ophthalmology. 1995;102:586–593.

65. Colthurst M, Williams R, Hiscott P, Grierson I. Biomaterials used in the posterior segment of the eye. Biomaterials. 2000;21(7):649–65.

66. Ho P, Chan I, Refojo M, Tolentino F. The MAI hydrophilic implant for scleral buckling - a review. Ophthalmic Surg Lasers. 1984;15:511–515.

67. D'Hermies F, Korobelnik J, Savoldelli M, Chauvaud D, Pouliquen Y. Miragel versus silastic used as episcleral implants in rabbits—an experimental and histopathologic comparative study. Retina. 1995;15:62–67.

68. Hubel D, Wiesel T, LeVay S. Functional architecture of area 17 in normal and monocularly deprived macaque monkeys. In: Cold Spring Harbor Symposia on Quantitative Biology.; 1976:581–589.

69. Wallman J, Turkey J, Trachtman J. Extreme myopia produced by modest changes in early visual experience. Science (80-). 1978;201(4362):1249–1251.

70. Winawer J, Wallman J. Homeostasis of eye growth and the question of myopia. Neuron. 2004;43(4):447–468.

71. Norton T. Animal Models of Myopia: Learning How Vision Controls the Size of the Eye. ILAR J. 1999;40(2):59–77.

72. Bagnoli P, Porciatti V, Francesconi W. Retinal and tectal responses to alternating gratings are unaffected by monocular deprivation in pigeons. Brain Res. 1985;338(2):341–345. doi:10.1016/0006-8993(85)90165-9.

73. Andison M, Sivak J, Bird D. The refractive development of the eye of the American kestrel (Falco sparverius): a new avian model. J Comp Physiol A. 1992;170(5):565–574.

74. McBrien N, Moghaddam H, New R, Williams L. Experimental myopia in a diurnal mammal (Sciurus carolinensis) with no accommodative ability. J Physiol. 1993;469:427–441.

75. Kroger R, Wagner H. The eye of the blue acara (Aequidens pulcher, Cichlidae) grows to compensate for defocus due to chromatic aberration. J Comp Physiol A. 1996;176(6):837–842.

76. Shen W, Vijayan M, Sivak J. Inducing Form-Deprivation Myopia in Fish. Invest Ophthalmol Vis Sci. 2005;46(5):1797–1803.

77. Turnbull P, Phillips J, Backhouse S. Emmetropisation in an invertebrate. In: International Myopia Conference.; 2013.

78. Gollender M, Thorn F. Development of axial ocular dimensions following eyelid suture in the cat. Vision Res. 1979;19:221–223.

79. Kirby A, Sutton L, Weiss H. Elongation of cat eyes following neonatal lid suture. Invest Ophthalmol Vis Sci. 1982;22:274–277.

80. Yinon U, Koslowe K. Eyelid closure effects on the refractive error of the eye in dark- and light-reared kittens. Am J Optom Physiol Opt. 1984;61:271–273.

81. Beuerman R, Chew S. Visual form deprivation induces myopia in the infant rabbit, which is reduced by muscarinic antagonists applied directly to the sclera. Soc Neurosci Abstr. 1993;19:1102.

82. Gao Q, Liu Q, Ma P, Zhong X, Wu J, Ge J. Effects of direct intravitreal dopamine injections on the development of lid-suture induced myopia in rabbits. Graefe's Arch Clin Exp Ophthalmol. 2006;244(10):1329–1335.

83. Young F. The effects of restricted visual space on the primate eye. Am J Ophthalmol. 1961;52:799–806.

84. Hoyt C, Stone R, Fromer C, Billson F. Monocular axial myopia associated with neonatal eyelid closure in human infants. Am J Ophthalmol. 1981;91:197–200.

85. Huang J, Hung L, Smith E. Effects of foveal ablation on the pattern of peripheral refractive errors in normal and form-deprived infant rhesus monkeys (Macaca mulatta). Invest Ophthalmol Vis Sci. 2011;16(52):6428–34.

86. Smith E, Ramamirtham R, Qiao-Grider Y, et al. Effects of foveal ablation on emmetropization and form-deprivation myopia. Invest Ophthalmol Vis Sci. 2007;48(9):3914–22.

87. Smith E, Hung L, Huang J, Arumugam B. Effects of local myopic defocus on refractive development in monkeys. Optom Vis Sci. 2013;90(11):1176–86.

88. Smith E, Hung L, Arumugam B, Huang J. Negative lens-induced myopia in infant monkeys: effects of high ambient lighting. Invest Ophthalmol Vis Sci. 2013;54(4):2959–69.

89. Smith E, Hung L, Huang J. Protective effects of high ambient lighting on the development of form-deprivation myopia in rhesus monkeys. Invest Ophthalmol Vis Sci. 2011;53(1):421–428.

90. Qiao-Grider Y, Hung L, Kee C, Ramamirtham R, Smith E. Recovery from form-deprivation myopia in rhesus monkeys. Invest Ophthalmol Vis Sci. 2004;45(10):3361–72.

91. Huang J, Hung L, Smith E. Recovery of peripheral refractive errors and ocular shape in rhesus monkeys (Macaca mulatta) with experimentally induced myopia. Vision Res. 2012;73:30–39.

92. Graham B, Judge S. The effects of spectacle wear in infancy on eye growth and refractive error in the marmoset (Callithrix jacchus). Vision Res. 1999;39(2):189–206. doi:10.1016/S0042-6989(98)00189-8.

93. Troilo D, Nickla D, Mertz J, Rada J. Change in the Synthesis Rates of Ocular Retinoic Acid and Scleral Glycosaminoglycan during Experimentally Altered Eye Growth in Marmosets. Invest Ophthalmol Vis Sci. 2006;47(5):1768–1777.

94. Troilo D, Quinn N, Baker K. Accommodation and induced myopia in marmosets. Vision Res. 2007;47(9):1228–44. doi:10.1016/j.visres.2007.01.018.

95. Troilo D, Nickla D, Wildsoet C. Form deprivation myopia in mature common marmosets (Callithrix jacchus). Invest Ophthalmol Vis Sci. 2000;41(8):2043–9.

96. Troilo D, Nickla D. The Response to Visual Form Deprivation Differs with Age in Marmosets. Invest Ophthalmol Vis Sci. 2005;46(6):1873–1881.

97. Troilo D, Totonelly K, Harb E. Imposed anisometropic, accommodation, and regulation of refractive state. Optom Vis Sci. 2009;86(1):E31–9.

98. Tigges M, Tigges J, Fernandes A, Eggers H, Gammon J. Postnatal axial eye elongation in normal and visually deprived rhesus monkeys. Invest Ophthalmol Vis Sci. 1990;31:1035–1046.

99. Hung L-F, Crawford M, Smith E. Spectacle lenses alter eye growth and the refractive status of young monkeys. Nat Med. 1995;1:761–765.

100. Hodos W, Kuenzel W. Retinal image degradation produces ocular enlargerment in chicks. Invest Ophthalmol Vis Sci. 1984;25:652–659.

101. Schaeffel F, Glasser A, Howland H. Accommodation, refractive error and eye growth in chickens. Vision Res. 1988;28(5):639–57.

102. Irving E, Sivak J, Callender M. Refractive plasticity of the developing chick eye. Ophthalmic Physiol Opt. 1992;12(4):448–456.

103. Wildsoet C, Wallman J. Choroidal and scleral mechanisms of compensation for spectacle lenses in chicks. Vision Res. 1995;35(9):1175–1194.

104. Zhu X, Park T, Winawer J, Wallman J. In a matter of minutes, the eye can know which way to grow. Invest Ophthalmol Vis Sci. 2005;46(7):2238–2241.

105. Glasser A, Troilo D, Howland H. The mechanism of corneal accommodation in chicks. Vision Res. 1994;34(12):1549–1566.

106. Glasser A, Murphy C, Troilo D, Howland H. The mechanism of lenticular accommodation in chicks. Vision Res. 1995;35(11):1525–1540.

107. Wallman J, Wildsoet C, Xu A, et al. Moving the retina: choroidal modulation of refractive state. Vision Res. 1995;35(1):37–50.

108. Howlett M, McFadden S. Form-deprivation myopia in the guinea pig (Cavia porcellus). Vision Res. 2006;46(1-2):267–283.

109. Hung L-F, Wallman J, Smith E. Vision-dependent changes in the choroidal thickness of macaque monkeys. Invest Ophthalmol Vis Sci. 2000;41(6):1259–1269.

110. Read S, Chakraborty R, Collins M. Changes in diurnal rhythms of choroidal thickness with monocular defocus in human eyes. In: Association for Research in Vision and Ophthalmology. Fort Lauderdale, FL; 2012:4453–D896.

111. McBrien N, Moghaddam H, Reeder A. Atropine reduces experimental myopia and eye enlargement via a nonaccommodative mechanism. Invest Ophthalmol Vis Sci. 1993;34(1):205–215.

112. Stone R, Lin T, Laties A. Muscarinic antagonist effects on experimental chick myopia. Exp Eye Res. 1991;52(6):755–758.

113. Cao J, Yang E-B, Su J-J, Li Y, Chow P. The tree shrews: adjuncts and alternatives to primates as models for biomedical research. J Med Primatol. 2003;32(123-130).

114. Müller B, Peichl L. Topography of cones and rods in the tree shrew retina. J Comp Neurol. 1989;282(4):581–594.

115. Norton T, McBrien N. Normal development of refractive state and ocular component dimensions in the tree shrew (Tupaia belangeri). Vision Res. 1992;32(5):833–842.

116. Metlapally S, McBrien N. The effect of positive lens defocus on ocular growth and emmetropization in the tree shrew. J Vis. 2008;8(3):1–12.

117. McKanna J, Casagrande V. Reduced lens development in lid-suture myopia. Exp Eye Res. 1978;26(6):715–23.

118. Norton T, Kang R. Morphology of tree shrew sclera and choroid during normal development induced myopia, and recovery. Invest Ophthalmol Vis Sci. 1996;37(3):1490–1490.

119. Norton TT, Rada JA. Reduced extracellular matrix in mammalian sclera with induced myopia. Vision Res. 1995;35(9):1271–1281.

120. Arumugam B, McBrien N. Muscarinic antagonist control of myopia: evidence for M4 and M1 receptor-based pathways in the inhibition of experimentally-induced axial myopia in the tree shrew. Invest Ophthalmol Vis Sci. 2012;53(9):5827–37.

121. Gao H, Frost M, Siegwart J, Norton T. Patters of mRNA and protein expression during minus-lens compensation and recovery in tree shrew sclera. Mol Vis. 2011;17(903-19).

122. Guo L, Frost M, He L, Siegwart J, Norton T. Gene expression signatures in tree shrew sclera in response to three myopiagenic conditions. Invest Ophthalmol Vis Sci. 2013;54(10):6806–19.

123. He L, Frost M, Siegwart J, Norton T. Gene expression signatures in tree shrew choroid during lens-induced myopia and recovery. Exp Eye Res. 2014;123:56–71.

124. Jobling A, Wan R, Gentle A, Bui B, McBrien N. Retinal and choroidal TGF-beta in the tree shrew model of myopia: isoform expression, activation and effects on function. Exp Eye Res. 2009;88(3):458–66.

125. Amedo A, Norton T. Visual guidance of recovery from lens-induced myopia in tree shrews (Tupaia glis belangeri). Ophthalmic Physiol Opt. 2012;32(2):89–99.

126. McBrien N, Arumugam B, Metlapally S. The effect of daily transient +4 D positive lens wear on the inhibition of myopia in the tree shrew. Invest Ophthalmol Vis Sci. 2012;53(3):1593–601.

127. Frost M, Norton T. Differential protein expression in tree shrew sclera during development of lens-induced myopia and recovery. Mol Vis. 2007;13:1580–8.

128. Jobling A, Gentle A, Metlapally R, Mcgowan B, Mcbrien N. Regulation of Scleral Cell Contraction by Transforming Growth Factor- Beta and Stress. J Biol Chem. 2009;284(4):2072–2079. doi:10.1074/jbc.M807521200.

129. Mcbrien NA, Jobling AI, Truong HT, Cottriall CL, Gentle A. Expression of muscarinic receptor subtypes in tree shrew ocular tissues and their regulation during the development of myopia. Mol Vis. 2009;15(December 2008):464–475.

130. McBrien N, Lawlor P, Gentle A. Scleral remodeling during development of and recovery from axial myopia in tree shrew. Invest Ophthalmol Vis Sci. 2000;41(12):3713–9.

131. Siegwart J, Strang C. Selective modulation of scleral proteoglycan mRNA levels during minus lens compensation and recovery. Mol Vis. 2007;13:1878–86.

132. Siegwart J, Norton T. The time course of changes in mRNA levels in tree shrew sclera during induced myopia and recovery. Invest Ophthalmol Vis Sci. 2002;43(7):2067–75.

133. Norton T. Experimental myopia in tree shrews. Ciba Found Symp. 1990;155:178–194.

134. Pardue M, Stone R, Iuvone P. Investigating mechanisms of myopia in mice. Exp Eye Res. 2013;114:96–105.

135. Prusky A, Alam N, Beekman S, Douglas R. Rapid quantification of adult and developing mouse spatial vision using a virtual optomotor system. Invest Ophthalmol Vis Sci. 2004;45(4611-4616).

136. Schmucker A, Schaeffel F. A paraxial schematic eye model for the growing C57BL/6 mouse. Vision Res. 2004;44:1857–1867.

137. Schmucker A, Schaeffel F. In vivo biometry in the mouse eye with low coherence interferometry. Vision Res. 2004;44(2445-2456).

138. Park H, Qazi Y, Tan C, et al. Assessment of axial length measurements in mouse eyes. Optom Vis Sci. 2012;89:296–303.

139. Wisard J, Chrenek M, Wright C, et al. Non-contact measurement of linear external dimensions of the mouse eye. J Neurosci Methods. 2010;187:156–166.

140. Tkatchenko T V, Shen Y, Tkatchenko A V. Analysis of postnatal eye development in the mouse with high-resolution small animal magnetic resonance imaging. Invest Ophthalmol Vis Sci. 2010;51(1):21–7. doi:10.1167/iovs.08-2767.

141. Tejedor J, de la Villa P. Refractive changes induced by form deprivation in the mouse eye. Invest Ophthalmol Vis Sci. 2003;44(1):32–36.

142. Schaeffel F, Burkhardt E, Howland H, Williams R. Measurement of refractive state and deprivation myopia in two strains of mice. Optom Vis Sci. 2004;81(2):99–110.

143. McFadden S, Wallman J. Guinea pig eye growth compensates for spectacle lenses. Invest Ophthalmol Vis Sci. 1995;36(4):S758.

144. Edwards M, Penny R, Lyle J, Jonson K. Brain growth and learning behaviour of the guinea-pig following prenatal hyperthermia. Experientia. 1974;30(4):406–407.

145. Ostrin L, Mok-Yee J, Wildsoet C. Behavioral Measures of Spatial Vision during Early Development in Pigmented and Albino Guinea Pigs. In: Association for Research in Vision and Ophthalmology.; 2011:52:6296.

146. Schmid KL, Wildsoet CF. Assessment of visual acuity and contrast sensitivity in the chick using an optokinetic nystagmus paradigm. Vision Res. 1998;38(17):2629–2634. doi:10.1016/S0042-6989(97)00446-X.

147. Howlett M, McFadden S. Emmetropization and schematic eye models in developing pigmented guinea pigs. Vision Res. 2007;47(9):1178–90. doi:10.1016/j.visres.2006.12.019.

148. Zhou X, Qu J, Xie R, et al. Normal development of refractive state and ocular dimensions in guinea pigs. Vision Res. 2006;46(18):2815–2823.

149. Howlett M, McFadden S. Spectacle lens compensation in the pigmented guinea pig. Vision Res. 2009;49(2):219–27. doi:10.1016/j.visres.2008.10.008.

150. Zeng G, Bowrey H, Fang J, Qi Y, McFadden S. The development of eye shape and the origin of lower field myopia in the guinea pig eye. Vision Res. 2013;76:77–88.

151. Jiang L, Long K, Schaeffel F, et al. Disruption of Emmetropization and High Susceptibility to Deprivation Myopia in Albino Guinea Pigs. Invest Ophthalmol Vis Sci. 2011;52(9):6124–6132.

152. Backhouse S, Phillips J. Effect of Induced Myopia on Scleral Myofibroblasts and in vivo Ocular Biomechanical Compliance in the Guinea Pig. Invest Ophthalmol Vis Sci. 2010. doi:10.1167/iovs.10-5387.

153. Chen B, Ma J, Wang C, Chen W. Mechanical behavior of scleral fibroblasts in experimental myopia. Graefe's Arch Clin Exp Ophthalmol. 2012;250(3):341–348.

154. McFadden S, Tse D, Bowrey H, et al. Integration of Defocus by Dual Power Fresnel Lenses Inhibits Myopia in the Mammalian Eye. Invest Ophthalmol Vis Sci. 2014;13.

155. Jungfeng M, Shuangzhen L, Wenjuan Q, Fengyun L, Xiaoying W, Qian T. Levodopa Inhibits the Development of Form-Deprivation Myopia in Guinea Pigs. Optom Vis Sci. 2010;87(1):53–60.

156. Tang R, Tan J, Deng Z, Zhao S, Miao Y, Zhang W. Insulin-like growth factor-2 antisense oligonucleotides inhibits myopia by expression blocking of retinal insulin-like growth factor-2 in guinea pig. Clin Exp Ophthalmol. 2012;40(5):503–511.

157. Zhi Z, Pan M, Xie R, Xiong S, Zhou X, Qu J. The Effect of Temporal and Spatial Stimuli on the Refractive Status of Guinea Pigs Following Natural Emmetropization. Investig Ophthalmol Vis Sci. 2013;54(1):890–897.

158. Jiang L, Zhang S, Schaeffel F, et al. Interactions of chromatic and lens-induced defocus during visual control of eye growth in guinea pigs (Cavia porcellus). Vision Res. 2014;94:24–32.

159. Liu R, Qiang Y, He J, et al. Effects of different monochromatic lights on refractive development and eye growth in guinea pigs. Exp Eye Res. 2011;92(6):447–453.

160. Long Q, Chen D, Chu R. Illumination with monochromatic long-wavelength light promotes myopic shift and ocular elongation in newborn pigmented guinea pigs. Cutan Ocul Toxicol. 2009;28(4):176–180.

161. Wang F, Zhou J, Lu Y, Chu R. Effects of 530 nm Green Light on Refractive Status, Melatonin, MT1 Receptor, and Melanopsin in the Guinea Pig. Curr Eye Res. 2011;36(2):103–111.

162. Di Y, Liu R, Chu R, Zhou X. Myopia induced by flickering light in guinea pigs: a detailed assessment on susceptibility of different frequencies. Int J Ophthalmol. 2013;6(2):115–119.

163. Leotta A, Bowrey H, Zeng G, McFadden S. Temporal properties of the myopic response to defocus in the guinea pig. Ophthalmic Physiol Opt. 2013;33(3):227–244.

164. An J, Hsi E, Zhou X, Tao Y, Juo SH, Liang CL. The FGF2 gene in a myopia animal model and human subjects. Mol Vis. 2012;18:471–478.

165. Cui D, Trier K, Zeng J, Wu K, Yu M, Ge J. Adenosine receptor protein changes in guinea pigs with form deprivation myopia. Acta Ophthalmol. 2010;88(7):759–65. doi:10.1111/j.1755-3768.2009.01559.x.

166. Dong F, Zhi Z, Pan M, et al. Inhibition of experimental myopia by a dopamine agonist: different effectiveness between form deprivation and hyperopic defocus in guinea pigs. Mol Vis. 2011;17:2824–2834.

167. Fang F, Pan M, Yan T, et al. The Role of cGMP in Ocular Growth and the Development of Form-Deprivation Myopia in Guinea Pigs. Invest Ophthalmol Vis Sci. 2013;54(13):7887–7902.

168. Huang J, Qu X, Chu R. Expressions of cellular retinoic acid binding proteins I and retinoic acid receptor-β in the guinea pig eyes with experimental myopia. Int J Ophthalmol. 2011;4(2):131–136.

169. Liu Q, Wu J, Wang X, Zeng J. Changes in muscarinic acetylcholine receptor expression in form deprivation myopia in guinea pigs. Mol Vis. 2007;13(May):1234–44.

170. Mao J, Liu S. Mechanism of the DL-alpha-aminoadipic acid inhibitory effect on form-deprived myopia in guinea pig. Int J Ophthalmol. 2013;6(1):19–22.

171. Mao J, Liu S, Qin W, Xiang Q, Wu X. Exogenous levodopa increases the neuro retinal dopamine of guinea pig myopic eyes in vitro. Eye Sci. 2011;26(4):211–216.

172. McFadden S, Howlett M, Mertz J. Retinoic acid signals the direction of ocular elongation in the guinea pig eye. Vision Res. 2004;44(7):643–653.

173. Wu J, Liu Q, Yang X, Yang H, Wang X, Zeng J. Time-course of changes to nitric oxide signaling pathways in form-deprivation myopia in guinea pigs. Brain Res. 2007;1186:155–63. doi:10.1016/j.brainres.2007.09.077.

174. Yang J, Xu Y, Sun L, Tian X. 5-hydroxytryptamine level and 5-HT2A receptor mRNA expression in the guinea pigs eyes with spectacle lens-induced myopia. Int J Ophthalmol. 2010;3(4):299–303.

175. Cui D, Trier K, Zeng J, Wu K, Yu M, Ge J. Adenosine receptor protein changes in guinea pigs with form deprivation myopia. Acta Ophthalmol. 2010;88(7):759–765.

176. Mao J, Liu S, Qin W, Xiang Q. Modulation of TGFβ(2) and dopamine by PKC in retinal Müller cells of guinea pig myopic eye. Int J Ophthalmol. 2011;4(4):357–360.

177. Wu J, Liu Q, Yang X, Yang H, Wang X, Zeng. Changes of nitric oxide synthase and cyclic guanose monophosphate in FD myopia in guinea pigs. Chin Med J (Engl). 2007;120(24):2238–2244. doi:10.1179/096992607X217967.

178. Mao J, Liu S, Dou X. Retinoic acid metabolic change in retina and choroid of the guinea pig with lens-induced myopia. Int J Ophthalmol. 2012;5(6):670–674.

179. Chen B, Wang C, Chen W, Ma J. Altered TGF-β2 and bFGF expression in scleral desmocytes from an experimentally-induced myopia guinea pig model. Graefe's Arch Clin Exp Ophthalmol. 2013;251(4):1133–1144.

180. Zhou X, Ye J, Willcox M, et al. Changes in protein profiles of guinea pig sclera during development of form deprivation myopia and recovery. Mol Vis. 2010;17:2163–2174.

181. Tian X, Cheng Y, Liu G, et al. Expressions of type I collagen, α2 integrin and β1 integrin in sclera of guinea pig with defocus myopia and inhibitory effects of bFGF on the formation of myopia. Int J Ophthalmol. 2013;6(1):54–8. doi:10.3980/j.issn.2222-3959.2013.01.11.

182. Wang Q, Zhao G, Xing S, Zhang L, Yang X. Role of bone morphogenic proteins in form-deprivation myopia sclera. Mol Vis. 2011;17:647–657.

183. Rymer J, Choh V, Bharadwaj S, et al. The albino chick as a model for studying ocular developmental anomalies, including refractive errors, associated with albinism. Exp Eye Res. 2007;85(4):431–442.

184. Nickla D, Wildsoet C, Wallman J. The circadian rhythm in intraocular pressure and its relation to diurnal ocular growth changes in chicks. Exp Eye Res. 1998;66:183–193.

185. Lu F, Zhou X, Zhao H, et al. Axial myopia induced by a monocularly-deprived facemask in guinea pigs: A non-invasive and effective model. Exp Eye Res. 2006;82(4):628–636.

186. Saltarelli D, C W, Nickla D, Troilo D. Susceptibility to form-deprivation myopia in chicks is not altered by an early experience of axial myopia. Optom Vis Sci. 2004;81(2):118–26.

187. Zhou X, Lu F, Xie R, et al. Recovery from axial myopia induced by a monocularly deprived facemask in adolescent (7-week-old) guinea pigs. Vision Res. 2007;47(8):1103–11. doi:10.1016/j.visres.2007.01.002.

188. Ouyang C, Chu R, Hu W. Effects of pirenzepine on lens-induced myopia in the guinea pig. Chinese J Ophthalmol. 2003;39(6):348–351.

189. Cheng Z, Li J, Li R, Li J. Effect of time limited form deprivation on the development of myopia in guinea pigs. Chinese J Ophthalmol. 2004;40(3):183–185.

190. Lu F, Zhou X, Jiang L, et al. Axial myopia induced by hyperopic defocus in guinea pigs: A detailed assessment on susceptibility and recovery. Exp Eye Res. 2009;89(1):101–8. doi:10.1016/j.exer.2009.02.019.

191. Deng Z, Tan J, Liu S, Zhao S, Wang J. The correlation between the regulation of recombinant human IGF-2 on eye growth and form-deprivation in guinea pig. Graefe's Arch Clin Exp Ophthalmol. 2010;248(4):519–25. doi:10.1007/s00417-009-1287-z.

192. Jiang L, Schaeffel F, Zhou X, et al. Spontaneous axial myopia and emmetropization in a strain of wild-type guinea pig (Cavia porcellus). Invest Ophthalmol Vis Sci. 2009;50(3):1013–9. doi:10.1167/iovs.08-2463.

193. Schmid K, Wildsoet C. Breed- and gender-dependent differences in eye growth and form deprivation responses in chick. J Comp Physiol A. 1996;178(4):551–61.

194. Troilo D, Li T, Glasser A, Howland H. Differences in eye growth and the response to visual deprivation in different strains of chicken. Vision Res. 1995;35(9):1211–6.

195. Guggenheim J, Erichsen J, Hocking P, Wright N, Black R. Similar genetic susceptibility to form-deprivation myopia in three strains of chicken. Vision Res. 2002;42(25):2747–2756.

196. Chen Y, Prashar A, Hocking P, et al. Sex, eye size, and the rate of myopic eye growth due to form deprivation in outbred White Leghorn chickens. Invest Ophthalmol Vis Sci. 2010;51(2):651–657.

197. Zhu X, Lin T, Stone R, Laties A. Sex differences in chick eye growth and experimental myopia. Exp Eye Res. 1995;61(2):173–179.

198. Chen Y, Hocking P, Wang L, et al. Selective breeding for susceptibility to myopia reveals a gene-environment interaction. Invest Ophthalmol Vis Sci. 2011;52(7):4003–4011.

199. Morgan I, Ashby R, Nickla D. Form deprivation and lens-induced myopia: are they different? Ophthalmic Physiol Opt. 2013;33(3):355–361.

200. Jung S, Lee J, Kakizaki H, Jee D. Prevalence of myopia and its association with body stature and educational level in 19-year-old male conscripts in seoul, South Korea. Invest Ophthalmol Vis Sci. 2012;53(9):5579–83. doi:10.1167/iovs.12-10106.

201. Lin L, Shih Y, Hsiao C, Chen C. Prevalence of myopia in Taiwanese schoolchildren: 1983 to 2000. Ann Acad Med Singapore. 2004;33:27–33.

202. Vitale S, Sperduto R, Ferris F. Increased prevalence of myopia in the United States between 1971-1972 and 1999-2004. Arch Ophthalmol. 2009;127(12):1632–9. doi:10.1001/archophthalmol.2009.303.

203. Hrynchak P, Mittelstaedt A, Machan C, Bunn C, Irving E. Increase in Myopia Prevalence in Clinic-Based Populations Across a Century. Optom Vis Sci. 2013;90(11):1331–1341.

204. Williams K, Hammond C. Prevalence of myopia and association with education in Europe. Lancet. 2014;383:S109.

205. Chang L, Pan C, Ohno-Matsui K, et al. Myopia-related fundus changes in Singapore adults with high myopia. Am J Ophthalmol. 2013;155(6):991–999.

206. Grosvenor T. Why is there an epidemic of myopia? Clin Exp Optom. 2003;86(5):273–5.

207. Saw S, Gazzard G, Shih-Yen E, Chua W. Myopia and associated pathological complications. Ophthalmic Physiol Opt. 2005;25(5):381–91. doi:10.1111/j.1475-1313.2005.00298.x.

208. Liu H, Xu L, Wang Y, Wang S, You Q, Jonas J. Prevalence and Progression of Myopic Retinopathy in Chinese Adults: The Beijing Eye Study. Ophthalmology. 2010;117(9):1763–1768.

209. Pan C, Cheung C, Aung T, et al. Differential Associations of Myopia with Major Age-related Eye Diseases The Singapore Indian Eye Study. Ophthalmology. 2013;120(2):284–291.

210. Gwiazda J. Treatment options for myopia. Optom Vis Sci. 2009;86(6):624–8. doi:10.1097/OPX.0b013e3181a6a225.

211. Wollensak G, Spoerl E. Collagen crosslinking of human and porcine sclera. J Cataract Refract Surg. 2004;30(3):689–695.

212. Wollensak G, Iomdina E, Dittert D, Salamatina O, Stoltenburg G. Cross-linking of scleral collagen in the rabbit using riboflavin and UVA. Acta Ophthalmol Scand. 2005;83(4):477–82. doi:10.1111/j.1600-0420.2005.00447.x.

213. Liu T, Wang Z. Collagen crosslinking of porcine sclera using genipin. Acta Ophthalmol. 2013;91(4):e253–57.

214. Paik D, Wen Q, Airiani S, Braunstein R, Trokel S. Aliphatic β-nitro alcohols for non-enzymatic collagen cross-linking of scleral tissue. Exp Eye Res. 2008;87(3):279–285.

215. Mattson MS. Understanding and treating eye diseases: mechanical characterization and photochemical modification of the cornea and sclera. 2008:V1–V32.

216. Slaughter B, Khurshid S, Fisher O, Khademhosseini A, Peppas N. Hydrogels in regenerative medicine. Adv Mater. 2009;21(32-33):3307–29. doi:10.1002/adma.200802106.

217. Tang S, Vickers S, Hsu H, Spector M. Fabrication and characterization of porous hyaluronic acid–collagen composite scaffolds. J Biomed Mater Res. 2007;82A(2):323–335.

218. Halbleib M, Skurk T, de Luca C, von Heimburg D, Hauner H. Tissue engineering of white adipose tissue using hyaluronic acid-based scaffolds. I: in vitro differentiation of human adipocyte precursor cells on scaffolds. Biomaterials. 2003;24(18):3125–3132. doi:10.1016/S0142-9612(03)00156-X.

219. Nesti L, Li W, Shanti R, et al. Intervertebral Disc Tissue Engineering Using a Novel Hyaluronic Acid–Nanofibrous Scaffold (HANFS) Amalgam. Tissue Eng Part A. 2008;14(9):1527–1537.

220. Liu H, Mao J, Yao K, Yang G, Cui L, Cao Y. A study on a chitosan-gelatin-hyaluronic acid scaffold as artificial skin in vitro and its tissue engineering applications. J Biomater Sci. 2004;15(1):25–40.

221. Solchaga L, Dennis J, Goldberg V, Caplan A. Hyaluronic acid-based polymers as cell carriers for tissue-engineered repair of bone and cartilage. J Orthop Res. 1999;17(2):205–213.

222. Cui F, Tian W, Hou S, Xu Q, Lee I. Hyaluronic acid hydrogel immobilized with RGD peptides for brain tissue engineering. J Mater Sci Mater Med. 2006;17:1393–1401.

223. Sahiner N, Jha A, Nguyen D, Jia X. Fabrication and characterization of cross-linkable hydrogel particles based on hyaluronic acid: potential application in vocal fold regeneration. J Biomater Sci Polym Ed. 2008;19(2):223–243.

224. Jha A, Tharp K, Ye J, et al. Growth factor sequestering and presenting hydrogels promote survival and engraftment of transplanted stem cells. Nat Commun (under Rev. 2014.

225. Rezania A, Thomas C, Branger A, Waters C, Healy K. The detachment strength and morphology of bone cells contacting materials modified with a peptide sequence found within bone sialoprotein. J Biomed Mater Res. 1997;37:9–19.

226. Wall S, Yeh C, Tu R, Mann M, Healy K. Biomimetic matrices for myocardial stabilization and stem cell transplantation. J Biomed Mater Res A. 2010;95(4):1055–66. doi:10.1002/jbm.a.32904.

227. Wang X, Chen W, Li Y, Gao T. Biomechanical Properties of Experimental Myopia in the Guinea Pig. In: Bioinformatics and Biomedical Engineering, 2008. ICBBE 2008. Shanghai; 2008:1825–1827.

228. Saha K, Keung A, Irwin E, et al. Substrate modulus directs neural stem cell behavior. Biophys J. 2008;95(4426).

229. Irwin E, Saha K, Rosenbluth M, Gamble L, Castner D, Healy K. Modulus-dependent macrophage adhesio and behavior. J Biomater Sci Polym Ed. 2008;19(1363).

230. Tsai C, Wu P, Fini M, Shi S. Identification of Multipotent Stem/Progenitor Cells in Murine Sclera. Invest Ophthalmol Vis Sci. 2011;52(8):5481–5487.

231. Miron-Mendoza M, Seemann J, Grinnell F. The differential regulation of cell motile activity through matrix stiffness and porosity in three dimensional collagen matrices. Biomaterials. 2010;31(25):6425–35. doi:10.1016/j.biomaterials.2010.04.064.

232. Dahlmann-Noor A, Martin-Martin B, Eastwood M, Khaw P, Bailly M. Dynamic protrusive cell behaviour generates force and drives early matrix contraction by fibroblasts. Exp Cell Res. 2007;313(20):4158–69. doi:10.1016/j.yexcr.2007.07.040.

233. Rhee S, Ho C, Grinnell F. Promigratory and procontractile growth factor environments differentially regulate cell morphogenesis. Exp Cell Res. 2010;316:232–244.

234. Lo C, Wang H, Dembo M, Wang Y. Cell movement is guided by the rigidity of the substrate. Biophys J. 2000;79(1):144–52. doi:10.1016/S0006-3495(00)76279-5.

235. Peng Y, Kau Y, Wen C, Liu K, Liu S. Solvent-free biodegradable scleral plugs providing sustained release of vancomycin , amikacin , and dexamethasone — An in vivo study. J Biomed Mater Res Part A. 2010;94(2):426–432. doi:10.1002/jbm.a.32697.

236. Gilhotra RM, Gilhotra N, Mishra DN. Piroxicam Bioadhesive Ocular Inserts : Physicochemical Characterization and Evaluation in Prostaglandin-Induced Inflammation. Curr Eye Res. 2009;34(12):1065–1073. doi:10.3109/02713680903340738.

237. Carcaboso AM, Chiappetta DA, Opezzo JAW, et al. Episcleral Implants for Topotecan Delivery to the Posterior Segment of the Eye. Invest Ophthalmol Vis Sci. 2010;51(4):2126–2134. doi:10.1167/iovs.09-4050.

238. Felt-Baeyens O, Eperon S, Mora P, et al. Biodegradable scleral implants as new triamcinolone acetonide delivery systems. Int J Pharm. 2006;322:6–12. doi:10.1016/j.ijpharm.2006.05.053.

239. Kim Y, Lim J, Kim H, Kim S, Shin J. A novel design of one-side coated biodegradable intrascleral implant for the sustained release of triamcinolone acetonide. Eur J Pharm Biopharm. 2008;70(1):179–186. doi:10.1016/j.ejpb.2008.04.023.

240. Shin JP, Park YC, Oh JH, et al. Biodegradable Intrascleral Implant of Triamcinolone Acetonide in Experimental Uveitis. J Ocul Pharmacol Ther. 2009;25(3):201–207. doi:10.1089/jop.2008.0086.

241. Meyer K, Palmer J. The polysaccharide of the vitreous humor. J Biol Chem. 1934;107:629–634.

242. Kleinberg TT, Tzekov RT, Stein L, Ravi N, Kaushal S. Vitreous substitutes: a comprehensive review. Surv Ophthalmol. 2011;56(4):300–23. doi:10.1016/j.survophthal.2010.09.001.

243. Schramm C, Spitzer M, Henke-Fahle S, et al. The Cross-linked biopolymer hyaluronic acid as an artificial vitreous substitute. Invest Ophthalmol Vis Sci. 2011;53(2):613–621.

244. Kogan G, Soltés L, Stern R, Gemeiner P. Hyaluronic acid: a natural biopolymer with a broad range of biomedical and industrial applications. Biotechnol Lett. 2007;29:17–25.

245. Pape LG, Balazs EA. The Use of Sodium Hyaluronate (Healon®) in Human Anterior Segment Surgey. Ophthalmology. 1980;87(7):699–705. doi:10.1016/S0161-6420(80)35185-3.

246. Greene P. Mechanical considerations in myopia. In: Grosvenor R, Flom M, eds. Refractive abnormalities - Research and clinical applications. Butterworth-Heinemann; 1991:287–300.

247. Cui W, Bryant M, Sweet P, McDonnel P. Changes in gene expression in response to mechanical strain in human scleral fibroblasts. Exp Eye Res. 2004;78(2):275–284.

248. Fujikura H, Seko Y, Tokoro T, Mochizuki M, Shumokawa H. Involvement of mechanical stretch in the gelatinolytic activity of the fibrous sclera of chicks, in vitro. Jpn J Ophthalmol. 2002;46:24–30.

249. Powell D, Mifflin R, Valentich J, Crowe S, Saada J, West A. Myofibroblasts. I. Paracrine cells important in health and disease. Am J Physiol. 1999;277(1):C1–C19.

250. Khaw P, Occleston N, Schultz G, Grierson I, Sherwood M, Larkin G. Activation and suppression of fibroblast function. Eye. 1994;8(188-195).

251. Nilsson S. Human retinal vascular obstructions. A quantitative correlation of angiographic and electroretinographic findings. Acta Ophthalmol. 1971;49:111–133.

252. Noell W. The origin of the electroretinogram. Am J Ophthalmol. 1954;38:78–90.

253. Fujino T, Hamasaki D. The effect of occluding the retinal and choroidal circulations on the electroretinogram of monkeys. J Physiol. 1965;180(4):837–845.

254. McLeod D, Hayreh S. Occlusion of posterior ciliary artery. IV. Electroretinographic studies. Br J Ophthalmol. 1972;56(10):765–769.

255. Fischer A, McGuire J, Schaeffel F, Stell W. Light- and focus-dependent expression of the transcription factor ZENK in the chick retina. Nat Neurosci. 1999;2:706–712. doi:10.1038/11167.

256. Zhang Y, Liu Y, Wildsoet CF. Bidirectional, Optical Sign-Dependent Regulation of BMP2 Gene Expression in Chick Retinal Pigment Epithelium. Invest Ophthalmol Vis Sci. 2012;53(10):6072–80. doi:10.1167/iovs.12-9917.

Appendix 1. Calculation of a correction factor for the refractive error data presented in Chapter 4

A1.1 Introduction

Retinoscopy is largely considered an objective method of measuring refractive error. However, examiner-based variability in refraction measurements is a well-known phenomenon (Bullimore, Fusaro, & Adams, 1998; Safir, Hyams, Philpot, & Jagerman, 1970; Zadnik, Mutti, & Adams, 1992), most often attributed to sources of variability such as standing outside one's own working distance and incorrect alignment with the subject's visual axis. Here we describe the calculation of a correction factor used in Chapter 4 to account for the biases in refractive error measurements performed by two different retinoscopists.

A2.2 Methods

The myopia control experiments described in Chapter 4 were performed over a 2-year period. Due to personnel changes in the lab, the refractive error measurements of guinea pigs were performed by two different examiners. The Diffuser group's measurements were performed by Examiner A, while the other two groups (Diffuer + HyA and Diffuser + Sham) were measured by Examiner B.

The refractive errors of the fellow (untreated) eyes were used to calculate the correction factor, since they were unaffected by the treatments. As shown in Figure A1-1, the refractive errors of the fellow eyes of guinea pigs measured by the two examiners were dissimilar, with the refractive errors measured by Examiner A trending more towards hyperopia than those measured by Examiner B (Figure 1). Though the means of the two groups were not significantly different (Examiner A: 2.64±1.75 D, Examiner B: 0.36±1.81. $p=0.09$, Mann-Whitney), it is still important to bring the means closer together to prevent incorrect conclusions from being drawn when different treatment groups are compared.

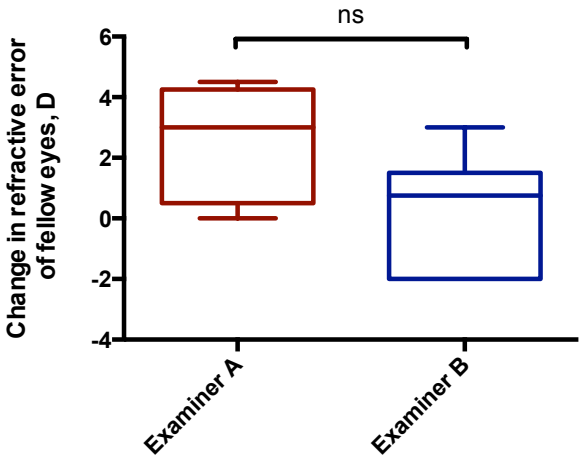

Figure A1-1. Change in refractive errors of fellow eyes, grouped according to which examiner performed the measurements.

To equalize the means of the two populations and ensure that accurate comparisons could be drawn between the treatment groups, a simple correction factor was calculated:

Mean refractive error of fellow eyes measured by Examiner A = 2.6428

Mean refractive error of fellow eyes measured by Examiner B = 0.3571

Correction factor = Mean (Examiner A) – Mean (Examiner B) = 2.2857

The correction factor was subtracted from the measurements obtained by Examiner A, equalizing the mean of that group to that of Examiner B (Figure A1-2).

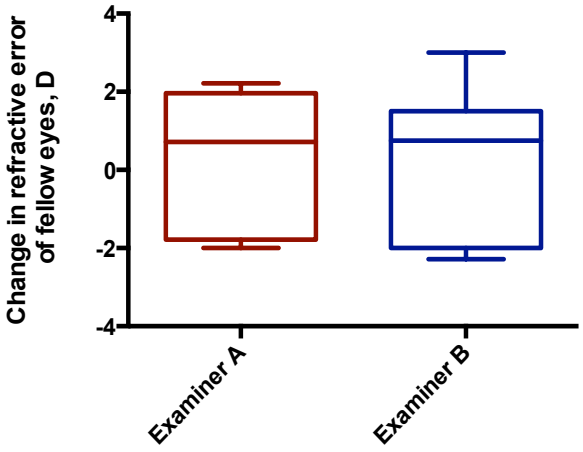

Figure A1-2. Change in refractive errors of fellow eyes, with a correction factor applied to Examiner A's measurements.

A2.3 Results and discussion

The effect of the correction factor – when applied to both treated and control eyes of animals measured by Examiner A – can be seen in Figure A1-3. Panel A presents uncorrected data, clearly showing the hyperopic bias of the examiner in the Diffuser group. Corrected data is shown in Panel B.

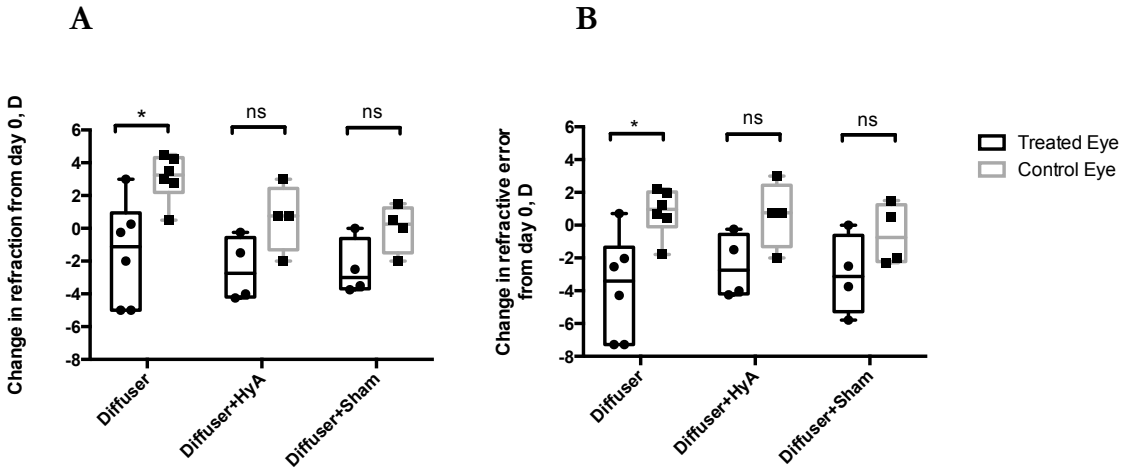

Figure A1-3. Uncorrected (A) and corrected (B) changes in refractive error over the total treatment period for treated and control eyes of guinea pigs treated with Diffusers, Diffusers+HyA, and Diffusers+Sham. Treated vs. control eye differences assessed with a Wilcoxon test (*$p<0.05$).

References

Bullimore, M., Fusaro, R., & Adams, C. (1998). The repeatability of automated and clinician refraction. *Optometry and Vision Science*, *75*(8).

Safir, A., Hyams, L., Philpot, J., & Jagerman, L. (1970). Studies in refraction. I. The precision of retinoscopy. *Archives of Ophthalmology*, *84*, 49–61.

Zadnik, K., Mutti, D., & Adams, A. (1992). The repeatability of measurements of the ocular components. *Investigative Ophthalmology & Visual Science*, *33*(7), 2325–2333.

Appendix 2. *In vitro* compatibility studies of N-isopropylacrylamide-based semi-interpenetrating polymer networks with guinea pig scleral fibroblasts

A2.1 Introduction

This appendix will describe preliminary studies undertaken to translate our group's previous research on hydrogel-based myopia control in chicks (Su, Wall, Healy, & Wildsoet, 2010). To that end, different formulations of the N-isopropylacrylamide (NIPAAm)-based semi-interpenetrating polymer network (sIPN) employed in those studies were synthesized, and their compatibility with primary guinea pig scleral fibroblasts assessed through live/dead staining and a proliferation assay.

A2.2 Materials and Methods

A2.2.1 Synthesis and rheological characterization of N-Isopropylacrylamide-based hydrogels

Unless specified, all chemicals were purchased from Sigma Aldrich and used without additional purification. The water used in the syntheses was ultra pure ATM type I reagent grade, purified in a MilliQ filter.

NIPAAm-based sIPNs were synthesized by redox radical addition polymerization at room temperature, in molar ratios of and 97:3: NIPAAm: acrylic acid in PBS without calcium or magnesium, as previously described (Chung et al., 2006; Kim, Chung, Gilbert, & Healy, 2005; Kim & Healy, 2003). The crosslinker concentration was varied from 1-4 mg/mL and the concentration of peptide-conjugated interpenetrating linear polyacrylic acid (pAAc) chain was varied from 0-210 μM.

Degradable acrylated peptide crosslinker was synthesized from a peptide sequence amenable to cleavage by MMP-2, -9, and -13 (Kim & Healy, 2003). A peptide sequence – Gln-Pro-Gln-Gly-Leu-Ala-Lys-NH_2 – (American Peptides) was reacted with acryloyl chloride and triethylamine, generating amide bonds between the peptide and acrylate groups and introducing bifunctional acrylate groups that can participate in the redox radical addition polymerization.

The linear interpenetrating chain of polyacrylic acid grafted with a cell-binding peptide (pAAc-g-RGD) was synthesized by first grafting linear polyacrylic acid (MW 450kDa; Polysciences, Inc) sequentially with maleimide side groups and a 15 amino acid-long RGD-containing peptide derived from bone sialoprotein (bsp-RGD(15), Ac-CGGNGEP**RGD**TYRAY-NH2, American Peptides).

Semi-interpenetrating polymer networks were synthesized by preparing a solution of NIPAAm, acrylic acid, acrylated crosslinker, and pAAc-g-RGD in calcium and magnesium-free PBS. The solution was purged of oxygen by bubbling it with dry nitrogen gas for 30 minutes, after which the solution was moved into a nitrogen glove box and 0.8 wt% ammonium persulfate and 4% v/v

N,N,N',N'-tetramethylenediamine (TEMED; Polysciences) were added as initiator and accelerator, respectively. The solution was vigorously mixed, then quickly pipetted into 24-well inserts (Millipore) and allowed to polymerize overnight. To prepare the hydrogels for cell culture, they were washed in excess PBS, sterilized with 70% ethanol, and washed again in PBS. For all washing steps, the hydrogels were taken through their Lower Critical Solution Temperature (LCST), thus allowing unreacted reagents to be expelled from the polymer matrix. The hydrogels were stored in sterile PBS at 4°C until used.

The mechanical properties of the hydrogel were characterized by measuring the complex shear modulus |G*| through dynamic oscillatory shear rheology (Anton Paar), using 25mm sanded parallel plates with a gap height of 1 mm. A humidity chamber was placed around the samples to prevent them from drying during measurements. Samples (n=3) were tested at 0.1-15Hz, 5% strain and 37°C.

A2.2.2 Cytocompatibility of sIPNs with guinea pig scleral fibroblasts

Cytotoxicity assay: To assess the short-term cytotoxicity of the synthesized hydrogels, primary guinea pig scleral fibroblasts were seeded over the surface of polymerized hydrogels at a density of $10x10^3$ cells/cm^2 and cultured for 7 days. Hydrogels were then stained for 30 minutes at 37°C with a Calcein AM/Ethidium Homodimer solution in PBS. Images were acquired using a fluorescence microscope (Nikon).

Alamar Blue proliferation assay: To quantify cell proliferation on the hydrogel surfaces and to determine its dependency on modulus and concentration of cell-binding peptide, a 14-day proliferation assay was performed with the non-toxic reagent Alamar Blue. Guinea pig scleral fibroblasts were seeded on the hydrogels (synthesized in 24-well Millipore inserts) or on tissue culture polystyrene (TCPS) plates alone at a density of $5x10^3$ cells/cm^2, for a total of $3x10^3$ cells and $9.5x10^3$ cells seeded onto the hydrogel and TCPS surfaces, respectively. Four to six replicates were tested for each condition. Cell numbers were assessed after 14 days using Alamar Blue (Life Technologies), according to the manufacturer's instructions. The reagent was first sterilized by filtering through a 200μm-pore syringe filter. The reagent was incubated with the samples for 2 h at 37°C, then the solution was carefully removed and its absorbance determined at 570nm.

A2.3 Results and discussion

A2.3.1 Rheological characterization of the sIPNs

The results of the rheological characterization of sIPNs synthesized with 1-4 mg/mL of crosslinker are shown in figure A2-1. For all hydrogels, the modulus increased slightly as a function of frequency. This tendency was especially marked for the 4 mg/mL hydrogels. The mean modulus of the hydrogels (averaged across all measured frequencies) was 97.38 ± 48.68, 206.90 ± 63.00, and 855.50 ± 193.90 Pa for the 1, 2, and 4mg/mL crosslinker hydrogels, respectively. The differences between the mean values were statistically significant ($p<0.0001$, Kruskal-Wallis test).

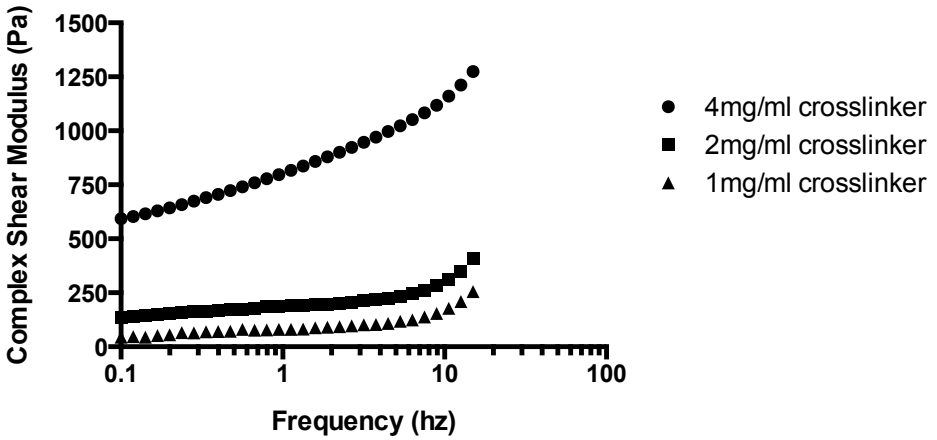

Figure A2-1 Rheological characterization of NIPAAm hydrogels at 37°C, plotted as complex shear modulus as a function of frequency, measured by oscillatory parallel plate rheology

Hydrogels stained with Calcein AM and Ethidium Homodimer were imaged by fluorescence microscopy after 7 days of culture. Composite images are shown in Figure A2-2. As expected, very few cells survived in the hydrogel containing no RGD peptide. The ones that did retained a rounded phenotype. Cells grew significantly more on the 105 and 210μM RGD hydrogels and adapted a more stellate phenotype. The hydrogels with 105μM RGD exhibited the highest amount of attached cells, with cell numbers increasing as a function of modulus. Comparatively fewer cells were attached to 210μM the hydrogels, suggesting that such a high a peptide concentration is deleterious to cell attachment and survival.

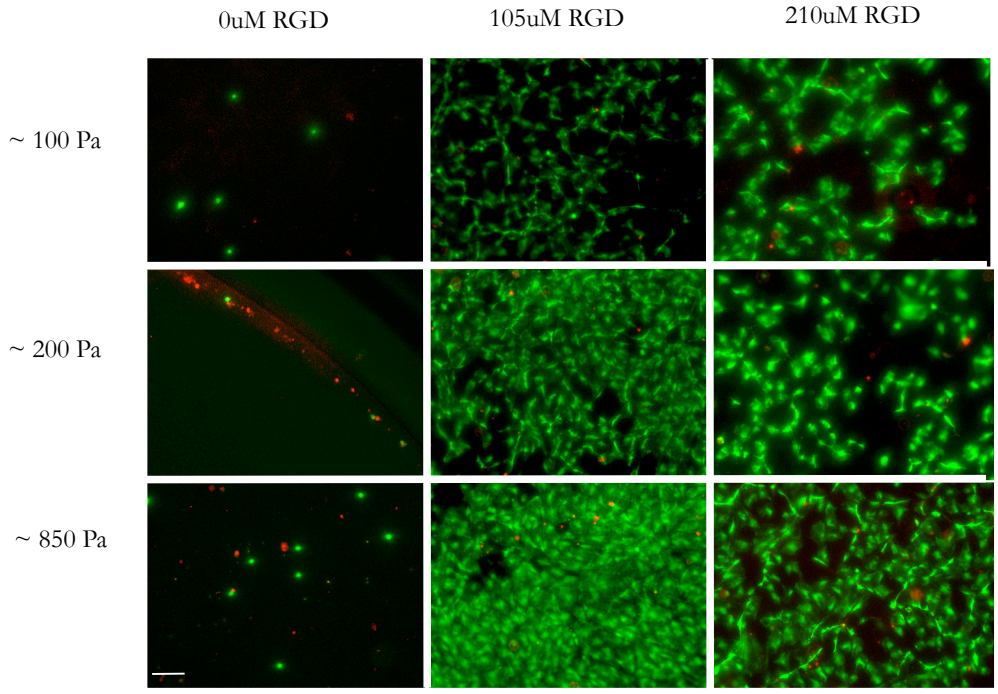

Figure A2-2. Representative live (green)/dead (red) images acquired after 7 days of 2D culture on NIPAAm-based hydrogels with varying modulus and bsp-RGD(15) (cell-binding peptide) concentration. Scale bars represent 100 μm.

Results of 14-day proliferation experiments are shown in Figure A2-3. For many of the hydrogels, the number of cells counted at day 14 was lower than the number of seeded cells ($3x10^3$ cells). Nonetheless, a surprising number of cells managed to survive on the 0μM RGD hydrogels, presumably by forming connections to neighboring cells in favor of connections to the matrix. No significant differences were found for each of the three moduli of the 0μM RGD hydrogels (2-way ANOVA, Tukey post-hoc test). Similarly to what we observed in the live/dead images, cells appear to proliferate slightly better on the 105μM RGD compared to the 210μM RGD gels. Within the 105μM RGD group, an increase in modulus resulted in an increase in proliferation. The 100 and 200 Pa hydrogels in the 210μM RGD group induced little cell proliferation, while the stiffer hydrogel was more conducive to cell growth.

Given the low cell numbers after 14 days of culture, we can speculate that there might have been a large amount of cell death shortly after seeding at day 0, and that the numbers measured at day 14 are the result of the proliferation of surviving cells. Since these hydrogels were not conducive to cell proliferation, we decided to pursue alternative hyaluronic acid-based hydrogels as a myopia control tool, as described in chapters 3 and 4.

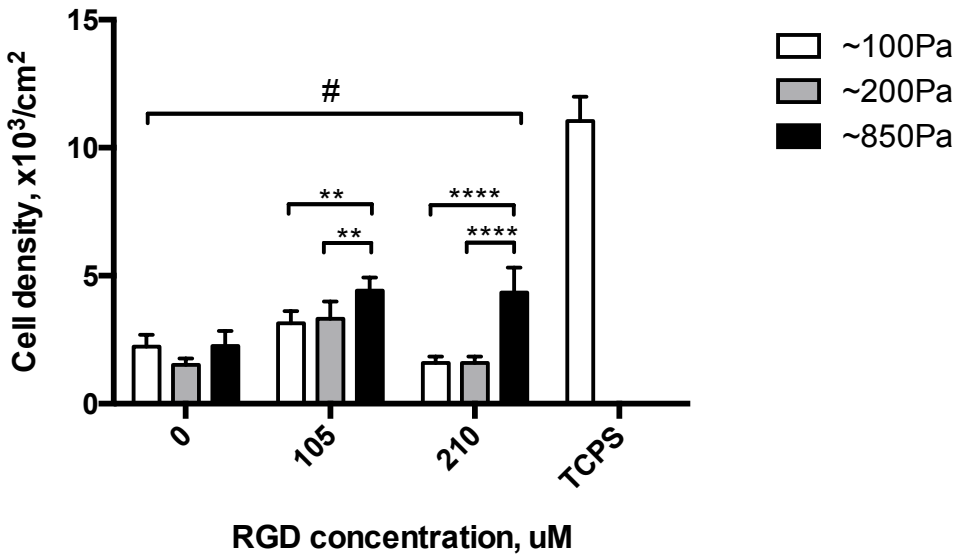

Figure A2-3. Guinea pig scleral fibroblast numbers after 14 days of culture on NIPAAm hydrogels, with RGD concentrations varying from 0-210 μM and modulus varying from 100-800 Pa, or on tissue culture polystyrene (TCPS, control). Columns represent mean + SD for 4-6 samples/condition. ** $p<0.01$, **** $p<0.0001$. # significant difference from TCPS, $p<0.0001$.

References

Chung, E. H., Gilbert, M., Virdi, A. S., Sena, K., Sumner, D. R., & Healy, K. E. (2006). Biomimetic artificial ECMs stimulate bone regeneration. *Journal of Biomedical Materials Research. Part A*, *79*(4), 815–26. doi:10.1002/jbm.a.30809

Kim, S., Chung, E. H., Gilbert, M., & Healy, K. E. (2005). Synthetic MMP-13 degradable ECMs based on poly(N-isopropylacrylamide-co-acrylic acid) semi-interpenetrating polymer networks. I. Degradation and cell migration. *Journal of Biomedical Materials Research Part A*, *75*(1), 73–88. doi:10.1002/jbm.a.30375

Kim, S., & Healy, K. E. (2003). Synthesis and characterization of injectable poly(N-isopropylacrylamide-co-acrylic acid) hydrogels with proteolytically degradable cross-links. *Biomacromolecules*, *4*(5), 1214–23. doi:10.1021/bm0340467

Su, J., Wall, S., Healy, K., & Wildsoet, C. (2010). Scleral reinforcement through host tissue integration with biomimetic enzymatically degradable semi-interpenetrating polymer network. *Tissue Engineering. Part A*, *16*(3), 905–16. doi:10.1089/ten.TEA.2009.0488

Appendix 3. Preliminary *in vivo* hydrogel injection studies

A3.1 Introduction

The project described in this dissertation depended greatly on reliable surgical procedures. This appendix will describe a few of the preliminary experiments conducted to optimize the surgery procedure and to determine the ideal hydrogel modulus for the myopia control experiments. Aspects of the preliminary surgeries different from the ones described in Chapter 4 are bolded.

A3.2 Materials and Methods

Elm Hill guinea pigs were anesthetized with a ketamine/xylazine cocktail (0.45/0.045 mg/kg body weight), placed over a warming pad, and covered with a sterile surgery blanket with an opening cut out for the eye. After cleaning the fur surrounding the eye with an alcohol pad, an eyelid retractor was positioned to increase visibility to the upper eye. A drop of local anesthetic was instilled onto the surface of the eye (0.5% Proparacaine Hydrochloride, Bausch & Lomb). An anchor suture (Reli® Plain Gut 5-0, Myco Medical Supplies) was threaded through the upper conjunctiva, secured with a hemostat, and gently pulled downwards in a nasal direction to roll the eye and facilitate access to the posterior sclera. Using surgical micro-scissors, an incision (**2-5 mm wide**) was made through the conjunctiva, episclera, and Tenon's capsule, exposing the sclera. The sclera was separated from its overlying tissues using blunt forceps. **The incision was not pre-sutured before the hydrogel/buffer injections.** At this point, the injection solution was prepared by mixing diluted HyA precursors with diluted crosslinker (for Diffuser + HyA group) and **allowing the polymer to start crosslinking for 2-3 minutes**. Approximately **100 µL** of hydrogel (for Diffuser + HyA group) or TEA buffer (for Diffuser + Sham group) were drawn through a syringe fitted with a curved 19G retrobulbar injection needle (Beaver-Visitec). The hydrogel/buffer was injected very slowly into the sub-Tenon's space (note that at this stage a variable amount of the hydrogel leaked back out of the incision; thus the volume of solution remaining at the injection site is also subject to variation, being as low as ~50 µL). The speed of injection is critical in this process, as too rapid injections can lead to the formation of bubbles and expulsion of much larger amounts of the hydrogel/buffer through the surgical incision. **The incision was closed with 2-3 single stitches**. Topical moxifloxacin hydrochloride solution (Vigamox, Alcon) was applied to the surface of the eye, the lid retractor was removed, any blood or fluid was very gently cleared away with sterile gauze. Guinea pigs were kept on a warming pad until completely recovered from anesthesia. Topical moxiflocaxin was instilled once daily for two days following the surgery. For the remainder of the study, the operated eyes were closely examined for signs of inflammation (redness, swelling, discharge, eyelid ptosis).

The ocular axial length of all animals was measured at baseline, then once weekly for 1-5 weeks after the surgery.

In the studies reported here, guinea pigs were injected with both 200 and 800 Pa hydrogels. On two occasions in which animals received 200 Pa hydrogel treatments, we investigated whether two 50 µL injections as opposed to a single 100 µL application would result in a more homogenous hydrogel

layer. For these surgeries, a 2-day recovery period was allowed between the surgeries. The second surgery was conducted by making an incision and injection through the inferior conjunctiva.

A3.3 Results and discussion

The surgical procedure described in this appendix caused more tissue trauma than the one ultimately used in our myopia control experiments (described in Chapter 4). In this case, the incision through the conjunctiva was just wide enough to admit the width of the needle; after the needle was placed through the incision to inject the hydrogel/buffer, it was moved around the surface of the eye to try distributing the polymer/buffer evenly. The movement of the needle caused some stress to the conjunctival tissue around the incision area, which led to post-surgical swelling that took 1-2 day to subside. Increasing the width of the surgical incision allowed for an easier movement of the needle and significantly decreased (in fact, effectively eliminated) the post-surgical tissue swelling.

A big modification from these original surgeries was the time of injection after mixing the monomer and crosslinker solutions. In these early studies, we sought to prevent an excessive amount of polymer from exiting the incision during the surgery by allowing it to polymerize for a few minutes, hence ensuring that it was less soft when injected. This practice, however, made the hydrogel more difficult to inject and resulted in a bolus of material becoming localized at a single spot, instead of a somewhat uniform layer covering most of the posterior pole.

Other aspects of these preliminary surgeries – which were eventually changed for the final studies – were the use of single sutures, only used to close the incision *after* the hydrogel/buffer injection. Unlike single sutures, loop sutures allow the incision to be closed more evenly and finalized by a single knot. Loosely suturing the incision prior to the hydrogel/buffer injection decreases the volume that leaks out of it and ensures more consistency between surgeries on different animals. Lastly, the use of a zero-dead-volume syringe allows for more precise control over the injected volume of solution

Changes in interocular difference of axial length for guinea pigs treated with 200 Pa hydrogels are shown in Figure A3-1. The graph depicts results for animals that received one (light blue lines) and two (dark blue lines) hydrogel injections. Three of the animals were monitored for one week after the surgery: in these guinea pigs, the treated eye was more elongated than the control eye, suggesting that the surgery has little effect on the rate of eye growth. Two guinea pigs were tracked for four weeks, and in their cases the treated eye grew slightly less than the control. In one of the animals, which was tracked for two weeks, the treated eye's growth rate was significantly slowed, such that the length of the treated eye was nearly 600 μm shorter than the control. A histological examination of the treated eye revealed a very large quantity of polymer accumulated in a single spot behind the sclera; it is likely that this implant pushed against the eye wall and led to a drastic decrease in eye length (Figure A3-2).

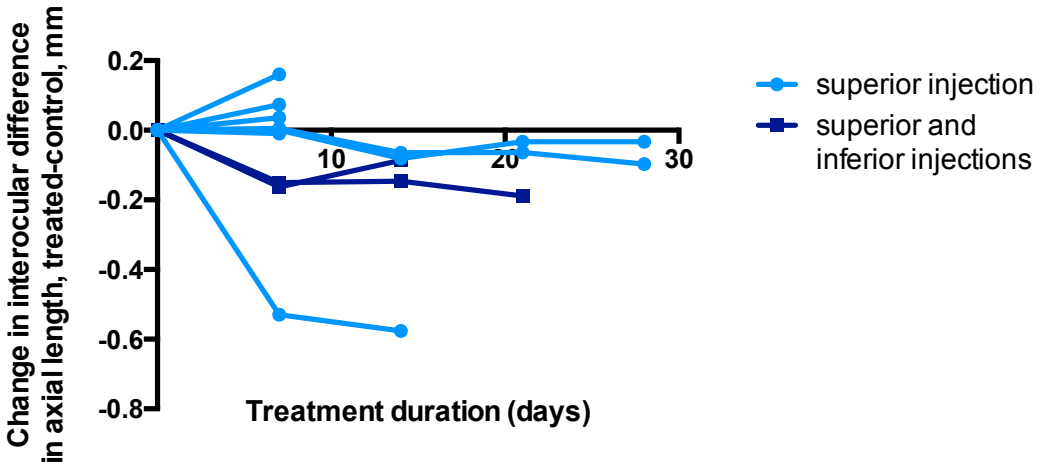

Figure A3-1. Individual longitudinal changes over the experimental period in interocular axial length for Elm Hill guinea pigs treated with superior and superior & inferior injections of 200 Pa 380 μM RGD hydrogels.

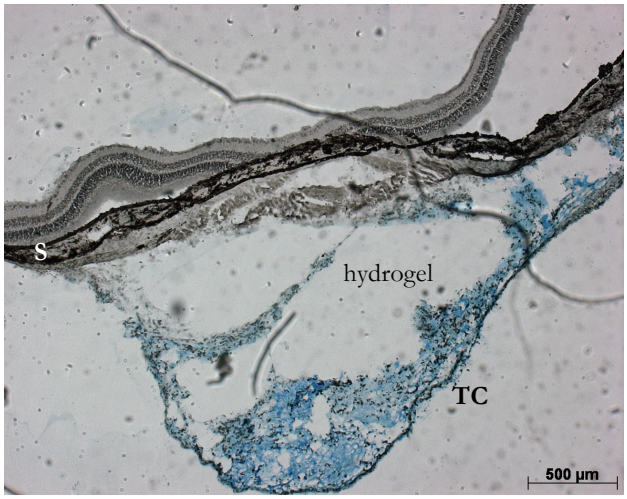

Figure A3-2. Posterior pole of a guinea pig eye after injection of 200 Pa 380μM RGD, stained with Alcian Blue. The section corresponds to the treated eye that exhibited a drastic decrease in the length in comparison to the control eye. Note the very large bolus of hydrogel, which could have been pushing against the eye wall. S: sclera. TC: Tenon's capsule.

Figure A3-3 shows the change in interocular difference of axial length described previously, with the addition of the ocular biometry data of guinea pigs treated with 800 Pa 380μM RGD HyA hydrogels. Aside from the exception discussed above, the 800 Pa hydrogels led to a stronger inhibition of ocular growth than the 200 Pa hydrogels. It also led to tissue deformation, as mentioned in Chapter 4. This, combined with the fact that the stiffer hydrogels were much more difficult to inject, led us to adopt the 200 Pa hydrogels for the myopia control *in vivo* studies.

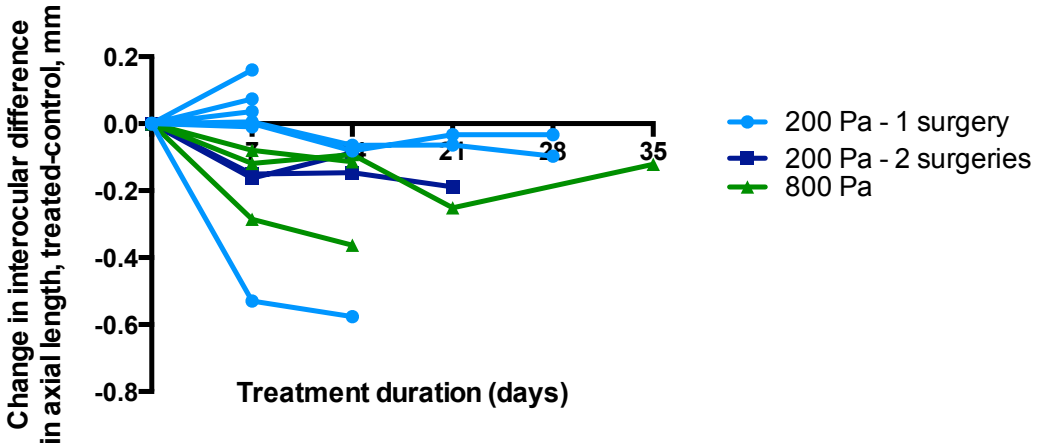

Figure A3-3. Individual longitudinal changes over the experimental period in interocular axial length for Elm Hill guinea pigs treated with superior injection of 800 Pa 380 μM RGD hydrogels, as well as superior or superior & inferior injections of 200 Pa 380 μM RGD hydrogels.